2018-01-22

Neuro-Electronic Interface: Interrogating Neuronal Function and Circuitry with Innovative Approaches

Wijdenes, Pierre

UNIVERSITY OF CALGARY

Neuro-Electronic Interface: Interrogating Neuronal Function and Circuitry with Innovative Approaches

by

Pierre Wijdenes

A THESIS

SUBMITTED TO THE FACULTY OF GRADUATE STUDIES

IN PARTIAL FULFILMENT OF THE REQUIREMENTS FOR THE

DEGREE OF DOCTOR OF PHILOSOPHY

GRADUATE PROGRAM IN BIOMEDICAL ENGINEERING

CALGARY, ALBERTA

JANUARY, 2018

Abstract

All nervous system functions, ranging from simple reflexes to complex behaviors and learning and memory, rely on networks of interconnected brain cells called neurons. Loss of various neuronal circuit functions, due either to stroke, epilepsy, trauma, Parkinson's, Alzheimer's or neurodegenerative diseases, renders the nervous system dysfunctional. Epilepsy alone is one of the most common and debilitating neurological disorder, which affects about 65 million people worldwide – representing 1% of the global population. Because natural replacement of injured or diseased nervous system tissue seldom, if ever, occurs, this loss of function is often irreversible and leaves patients incapacitated for life. The lack of fundamental knowledge in the field of neurological disorders, such as epilepsy, owes its existence to the intricacies of neuronal networks, and our inability to monitor their activities at the resolution of individual neurons. Thus, several laboratories in the world have developed brain-chip interface technologies that allow the interrogation of neuronal function non-invasively and over an extended time period. A variety of neuro-electronic interfaces now allow fundamental understanding of brain function, ranging from monitoring ion channel activities [1–3], to synaptic plasticity [4], and brain-controlled prosthetic devices [4–9]. However, there are several limitations to the existing micro-electrode designs, their biocompatibility and resolution, when monitoring both normal and perturbed activity patterns, for example during epilepsy**. Thus, the main objective of my thesis was to develop a set of novel micro-electrode arrays (MEAs) that could fill this technological gap, allowing for the detection, characterization, and modulation of neural activity from individual cells to neuronal networks.**

The research presented here focuses on the design parameters, fabrication techniques and protocols used to validate the in-house devices developed during my PhD research. I investigated and established essential criteria such as integrated substrate biocompatibility and the ability of my devices to record neural activity at a resolution higher than commercially available chips. Neural activity recorded using newly developed neuro-chips permitted the acquisition of high resolution recordings which could then be analyzed computationally to characterize and differentiate activity patterns recorded from single cells and entire neural networks. Together, these studies not only allowed me to develop novel MEA technologies, but will also provide researchers with unique opportunities to better understand cellular and network properties.

Preface

"Man cannot discover new oceans unless he has the courage to lose sight of the shore"

– André Gide

"***Whatever happens, the Earth keeps turning***"

– Dad

Acknowledgements

I initially joined Dr. Syed's laboratory as an intern in Summer 2009 and got exposed for the first time, to the notion of brain-chip interfaces, a field that I have always been passionate about. Despite this incredible experience, I thought I would never have the courage to pursue a PhD; I thought that it was simply "not something for me". But as we also say in France, "only stupid people do not change"… And as if a magnet was left for me in this place, I came back to Calgary in 2012 to start this incredible journey and never a single second did I regret this decision. Throughout this journey, I have been surrounded by some of the most intelligent and genuine people I ever met in my life, and learning from and with them has been a true honor. To all the people that have been a part of my academic adventure, I am sincerely grateful for your support for it helped me grow as an individual and become the person I am now.

Dr. Syed, being the lab's Frenchy was a true honor. You taught me so many valuable skills that I am taking away with me, and two in particular will always stand on for the rest of my life. First, "thinking is a hard thing" that often generates more questions than answers; but it is also a gift, a privilege, that enables us to be "touched by God" every time the bulb lights up. Second, you taught me how to lead as a servant, a middle man that listens, serves and inspires individuals, to effectively leverage their natural strengths so that they can realize their full potential. The success of the ones we support become our own successes, and this is one of the most humbling and gratifying experience. Naweed - thank you. Also, sorry I didn't bring you a Nobel prize…!

Wali, you are a true artist and a friend that we can always count on. In fact, I think you never turned your back to any of my requests, even when they were stupid or difficult! It was your cell culture skills that brought my research into reality. Also, thank you for giving all of us a bad time when we are late or don't work hard enough, I will somehow miss that.

Jean, you always managed to surprise me by solving technical issues I had with my experiments. I will repeat it one more time: you should have been an engineer! Thank you for your support and work in the lab, things would not happen smoothly without you.

Carolyn, you are the most efficient administrator I have ever met. You are THE go to person to get things done. Thank you very much for keeping everyone on track and helping us navigate the mazes of the university.

Thank you to all my lab mates: Tara for correcting so many time my Frenglish; Collin my best bud; Angie the (super) smart cookie; Ryden my young padawan; Simon the eagle eye; Camilla; Fenglian; Michael; Hasan; Andrew; Thomas; Eugeni; Cezar; I am so thankful that our roads crossed and that I got the chance to learn by your side.

To my committee members: Dr. Dalton, Dr. Rho and Dr. Teskey, thank-you for your support and encouragement. Having you guide me and believe in my research was an honor.

To the Biomedical Engineering program: Dr. Kallos, Lisa Mayer, and Lisa Mullaney for enabling students like myself to follow their passion.

To my family and friends: Mom, Dad, Sister, for encouraging me to always follow my dreams, and making me believe that nothing is impossible; Jen, John, Donna, Terry, thank you for your unconditional love and support; the Adams, you guys just rock; Jan, Carolyn, Nichole Van Minnen, thank you for your support welcoming me to Calgary and making both my arrivals so enjoyable.

And finally, I would like to express my gratitude for this opportunity to access the knowledge and resources present at the University of Calgary facility that allowed me to optimize the design of our MEAs and improve specific fabrication characteristic that were so fundamental for my project. This work would also not have been possible without the generous support of the Antje Graupe Pryor Foundation and its Werner Graupe International Fellowship in Engineering.

Table of Contents

List of Tables

List of Figures

AED	Anti-epileptic drug
aCSF	Artificial cerebrospinal fluid
AFM	Atomic force microscope
An^-	Anions
AP	Action potential
ATP	Adenosine triphosphate
Ca^{2+}	Calcium
CAGR	Compound annual growth rate
CM	Conditioned media
CNS	Central nervous system
DBS	Deep Brain Stimulation
DM	Defined media
EEG	Electroencephalogram
EPSP	Excitatory post-synaptic potential
FET	Field-effect transistor
IPSP	Inhibitory post-synaptic potential
ISI	Inter-spike interval
K^+	Potassium
LPeD1	Left pedal dorsal 1
MEA	Multi-electrode array
MRI	Magnetic resonance imaging
MW-MEA	Multi-well multi-electrode array

Mg^{2+}	Magnesium
Na^{+}	Sodium
NBM	Neurobasal medium
NT-MEA	Neural tissue multi-electrode array
PDMS	Polydimethylsiloxane
PNS	Peripheral nervous system
PTP	Post-tetanic potential
PVD	Physical vapor deposition
RPeD1	Right pedal dorsal 1
R_{seal}	Sealing resistance
SEM	Scanning electron microscope
SNR	Signal-to-noise ratio
SS-MEA	Soma-soma multi-electrode array
VD4	Visceral dorsal 4
VNS	Vagus nerve stimulation

Chapter 1: Introduction

1.1 General introduction

Going through a day in life can appear trivial for most of us. We get up in the morning, have a cup of coffee, go to work, interact with people, exercise and participate in various activities. It is however not immediately obvious how our bodies and organs are controlled and can perform such tasks with little conscious effort, allowing us to walk, speak, or breath. And this does not even take into consideration the emotions and feelings we may experience in our life. We just do it… Or shall we say, something does it for us.

Indeed, we now know that the Central Nervous System (CNS, which is composed of the brain and spinal cord) works in unison with the Peripheral Nervous System (PNS, composed of ganglion and nerves). While the brain is in charge of processing and integrating information that it receives and perceives, the PNS act as a relay that communicates input and output information between the CNS and the different organs and muscles. So the question that naturally arises is how such a complex system can integrate and communicate information required to eventually evoke an eye blink or a heartbeat? What is the nature of this information that results in our sensing of the world around us and moving within it? To answer these questions, understanding the brain is key, and this is the reason why the field of neuroscience has considerably expanded in the last century.

The human brain is composed of a population of no more than 85 to 100 billion neurons [10], considered to be the fundamental building blocks of the central nervous system. But the number of neurons present in our brain do not solely explain the astounding cognitive capacities of the human brain compared to other mammals. For example, the adult brain from an African elephant (*Loxodonta*) possess an estimated 257 billion neurons [11], but does not appear to have a greater functional and cognitive capacity than a human. Thus, to solve the enigma of the human brain capacity, we need to look at how these billions of neurons interconnect: through a specialized communication structure called a synapse. Digging a bit deeper, it is actually the sum of these estimated 1.5×10^{14} synapses that enables the complex and high level function performed by the human brain [12]. This represents literally 75 times more synapses present in each and every single human brain, than galaxies in the observable universe. When interconnected, these neurons form dense, complex, highly malleable, and feedback loop networks that are responsible for all actions, feelings and thoughts, these being conscious or not.

Therefore, to permit repair of damaged parts of the nervous system and offer appropriate treatments to those affected by neurological disorders, it is essential that we understand in the first place how neural networks form and develop, as well as how the CNS interpret and process information. However, concurrently recording from large neural ensembles remains a daunting challenge to say the least.

This chapter will provide a review of the main building blocks required to form a neural network, and how its dysfunction can cause neurological disorders, including epilepsy. Further, an

overview of the history of Multi-Electrode Arrays technology used in electrophysiology will be provided, as well as a description of their current limitations impacting our understanding of brain functions.

1.2 Fundamental of Neuroscience

1.2.1 Neurons as the main building blocks

Neurons are the main fundamental building blocks that comprise our nervous system (CNS and PNS), and play an essential role in the detection, processing and transmission of biological messages. They are electrically excitable cells, that when interconnected with other neurons, can transmit information between themselves and with other neural or non-neural cells. Different types of neurons exist, including sensory, motor and inter-neurons, each with specific functions, sizes (4 – 125 µm in diameter) and electrochemical properties.

More specifically, the process used by a neuron to receive, treat and send information is described as follow [13]. The structure of a neuron can be broken down into five main components: the dendrites, the soma, the axon hillock, the synaptic terminals, and the axon (Figure 1). First, dendrites serve as a mesh of electrical receptacles that integrate the synaptic inputs from neighboring neurons. This integration is considered to be both spatial and temporal: spatial because it aggregate the inhibitory or excitatory information provided by neighboring neurons; and temporal because the compiled rapid electrochemical stimuli are summed together to form one unique signal. Once received, the information is sent to the cell body, also called soma, a spherical structure where the cell nucleus is found. The soma is responsible for maintaining the health and functionality of the cell, but do not participate per se in the processing of the electrical information. In fact, it is at the site of the axon hillock that incoming electrical signals are filtered, integrated

and triggered. After receiving the synaptic inputs from multiple dendrites in the form of Inhibitory Post-Synaptic Potentials (IPSPs) or Excitatory Post-Synaptic Potentials (EPSPs), the sum of these aggregated signals is required to reach a certain threshold necessary for further propagating the output signal along the axon. The axon is a uniform elongation of nerve fiber (length up to ~ 1 meter [14]) that spreads from the cell body to the synaptic terminals. The role of glial cells, is in part, to support neuron functioning by insulating the axon with a fatty substance called myelin. While a larger axon diameter usually means that the information can travel faster, it is mostly the presence of this myelin sheath around the axon that permits the preservation and fast transfer of the electrical signals to the synaptic terminals. In turn, the synaptic terminal converts the electrical signal into a release of chemicals called neurotransmitters, that will bind to receptors located on an adjacent neuron (see next section for more details).

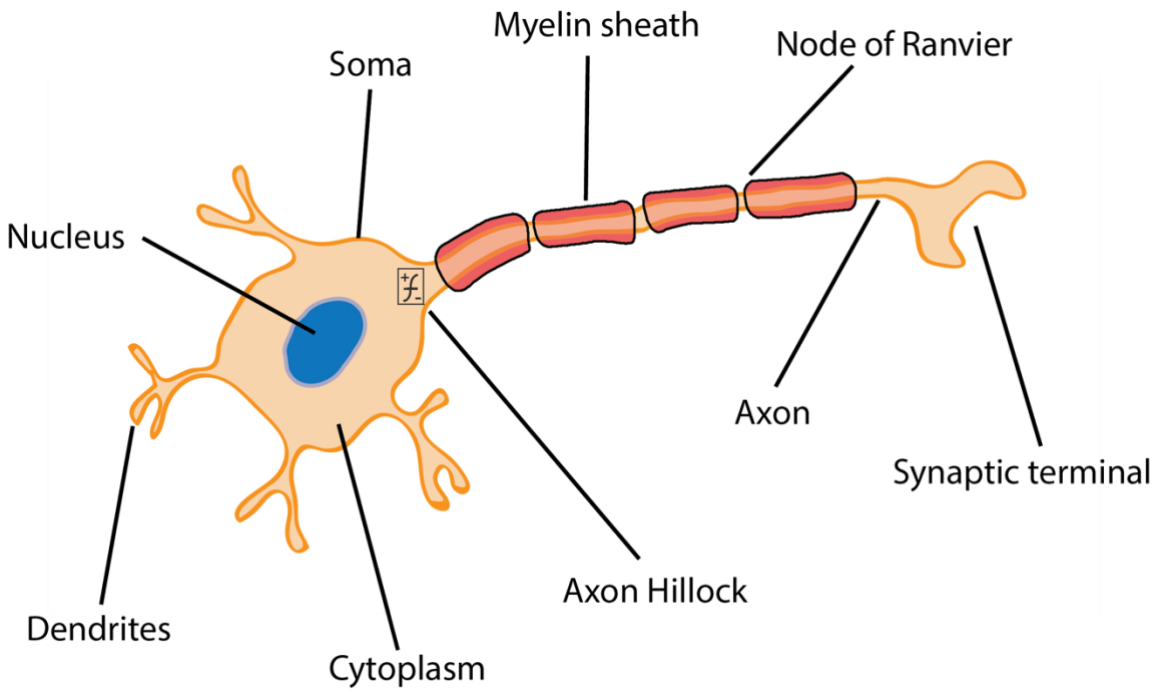

Figure 1: Schematic of a neuron

Schematic of a neuron, a specialized cell that transmit information in the nervous system. The dendrites convert afferent information from other neurons into electrical impulses that is then treated at the axon Hillock. The signal is then transmitted to the synaptic terminals through the axon. An insulating layer (myelin sheath) improves the conduction properties of the electrical impulses.

1.2.2 Passive membrane and action potential propagation

As described previously, neurons are individual nerve cells that transmit electrochemical signals [13]. It is important to consider that like most living cells, neurons have a selectively permeable membrane consisting of a phospholipid bilayer impermeable to ions. These phospholipids are themselves made of two elements: a hydrophilic head facing the extracellular solution and a hydrophobic tail facing the intracellular fluid (Figure 2). However, proteins function embedded within this layer allow for specific ions and molecules to cross the membrane. As described below, these inward and outward flows are fundamental for the neurons to function.

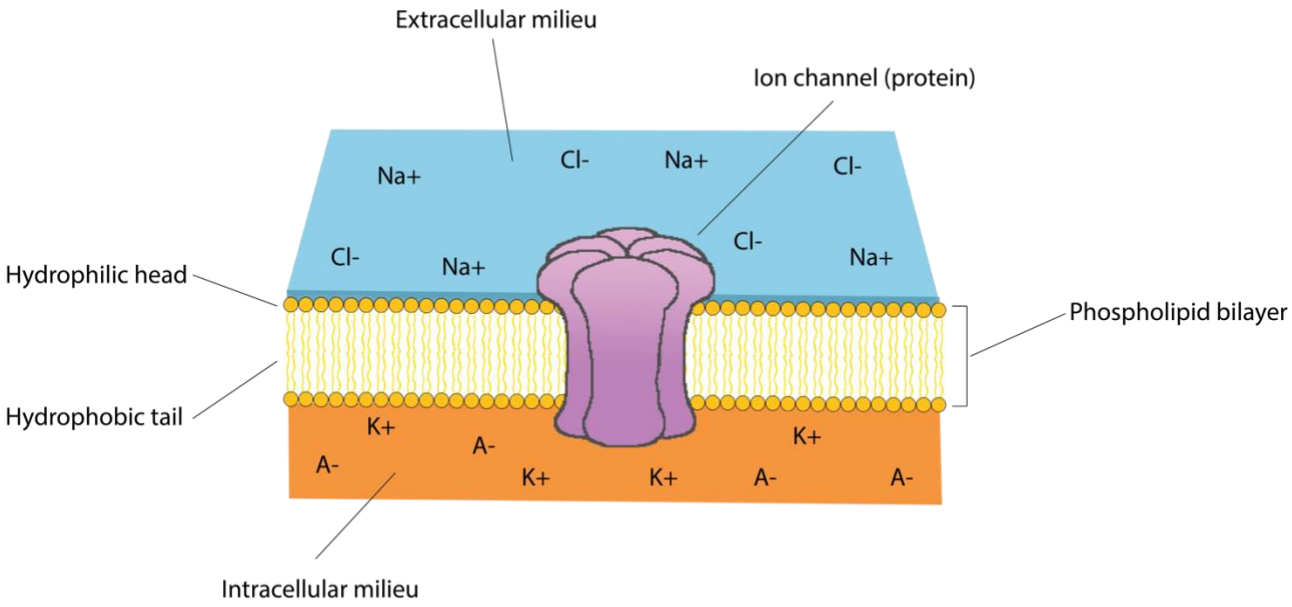

Figure 2: Schematic representation of the neuronal membrane

Schematic representation of the neuronal membrane. Ion channels are embedded in a membrane consisting of a phospholipid bilayer that is impermeable to ions. These channels can selectively permit ions to cross the membrane.

First, to fully grasp the electrochemical interplay that occurs at the neuronal level, it is important to understand that four major ions are distributed in different concentrations on both sides of the phospholipid bilayer: Anions (An^-) mostly contributed by proteins, sodium (Na^+), chloride (Cl^-) and potassium (K^+). While Cl^- and Na^+ are more concentrated outside the cell, the concentration of K^+ and An^- is considered higher in the intracellular milieu [13]. When a neuron is at rest (i.e. when no signal is being processed or transferred), the separation of chargers is preserved by proteins called ion channels and pumps: active Na+ / K+ ionic pumps create an influx of K^+ ions and efflux of Na^+ ions, compensated by an additional efflux of K^+ ions though open K^+ ion channels. This leaves the intracellular milieu at a lower electric potential than the surrounding extracellular solution, and results in a negative transmembrane potential in the range of -40 to -90 mV, also called the resting membrane potential. The electrical potential difference across the cellular membrane is also called transmembrane potential V_m and is defined by the relation: $V_m = V_{in} - V_{out}$.

The information that propagates all the way from the dendrites to the synaptic terminal by means of an electrochemical signal, also called the action potential, is generated as follows: A stimulus, created by either the activation of membrane receptor proteins (chemical stimulus) or a charged electrode (electrical stimulus), initiates a depolarization (loss of charge difference) across the cell membrane. This generates an influx of Na+ ions into the cells through sodium channels which results in an increase of the membrane's resting potential. If the membrane potential increases to the point of reaching a threshold (varying between neurons and animal models), it causes voltage-gated ion channels to open, creating an additional influx of Na+ which depolarizes

the membrane rapidly. Then, an efflux of K^+ ions will hyperpolarize the membrane and participate in the restoration of the original ion concentrations found at rest through Na^+ potassium pumps present in the cell membrane.

Action potentials can be considered as "all-or-none" signals, even if differences exist in terms of action potential durations or amplitudes. In addition, the pioneering work of Hodgkin and Huxley in 1952 [15] facilitated our understanding of these phenomena by comparing the membrane as a capacitor separating ionic charges, and the ion channels as resistors allowing current flow.

1.2.3 Synapses

A synapse is a specialized structure found between two neurons that follows a developmental process, otherwise known as synaptogenesis. First, neurons will naturally extend their axons and dendrites with the guidance of extracellular cues [16,17]. Following a dynamic process that is regulated in response to both extrinsic cues and intrinsic molecular programs [18,19], two pre- and post-synaptic neurons will then form a synapse between their respective axon and dendrites [20,21]. This synapse can be of two forms: electrical or chemical (Figure 3).

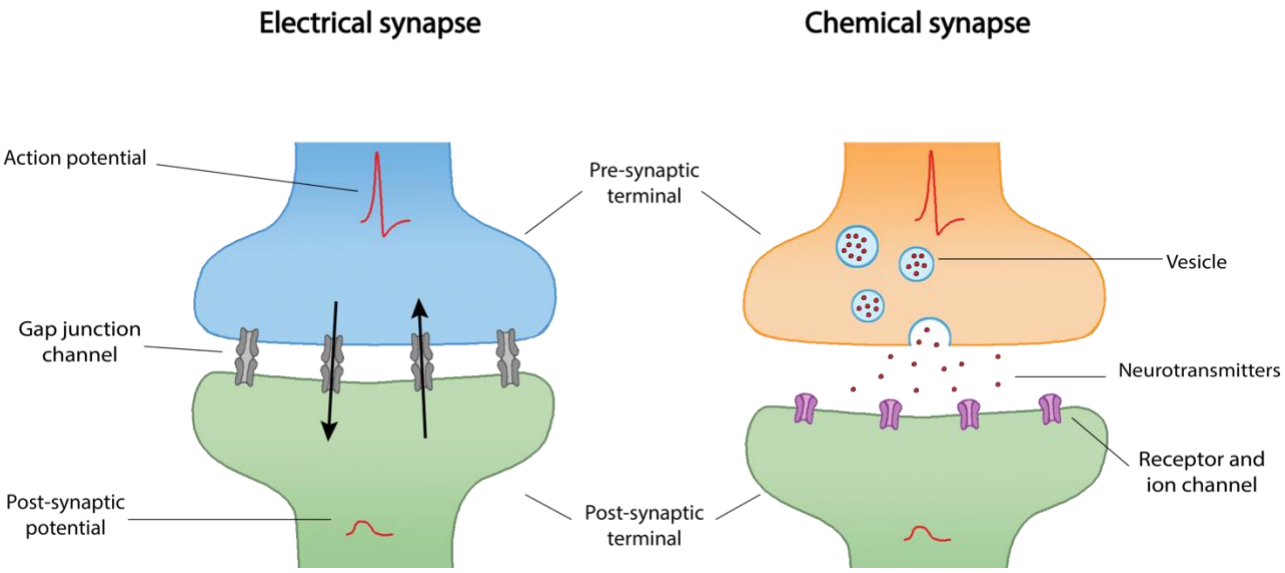

Figure 3: Schematic of two forms of synapses

Schematic of two forms of synapses: electrical (left) or chemical (right). The pre- and post-synaptic membranes of an electrical synapse are connected by gap junction channels that allow current to pass freely, and in both directions, from one neuron to the next. In comparison, the transfer of information in a chemical synapse requires the release of specific neurotransmitters. Following a depolarization of the pre-synaptic terminal, synaptic vesicles open at the membrane and release neurotransmitters into the synaptic cleft. These neurotransmitters then bind to receptors present in the post-synaptic membrane, resulting in a potential change in the post-synaptic neuron.

Electrical synapses are composed of gap junctions that permit a physical linkage between the pre- and post-synaptic interconnected membranes. Thus, the current (ion movements) can freely move between the cytoplasm of one cell to the other; so can a variety of substances including ATP (adenosine triphosphate) and other messengers. While they are considered the fastest mode of communication between neurons [17], they represent the minority of synapses in the mammalian nervous system. In comparison, a chemical synapse transduces an electrical signal generated by a pre-synaptic neuron into the release of chemical signals, also called neurotransmitters [17], which diffuse across a synaptic cleft (physical separation between the pre- and post-synaptic cells). These neurotransmitters then bind to specific receptors located on the post-synaptic membrane that extend into the postsynaptic cytoplasm, which will in turn open ion channels and result in a change of membrane potential of the receiving cell [22].

An additional confounding element of neuronal complexity is that the synapses are not hardwired, not is their efficacy static. Indeed, the synaptic transmission between paired neurons exhibits high degree of "plasticity", whereby the potential of a synapse can either be augmented (potentiated) or attenuated (depressed) depending on their surrounding environment and level of activation [23]. Interestingly, some of these changes can be transient (milliseconds to seconds, [24]), or persist for much longer periods of time (hours to days, [25]). Overall, the nature of these synapses establishes a very fundamental component called brain plasticity, that allows entire networks in the nervous system to appropriately respond to sensory inputs and ultimately help organisms adapt to changing environments. This capacity also forms the basis for short and long-term modulations that underlie learning and memory.

1.3 The importance of neural networks

Recent studies in the field of neuroscience underscore the fact that in order to understand even the simplest brain function, it is critical that we develop model systems with simple behaviors and well defined neural networks [26]. In both animals and humans, several approaches using specific electrographic oscillation frequency detection or imaging techniques have been developed to characterize existing neuronal networks [27]. These approaches are however facing several challenges, including: 1) Brain plasticity often involves cross-network interactions and any short or long-lasting changes caused by single or repetitive experiences can significantly affect how these networks operate; 2) Many neuronal network connectivity changes occur during developmental stage of organisms, and the age and maturation of the model studied always need to be considered [28].

Finally, it is important to recognize that neuroplastic changes can be either beneficial or harmful for an organism. For example, as described in the next sections, intense and repetitively occurring seizures can alter brain structures or even induce neurogenesis [29–31]. More precisely, structural reorganization of the mossy fiber in the hippocampus of patients suffering from epilepsy can contribute to even more repetitive and severe seizures [32–34], leaving some patients debilitated for life.

Only after understanding the basis of network formation and how these networks operate in normal conditions, will we be able to understand how alterations in the central nervous system

(CNS) result in neurological disorders. Unfortunately, this lack of knowledge precludes the development of needed therapies that can effectively target CNS neurodegeneration and alleviate human suffering from these disorders.

1.4 Dysfunctional networks and neurological disorders

A neurologic deficit can be defined as a functional abnormality of a body area due to interruption in the normal function of the nervous system (including the brain, spinal cord, or peripheral nerves). It affects patients suffering from neuro-degenerative diseases (such as Parkinson, Alzheimer, Epilepsy, stroke), mental and neurological disorders (depression, mood disorders, epilepsy), but also from trauma and injuries resulting in organ dysfunction and partial or total body paralysis. So far, pharmaceutical therapies have failed to develop effective treatments either to prevent or cure these deficits. Pharmaceuticals can at best slow down the progression of the disease but the required lifetime medication results in disastrous side effects (physical and cognitive deficits, behavioral disorders, social exclusion). Thus, because such neurologic deficits cannot be sufficiently treated, the resulting loss of function is often irreversible, leaving patients debilitated for life.

The cost of drugs required to manage these patients also remains a determining factor as many of them are extremely expensive and therefore not affordable for people with low income or without substantial health care coverage. Any solution for these problems would bring great relief to patients and positively impact their quality of life. Statistically, it is estimated that around 1.4 billion people in the world suffer from some form of neurologic deficit [35]. In the United States alone, the National Institute of Mental Health (NIMH) estimates that about 1 in 4 American adults

suffer from a diagnosable mental disorder in any given year, with nearly 6% suffering serious disabilities as a result [36]. Moreover, the rapidly growing global population coupled with the increasing life expectancy will considerably increase this number in the near future [36,37]. Consequently, the significant socio-economic cost related to neurologic deficits is expected to rise.

Understanding the fundamental cellular and molecular mechanisms underlying neuronal network function is indeed essential to solving neural disorders involving complex neural systems such as seen in epilepsy. In parallel, the sophistication and complexity of both micro and nano-technology fabrication processes have considerably impacted the development of biomedical devices such as neuro-electronic hybrids. In this regard, the neuroscience and computational fields have found tremendous support to explore novel biological and electrophysiological principles. To better manage and treat epilepsy, it is therefore imperative that we take advantage of these technological progresses to characterize neural activity from single cells to complex networks, and develop compounds offering better treatment efficacy.

1.5 Potential of neuro-technologies

The latest biotechnological developments now permit new engineering based solutions to help, in some cases, patients suffering from neurological disorders. Several research groups and emerging biotechnology industries have recently begun focusing on developing bionic devices with the intent of regaining lost neural function through hybrid technologies. Once a "fantasy" term derived from science fiction, it is clear that neuro-technology is an emerging field. Using direct communication pathways between the nervous system and an external electronic device, neural interfaces are directed at restoring and also augmenting human sensory-motor or cognitive functions [38]. After many years of animal experimentation, neuro-prosthetic devices started to be successfully implanted in humans in the mid-1980s. A variety of neuro-electronic interfaces currently available allow fundamental research aimed at understanding neurologic deficits. Moreover, a variety of these devices are currently being used clinically including the following: cochlear implants [39,40], deep brain stimulation (DBS) for Parkinson's disease and vagus nerve stimulation (VNS) for epilepsy [41–44], artificial retina [45,46], and heart stimulation [47,48]. Not only do they offer successful improvement in terms of individual health, but they also enable patients to reclaim some productivity and improved quality of life.

However, all these devices are aimed at stimulating or enhancing brain function, and not to record activity from it; thus, hindering any option to create a feedback loop system required for a beneficial bionic hybrid. Additionally, researchers are just starting to understand the longer term side effects of these electrical stimulations on brain rewiring and "collateral damage" to the

impacted circuits. Many of these chronic side effects impact the CNS leaving patients with additional symptoms and cognitive impairments including learning, memory and speech [49–51]. Finally, and maybe most importantly, they do not cure the patients, but rather help them cope with symptoms they experience.

Significant progress in understanding brain functions and neuro-degenerative diseases thus requires a much deeper understanding of the cellular and molecular mechanisms that underlie neural network function. Progress in this area has been hampered, in part, due to our limited capacity to record and monitor neural activity at a high-resolution from either single or multiple inter-connected neurons over an extended period of time. This inability to accurately monitor individual neurons and their synaptic activity precludes fundamental understanding of brain function under normal and various pathological conditions. Thus, research in neuroscience and electrophysiology requires the support of new tools that can help develop a better understanding of some of the fundamental building blocks forming neural networks: the neurons and their synapses.

While traditional intracellular recording electrodes and/or patch clamp electrodes remain the gold standard in the field of electrophysiology for recording and analyzing neuronal activity at a single cell level, these approaches are limited in that only a few neurons can be recorded concurrently (two being the maximum in most cases). In addition, these techniques are invasive and only allow short-term recordings (minutes to hours at best). To overcome these limitations, recent advances in Micro-Electrode Arrays (or Multi-Electrode Arrays - MEAs*)* now enable *in-vitro* extra-cellular recording (or stimulation) of a multitude of neurons simultaneously and over

several consecutive days [52–55]. From single cells to a variety of bio-electrically active tissues, MEAs are progressively changing the field of electrophysiology by offering new opportunities to investigate neural development, plasticity, and electrical interactions among cultured elements. The following sections describe the evolution of MEAs, their applications, and some of the limitations associated with them.

1.5.1 History and evolution MEAs

In 1972, more than 40 years ago, Thomas et al. [56] were the first to provide a description of multi-electrode arrays for recording spike behaviors from cultured neural cells and acute tissue. This approach was further developed by Gross et al. in 1977 [57,58], and the ability to stimulate was then added by Jobling et al. in 1980 [59]. However, to point out a main challenge that arose very early on, the amplitude of the recorded signals from cultured cells had a difference of a factor of about 1000 compared to intra-cellular techniques [60]. Jobling et al. reported in 1980 [59] the development of a Field-Effect Transistor (FET) on a silicon chip to successfully record activity from hippocampal slices. However, this work was not pursued (until later by Fromherz et al. in 1991 using large leech Retzius cells [61].

Later on, it was discovered that modified MEAs could be used in different experimental conditions to increase the probability of recording activity from vertebrate or invertebrate neurons [62]. Researchers also expanded their field of studies by using MEAs to record activity from the

intact brain slices of mice [63,64] or the retina [65]. By the beginning of the 21st century, the focus gradually switched from trying to record extracellular activity with the same resolution as intracellular electrodes (which had very limited success [66,67]) by using MEAs for studying plasticity of cortical networks, in which typically every electrode of the MEA can record activity simultaneously [68]. To allow this, two factors needed to be improved: 1) the maintenance of a biocompatible extra-cellular milieu required for the cells to survive, and 2) the ability to perform stable recording by maintaining a continuous and prolonged contact between the electrodes and the neurons. While Potter et al. [69] successfully demonstrated the ability to record neural network activity for extended periods of time (> 1 month), the Fromherz group investigated the fabrication of a picket fence around each electrode to hold neurons in place and study small interconnected networks from snails [70]. More recently, research groups around the world have attempted to adapt the morphology of micro-electrodes, creating three-dimensional structures, but with limited success, as described in the next sub-sections.

In summary, while the research community witnessed a variety of different explorations and new opportunities offered by MEAs in the last four decades, additional challenges still needed to be solved, and technologies developed, in order to further our knowledge of neural activity, from single cells to large complex networks [71,72].

1.5.2 Application of MEAs

Recent breakthroughs in micro- and nano-scale fabrication processes have advanced the development of neuro-electronic hybrid technology and now allow many major types of traditional electrophysiology experiments to be conducted. From single cells to large complex networks, MEAs offer numerous opportunities to further understand intricacies of brain functions like drug screenings [73], or even stimulating brain regions when positioned on a flexible membrane (flex-MEA [74]) and implanted *in-vivo*. However, MEAs are not always the best options depending on application and experimental goals, and it is therefore important to consider both their strengths and weaknesses. Their major assets are:

1. The capability to collect data from multiple electrode sites simultaneously, thus allowing the mapping of cultured neurons and acute brain slices;
2. The ability to perform longer term continuous recording at a single cell level compared to traditional intracellular techniques;
3. The possibility among an array of electrodes to quickly and locally switch stimulation and recording.

In the field of neuro-engineering, several research groups have tried, with limited success, to increase the signal quality or the electrical coupling coefficient, recorded between the micro-electrodes on the MEAs and cultured neurons. As a result, several reported factors [75–78] have been identified as crucial aspects associated with attaining high signal-to-noise ratios: 1/ increased

sealing resistance by improving the adhesion between the cells and the electrodes; 2/ decreased input impedance of the di-electric electrodes; 3/ the neuronal current magnitude, itself being a function of the cell size, ion channels concentration and location. Because the electrode impedance is mainly a result of the materials used, research focus is often targeted on increasing the sealing resistance (Rseal) by modifying the shape of the electrodes in order to increase the signal-to-noise ratio (SNR).

Based on the different factors cited above, neuronal activity recording and stimulating devices have been prototyped to enable better cellular exploration [79–82]. For example, a multitude of penetrating and non-penetrating nanopillar electrodes [77,83,84], carbon nanotube electrodes [85,86], mushroom-shaped protruding micro-electrodes[87], patch-clamp devices [88], traditional 8x8 micro-electrode arrays (MEAs) etc. have been used to record neuronal activities. Among such devices are three-dimensional and planar micro-electrodes, each with their respective advantages and disadvantages.

1.5.3 Limitations of MEAs and opportunities for development

Bearing these advantages in mind, our understanding of neuronal network phenomena and associated electrophysiological processes is still in its infancy. This is, in large, due to technical limitations (i.e. unstable prolonged recordings and low signal-to-noise ratio) that still need to be solved.

Indeed, three-dimensional electrodes generally monitor activity over a limited period of time (maximum 2 days using mushroom-shape electrodes [75]) due to the intrusive nature of these three-dimensional structures that compromise neuronal cell membrane and network integrity, thereby disrupting their connectivity and cellular viability. Indeed, neuronal adhesion and firm contact with the recording site are prerequisites for longer-term sustainable recordings. Neurons grown in culture tend to pull away from the recording sites due to physical tension applied by either their elongating growth cones or neurites. This, in turn, results in the neurons losing contact with the recording site, reducing the stability of the recorded signal. Several approaches have been used to restrain this natural movement; many of which involve using three-dimensional micro-structures to restrain neurons to their recording sites [70]. However, these approaches have a limited success rate (e.g. spike and mushroom electrodes) as neurons eventually experience membrane rupture, cytosol leakage and cell death within a short period of time [70,75].

In addition, recordings from MEAs are always obtained at a much lower signal resolution compared to their intracellular electrode counterparts. This can be attributed to many different factors, including the following: the micro-electrode materials, the interfacing between a cell and the surface of the micro-electrode, or the presence of glia cells when recording from mammalian cultures that reduces the probability to record activity. More specifically, they are not adapted for the detection and measurement of subthreshold synaptic current. This is a serious limitation that hampers studies of neural network formation, plasticity, and dysfunction, thus motivating the development of new approaches.

Overall, MEAs are still not designed to investigate and characterize individual neurons and neural networks at a resolution high enough to help understand the causes of various neuro-degenerative and network related pathological conditions. Three-dimensional electrodes tend to allow for high fidelity recordings with the drawback being that they can only do so over a short-term period (hours to days). On the other hand, planar micro-electrodes permit longer-term recordings (weeks to months), at the expense of a low signal resolution [75]. Ideally, combining both advantages (i.e. high fidelity and long-term recordings) could offer new opportunities to monitor and record subtler aspects of neural brain activity.

1.6 Specific Aims

Taking into consideration these limitations, and the urgent need to develop new tools that can perform long-term recordings at a higher signal-to-noise resolution than commercially available devices, I decided to focus on the design and fabrication of MEAs that could give researchers a better understanding of brain functions and dysfunction. Thus, the **main objective of my PhD research was to design and develop novel micro-electrodes that may allow high fidelity neural recording over extended periods of time, from single cells to complex networks found *in-vivo*.** I had three specific aims:

Specific aim #1: To develop and validate computationally a first in-house novel MEA (SS-MEA) for long-term high fidelity neural activity recordings, non-invasively, from single and paired cells from invertebrates (chapter 3).

Specific aim #2: To extend the findings from aim #1 and develop a second MEA (MW-Chip) capable of recording network activity from mammalian cortical cultured cells (chapter 4).

Specific aim #3: To develop a novel three-dimensional MEA (NT-Chip) that will enable activity recordings from healthy neural networks located inside acute hippocampal brain slices from mice (chapter 5).

Chapter 2: Materials and Methods

Whereas more specific details of various protocols and fabrication techniques are given in the relevant sections of the thesis, this chapter provides an overview of methodologies that have been used throughout.

2.1 Animal models and specific care

Three animal models were used throughout my research to meet the experimental needs of the desired objectives. Initially, the freshwater snail *Lymnaea stagnalis* was used as a model organism to study neural activity at a single cell level in order to optimize and customize the planar nano-edge micro-electrodes (chapter 3). I then moved to mammalian models using both cultured cortical and hippocampal cells from P0-P1 Sprague Dawley rats (chapter 4), and wild-type (P35) control mice to perform brain slice recording using an array of three-dimensional gold micro-electrodes (chapter 5). A general description of all models used herein is presented below. All experiments and procedures presented here that involved animals were performed in accordance with the standard regulations established by the Canadian Council on Animal Care. All animal protocols were approved by the Ethic Committee of the University of Calgary.

2.1.1 Freshwater snail Lymnaea stagnalis model

To overcome the challenges posed by the complexity of the mammalian neural network, the Syed lab has been using the freshwater snail *Lymnaea stagnalis* (Gastropod, Pulmonata, Basommatophora, Lymnaeidae) (Figure 4) as a model system to investigate fundamental neuronal properties, synaptogenesis (formation of synapses) and network formations. This invertebrate model provides larger neurons (30 – 80 µm diameter, compared to 6 – 25 µm for mammalians) that are both structurally and functionally well characterized. Moreover, single neurons can be manipulated with great ease [89], allowing their precise juxtaposition on standard plastic/glass culture dishes and MEAs to be precise.

Figure 4: Lymnaea stagnalis

A photography showing *Lymnaea stagnalis* - a freshwater pulmonate snail.

2.1.1.1 Animal Rearing

The stocks of freshwater snail *Lymnaea stagnalis were* derived from an inbred population obtained from the Free University of Amsterdam (the Netherlands). They were raised and maintained in Calgary for several decades. Snails were maintained at room temperature (20-21°C) in a well-aerated aquarium with filtered and dechlorinated tap water. The animals were fed on a regular basis (twice a week on average) with fresh romaine lettuce and once a week with Purina Trout Chow® (Purina Mills, MO, USA).

2.1.1.2 Dissection

Neurons were isolated and cultured as described in Syed, et al [90]. Specifically, their removal from the aquarium, 1 to 2 months old animals, with a shell length of 15-20 mm, were carefully de-shelled with a pair of blunt forceps. Caution was taken to inflict minimal damages to the animal tissue during this step. They were then anesthetized for 10 minutes in a saline solution (all in mM: 51.3 NaCl, 1.7 KCl, 4.0 $CaCl_2$,1.5 $MgCl_2$) mixed with Listerine TM (ethanol, 21.9%; methanol, 0.042%), the final concentration of Listerine being 10%. After 10 minutes, animals were transferred to a culture Sylgard dish containing saline solution, and pinned down appropriately to facilitate the dissection using insect pins. A dorsal midline incision was made on the animal's anterior body using fine forceps and dissection scissors (Fine Science Tools, #5, BC, Canada). The central ring ganglia were then exposed by spreading and pinning the skin and other organs further with the aid of insect spins. After severing the nerves and other connective tissues surrounding the

brain area, the central ring ganglia were extracted and isolated in a saline solution containing antibiotic (gentamicin, 50 μg/mL). Central ring ganglia comprising the brain (Figure 5, a) were then washed three times in a gentamicin saline solution (each 10 minutes' wash).

a)

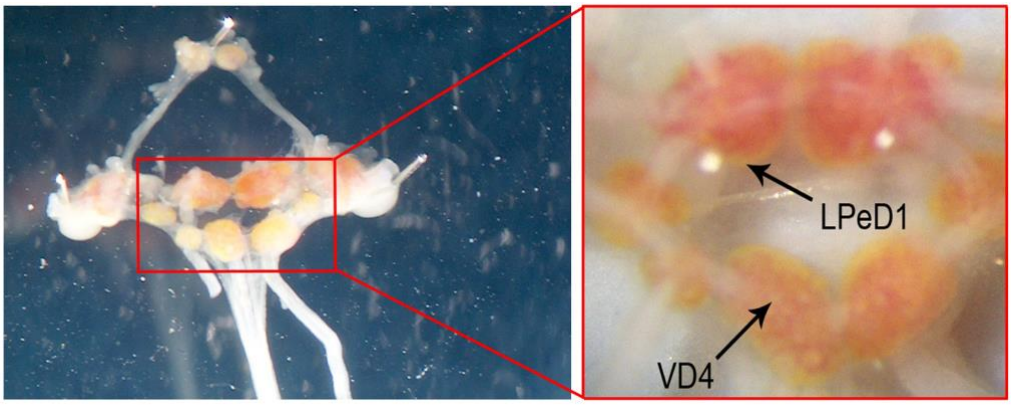

b)

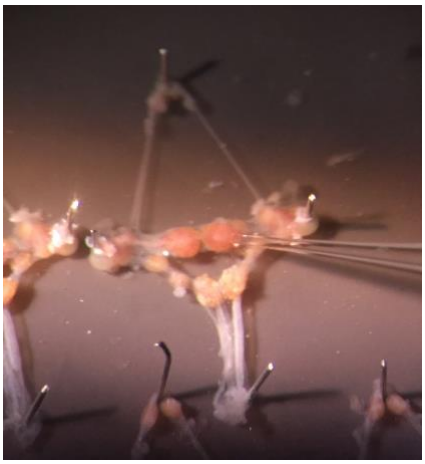

Figure 5: Central ring ganglia from Lymnaea stagnalis

Central ring ganglia from *Lymnaea stagnalis. a)* The central ring ganglia were extracted from the animal, and maintained in normal saline solution. The cerebral ring ganglia was pinned onto a Sylgard dish and specific neurons (e.g. visceral dorsal 4, VD4, and left pedal dorsal 1, LPeD1) could be identified under a dissection microscope. b) After the brains were pinned down in the culture dish, individually identified neurons were isolated by applying a gentle suction applied through a fire-polished glass pipette. The isolated neurons could then be individually juxtaposed on an MEA micro-electrode.

2.1.1.3 Culture

Following their isolation, brains were treated with trypsin enzymes for 20 minutes (2 mg/mL; T-4665; Sigma-Aldrich, St Louis, MO, USA) and with trypsin inhibitor for another 15 min (2 mg/mL; T-9003; Sigma-Aldrich, St Louis, MO, USA). During both treatment conditions, dishes were gently agitated every 5 minutes to facilitate the enzymatic softening of the tissue. Following these two treatments, brains were pinned dorsal side up onto a smaller Sylgard culture dish containing a high osmolality Defined Media (DM, 180-195 mOsm). Fine forceps were then used to manually remove both the outer and the inner sheaths of the ganglia, exposing some of the neurons of interests. Depending on the experimental needs, specific *Lymnaea* neurons were isolated by applying a gentle suction through a fire-polished and Sigmacote® treated glass pipette (SL2; Sigma-Aldrich, St Louis, MO, USA) (Figure 5, b). Neurons were then transferred to pre-defined culture conditions with the help of fire-polished glass pipette attached to a Gilmont syringe. A gentle suction was applied to extract neurons and the isolated somata and their axons were then gently juxtaposed against the surface of the devices containing the micro-electrodes (e.g. planar micro-electrodes recording sites) [91].

The ability to select each time the same neuron from any *Lymnaea* brain provided incredible consistency in our experiments. For my own experimental needs, I mainly used left pedal dorsal 1 (LPeD1), ventral dorsal 4 (VD4), and right pedal dorsal 1 (RPeD1) which have been previously well characterized [90–92].

2.1.1.4 Media

For all experiments involving *Lymnaea*, neurons were cultured either in Defined Media (DM – does not contain any trophic factors) or Conditioned Media (CM – contains brain derived trophic molecules). While DM (trophic factors-free, 50% L-15 medium with 20 μg/mL of gentamicin and inorganic salts at mM: 40 NaCl, 1.7 KCl, 4.1 $CaCl_2$, 1.5 $MgCl_2$ and 10 HEPES at pH 7.9) lacks trophic factors that are naturally present in the animal, and required to promote neural growth and synaptogenesis also seen *in-vivo* [93]; CM in contrast, contains these trophic factors which are required for growth and synapse formation [91].

Specifically, for a total of 6 ml of CM, 12 isolated brains from 3-5 months old (shell length 20-30 mm) animals were transferred through a series of ten washing containing gentamicin saline for 10 minutes each. This step was necessary to "wash" the brains and minimize bacterial contamination. Every 5 minutes, plastic dishes (3001, Sigma-Aldrich, St Louis, MO, USA) were genteelly agitated. After the last "wash", brains were transferred to an autoclaved Sigmacote® (Sigma-Aldrich, St Louis, MO, USA) treated glass petri dish containing 6 mL of DM and placed in a humidified incubator at room temperature. After 3 days, the CM was collected into 2 mL tubes and kept frozen at – 20 °C until used. This process could be repeated two more times by increasing the incubation time to 5 and 7 days respectively, and therefore collecting an additional 12 mL of CM.

2.1.2 Sprague Dawley rat model

To meet the experimental needs in chapter 4, mammalian neurons from P0-P1 Sprague Dawley rat pups were obtained. Neurons from young animals were harvested because of their naturally occurring spontaneous activity that has been shown to be more prominent than in cells from mature and fully developed adult rats [94].

2.1.2.1 Rearing condition

All animal procedures were approved by the University of Calgary's institutional animal use and care committee and in accordance with the standards established by the Canadian Council on Animal Care. Female pregnant rats were given food and water ad libitum and kept on a 12-hour light/dark cycle to mimic day patterns. The day that the mother gave birth (P0) or on the following day (P1), pups were sacrificed and cortical and hippocampal neurons harvested.

2.1.2.2 Dissection

The rat pups (P0 or P1) were anesthetized on ice, sacrificed and an incision was made behind the skull. The skull was then peeled off to expose the brain which allowed the dissection of the cortex and hippocampus. Both cortex and hippocampi were dissected in HBSS containing 10 mM HEPES (310 mOsm, pH 7.2), and treated with an enzyme mixture for 20 minutes at 37 °C containing papain (50 U/mL), 150 mM $CaCl_2$, 100 µM L-cysteine, and 500 µM EDTA in

neurobasal medium (NBM). Tissue was then washed three times with NBM that was supplemented with 4% FBS, 2% B27, 1% penicillin-streptomycin and 1% L-Glutamine.

2.1.2.3 Cell dissociation and culture media

Neurons from the cortex and hippocampus were dissociated separately by trituration with polished glass Pasteur pipettes, and plated at a high density onto clean, sterilized and coated Multi-Electrode Arrays (see MEA preparation protocol below) containing supplemented NBM as above. The following day, the culture media was changed to NBM supplemented with 2% B27, 1% penicillin-streptomycin and 1% L-Glutamine, i.e. as described above but without the FBS; this was meant to limit glial cells proliferation. Neurons were maintained in an incubator at 37 °C with 5% CO_2 and approximately 50% of the culture media was changed every 2-3 days.

2.1.3 Wild-type (P35) mice model

In chapter 5, I used brain hippocampal tissue from control mice that were provided by Dr. Gavrilovici, in collaboration with Dr. Rho's laboratory at the Alberta Children's Hospital Research Institute, University of Calgary, to investigate the recording capability of our three-dimensional micro-electrodes.

2.1.3.1 Rearing condition

C3HeB/FeJ mice were purchased from Jackson Laboratories (Bar Harbor, ME, U.S.A.), and the colony was maintained in the Animal Resource Facility at the Cumming School of Medicine, University of Calgary. Mice were given food and water ad libitum and kept on a 12-hour light/dark cycle. Wild type (+/+) mice at P35 (postnatal day 35) were used in this study and all procedures involving animals were conducted in accordance with the National Institutes of Health guidelines and the EU Directive 2010/63/EU.

2.1.3.2 Dissection, brain slicing and media

On the day of the experiment, animals were anesthetized (Ketamine–Dormitor mixture; 0.1 ml/100 g; i.p.), sacrificed, and their brains were removed and quickly placed into ice cold, oxygenated (95% O_2 / 5% CO_2) artificial cerebrospinal fluid (aCSF; all in mM: 86 NaCl, 3 KCl, 4 $MgCl_2$, 1 NaH_2PO_4, 75 sucrose, 25 glucose, 1 $CaCl_2$, and 25 $NaHCO_3$). Coronal slices (300 to 500 μm; 1.5 to − 0.3 mm relative to Bregma) containing the hippocampus were prepared using a Leica VT 1000S vibratome [95–97]. These slices were then placed in aCSF containing (in mM) 124 NaCl, 4.5 KCl, 1 $MgCl_2$, 10 glucose, 1 $CaCl_2$, and 26 $NaHCO_3$ at 32°C for 30 min to recover, and remained afterwards in a aCSF bath at room temperature (22-24°C) until used [98]. All solutions used during this process were maintained at pH 7.4 and bubbled with 5% CO_2 / 95% O_2 (carbogen).

2.2 MEA Fabrication

During my PhD research, I designed, developed and participated in the fabrication of several MEAs that are presented in the next chapters. More specifically, three newly developed MEAs were particularly effective in answering the specific experimental questions: the Soma-Soma MEA with nano-edge micro-electrodes (chapter 3), the Multi-well MEA (chapter 4), and the three-dimensional gold micro-electrodes MEA (chapter 5).

All MEAs designed in this thesis shared a common photolithography fabrication process (Figure 6). Specific differences are detailed in the relevant chapters, but the core fabrication technology is described here to avoid repetition. Briefly, all our custom designed MEAs were fabricated using a two-mask photolithography process on 49x49mm glass, 1mm thick. Gold (200 to 600nm thick) was deposited on a chrome adhesion layer (10 to 50 nm thick) using a Physical Vapor Deposition technique (PVD) – sputter deposition (CMS-18, Kurt K Lesker Co., Pennsylvania, USA). HPR504 (Fujifilm, USA) was then spin-coated (WS-650-23B, Laurell Technologies Corp., North Wales, Pennsylvania, USA) on the 49 x 49 mm substrate and soft-baked. To create the desired patterns of the MEAs (wires and electrodes), several photomasks were used. These masks block light in specific areas and allow images to be produced when placed in an exposure system (i.e. mask aligner). Following exposition to UV light with the aid of a mask aligner (MA/BA 6, Suss Microtec, Corona, California, USA), we used in the following order, Microposit developer 354 (Dow Chemical Corp., Midland, Michigan, US), gold etchant (potassium Iodide mixed in house from solid Iodide and Potassium Iodide crystals, VWR Canada)

and chrome etchant (Acetone, IPA - VWR Canada) to develop the electrodes and traces patterns. An epoxy based photoresist layer – SU8 2000.5 (SU8 Developer, Remover PG - MicroChem Corp, Newton, MA, USA) – was then deposited to provide an insulation layer over the electrode traces. Openings in the SU8 photoresist layer were left usually around the main electrode arrays that remained bare of insulation for stimulation/recording purposes.

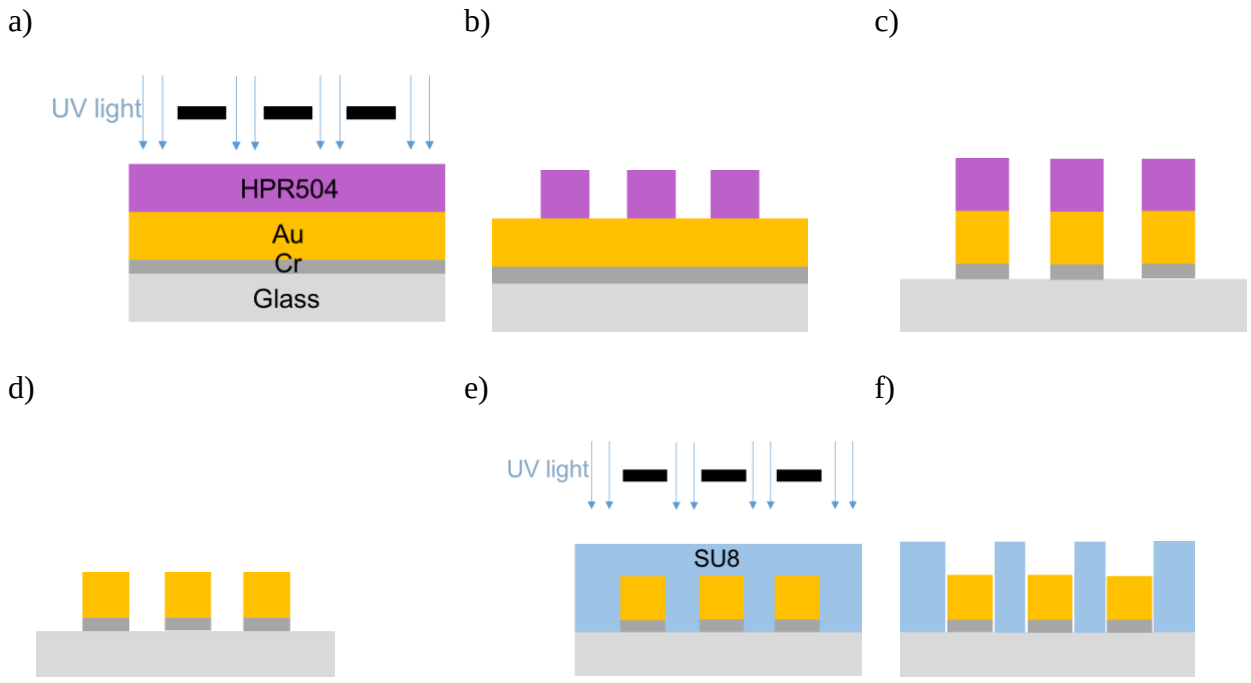
a)
b)
c)
UV light
HPR504
Au
Cr
Glass
d)
e)
f)
UV light
SU8

Figure 6: Schematic of the process followed to fabricate the MEAs

Schematic of the basic underlying process followed to fabricate the MEAs (dimensions not on scale). a) Following the deposition of chrome, gold and HPR504 (positive photoresist), a mask was used to locally expose the photoresist to UV light. b) Microposit developer 354 allowed the soluble HPR504 to be removed. c) Gold and chrome etchant were used to develop the micro-electrode and trace patterns. d) The remaining HPR504 was then removed with acetone. e) SU8 was deposited to provide an insulation layer over the electrode traces, and a second mask was used to locally expose SU8 to UV light. f) Finally, remover PG was used to remove the soluble SU8. The remaining SU8 was then cured to give its mechanical properties.

When using fabrication equipment such as the spin coater or the mask aligner, or when undergoing etching or baking steps, certain variables like the UV exposure time, spin acceleration and final speed, baking time, etc. were adapted as necessary to permit the fabrication of desired electrodes and wire structures. Sizes and intervals between electrodes were also adjusted according to experimental needs using different in-house designed photomasks. Again, more information regarding each fabricated MEAs is available in chapter 3, 4 and 5.

Most MEAs presented in this thesis were fabricated jointly in collaboration with Dr. Dalton at the Advanced Micro/nanosystems Integration Facility (AMIF - University of Calgary). However, while all masks used for MEAs fabrication were designed at the University of Calgary using Autocad (Autodesk, CA, USA), the masks production was out-sourced (MicroFIT Co. Ltd., South Korea or Photoscience Inc., California, USA).

Following the fabrication step, every MEAs as inspected under an optical microscope for any defects, and a quality control was conducted using atomic force microscopy (AFM, NanoWizard 4 BioScience, JPK Instruments, Germany) and a surface profilometer (KLA-Tencor, P6, CA, USA).

2.3 MEA preparation

After fabrication, and before any cells were cultured, all MEAs underwent a washing, cleaning, sterilization and coating process. While the coating processes differed depending on the animal models used for our experiments, every other process remained the same. A brief description is provided below.

2.3.1 Washing, cleaning and sterilization processed

After inspection for any defects or debris under an optical microscope, MEAs were rinsed extensively (30 to 50 times) with filtered, autoclaved distilled water. This ensured complete removal of any fabrication residues deemed harmful for cell culture. Also, following every experiment, MEAs were washed in a similar way to remove cell residues and previous coatings. To completely remove any cell residues, MEAs followed a cleaning procedure using a 10% tergazyme solution. Again, MEAs were extensively rinsed with filtered, autoclaved distilled water to ensure complete removal of any enzymatic solution that would be considered harmful to the cells. On rare occasions, we used diluted household bleach (5.25% Sodium Hypochlorite diluted with a ratio of 1:500) to remove residues or potential fungus. MEAs were then sterilized with 70% ethanol for 30 minutes and rinsed 3 times with filtered autoclaved distilled water.

2.3.2 Coating procedure for Lymnaea Stagnalis snail neurons

1 to 2 mL of 1:1 Poly-L-Lysine (PLL, 7.7 mM, Sigma-Aldrich, St Louis, MO, USA) was added inside the MEA chambers to facilitate cellular adhesion and growth, and allowed to rest for 30 minutes at room temperature. Once removed with vacuum, the MEA were rinsed with a combination of filtered autoclaved distilled water and filtered saline autoclaved water (all in mM: 51.3 NaCl, 1.7 KCl, 4.0 $CaCl_2$,1.5 $MgCl_2$), and left to air dry for 20 minutes. MEAs were then sealed in plastic dishes with parafilm and stored at low temperature (4-6 °C), or used the same day. I preferred to use MEAs within 1 to 2 weeks following the coating procedure as the Poly-L-lysine seems to degrade thus losing its adhesive properties.

2.3.3 Coating procedure for Sprague Dawley rat neurons

The coating procedure for Sprague Dawley rat neurons started 2 days before the experiments. Briefly, MEAs were coated with Poly-D-Lysin (PDL, 30 µg/mL Sigma-Aldrich, St Louis, MO, USA) and Laminin (2 µg/mL, Sigma-Aldrich, St Louis, MO, USA) in a two steps process. First, PDL was diluted in Phosphate-Buffered Saline (PBS, all in mg/mL: 12.7 Na_2HPO_4, 2.65 NaH_2PO_4,$2H_2O$, 85 NaCl) and the MEA chambers were filled with 1 ml of this solution. MEAs were gently agitated to ensure even coating of the surface and placed in an incubator (37°C, 5% CO_2) for 24 hours. The following day, the PDL/PBS solution was removed and replaced with 1mL of Laminin/PBS. Similarly, MEAs were gently shaken and placed in the incubator for 24 hours.

Only 15 to 30 minutes before neuronal plating, the Laminin/PBS solution was removed and the surface was rinsed with PBS and filtered, autoclaved distilled water.

2.4 Electrophysiology recording equipment

Throughout my PhD research, both intracellular and extracellular recording techniques were used depending on the experimental requirements. More specifically, conventional intracellular recordings were only used for the invertebrate neurons to record cellular membrane potentials, neuronal activity, and pre/post-synaptic potentials.

2.4.1 Intracellular recording

Using a vertical pipette puller (David Kopf Instruments, USA, 700C), glass microelectrodes (1.5 mm internal 31 diameter; World Precision Instruments, Sarasota, FL, USA) were pulled with resistances in the range of 20-60 MΩ, filled with a saturated solution of K_2SO_4, mounted on micromanipulator (MPC-200, paired with ROE-200 and MP285 motorized drivers; Sutter Instrument, CA, USA) and connected to an amplifier (Digidata 1322A or Digidata 1440A; MDS Inc, Toronto, Canada). A silver wire (99%) was positioned into the cell culture solution as a reference ground electrode. Before impaling the cells, an upright microscope (Olympus BX61WI; Olympus Canada, Ontario, Canada) was used to visualize neurons and the electrodes. Manipulation of the glass microelectrodes to bring them close to the neurons enabled the cells (single or paired configuration) of interest to be impaled. DC Current was injected into the somata using an amplifier (Dual Channel Intracellular Recording Amplifier IR-283; Cygnus Technology, Delaware Water Gap, PA, USA) to record and stimulate the cells, and the amplified electrical signal was then digitized and visualized through Axoscope 9.0 (MDS Inc, Toronto, Canada).

2.4.2 Extracellular recording

Once properly coated, both in-house and commercially available MEAs were used to record neuronal activity extracellularly from cells in direct contact with the micro-electrodes. Neuronal activity was recorded by an MEA amplifier and PCI acquisition card (MEA1060; Multichannel Systems, Reutlingen, Germany) and visualization was made using the software MC_Rack and MEA_Select (Multichannel Systems, Reutlingen, Germany). For experiments involving mammalian models only, software TCX-Control was used to control the temperature regulator and heated cannula (respectively TC02 and PH01, Multichannel Systems, Reutlingen, Germany). On specific occasions, stimulations could be induced by STG 4004 stimulator controlled by the software MC_Stimulus II (both from Multichannel Systems, Reutlingen, Germany).

The recordings were compiled and processed using MC_DataTool and MC_Rack software respectively. More precisely, a spike detector present in MC_Rack allowed the extraction of timestamp associated with each individual action potential. These outputs were then imported and processed by Excel (Microsoft; Redmond, WA, USA) to better analyze activity frequency or the time elapsed between two adjacent action potentials, known as interspike intervals (ISI).

2.5 Computational simulation and statistical analysis

Computational simulation was performed using the built in *Electric Currents* module in COMSOL Multiphysics (COMSOL Inc., Burlington MA), a software based on finite element analysis. Statistical analysis and data visualization to characterize activity from intra and extra-cellular recordings were performed using the following software: SPSS (IBM, Armonk, NY, USA), Excel Microsoft (Microsoft, Redmond, WA, USA) and Matlab (The Mathwork Inc., Natick, MA, USA).

Chapter 3: Development of a bio-mimicking planar micro-electrodes with nano-edges

This chapter comprises sections published in the following manuscripts, patent or presented at conferences:

Manuscripts:

- **Wijdenes P.**, Ali H., Armstrong R., Zaidi W., Dalton C., Syed N.I. *A novel bio-mimicking, planar nano-edge micro-electrode enables enhanced long-term neural recording*. Scientific Reports (Nature Publishing Group), **6**, 34553 (2016).

- **Wijdenes P.**, Luk C.C., Lee A.J., Zaidi W., Leung A., Wong N. and Syed N.I. *Trophic Factor Induced Activity Patterns Regulate the Expression of Excitatory Acetylcholine Receptors in Lymnaea Neurons*. Scientific Reports (Nature Publishing Group), **5**, 9523 (2015).

- Ghazavi A., Westwick D., Xu F., **Wijdenes. P**, Syed N., Dalton C. *Effect of planar micro-electrode geometry on neuron stimulation: finite element modeling and experimental validation of the efficient electrode shape.* Journal of Neuroscience Methods. **248**, 51-8 (2015).

Conferences:

- **Wijdenes P.**, Ali H., Syed N.I., Dalton C. *Simulations of micro-electrode and neuron interfaces enable long-term and high fidelity recordings*. COMSOL Conference, Boston, USA - Poster presentation (2016).

- **Wijdenes P**., Dalton C., Armstrong R., Zaidi W., Syed N.I. *Development of a planar micro-electrode array offering long-term, high-resolution neuronal recordings*. IFMBE Proceeding. **51**, 1173-1176, Toronto, Canada - Podium presentation (2015).

- **Wijdenes P.**, Dalton C., Armstrong R., Zaidi W., Syed N.I. *Long-term neuronal recording and analysis of patterned activity using multi-electrode arrays*. Biomedical Engineering Society, Tampa, USA - Poster presentation (2015).

- **Wijdenes P.**, Luk C., Dalton C., Armstrong R., Lee A., Syed N.I. *A novel microchip with high temporal resolution for detecting synaptic potentials*. Alberta Biomedical Engineering Conference, Banff, Canada - Podium presentation (2013).

Patent:

- **Wijdenes P.**, Dalton C., Syed N.I. *Novel planar micro-electrodes with unique morphological structure for enhanced neural recording*. US 62277803 (2015). Filled application, PCT Status

3.1 Introduction

To overcome some of the challenges posed by existing MEAs and improve upon their fundamental characteristics required to increase the strength of the recorded signals, I first used them to record extra-cellular activity from the *Lymnaea* model specifically. As explained previously in chapter 2, the advantage of this invertebrate system is that it allows recapitulation of synaptic and network phenomenon that is not always attainable using mammalian preparations. In addition, both the expertise and equipment needed to study intracellular neural activity from cultured single and paired *Lymnaea* neurons was well established in Dr. Syed's lab.

However, based on the information presented in chapter 1, it became apparent to me that commercially available MEAs are mostly dictated for market needs and therefore mainly designed for mammalian neurons [79,99]. Again, these devices do not permit high resolution recording (only < 1mV [75]), therefore limiting the ability to record from invertebrate neurons. When used with the *Lymnaea* model, most of its neurons move away from their MEA recording electrode sites 1 to 2 days after plating, thus preventing us from conducting longer-term experiments [70]. Finally, commercially available MEAs are not specifically designed to record neural activity from pre- and post-synaptic cells cultured in a soma-soma configuration, this being a possibility [89,91,92] that I wished to exploit further. To achieve my goals, I therefore designed and fabricated my own novel MEA for *in-vitro* neural recording, specifically a Soma-Soma MEA with nano-edges (SS-MEA). I hypothesized that this new device would allow better recording resolution than standard commercialized MEAs and maintain long-term recordings (> 2 weeks).

This chapter presents the main results associated with the design and development of this new device, which also served to help establish the fabrication standards used for all other devices presented in the following chapters. The section bellow describes the order in which my endeavors perused:

- The fabrication process associated with the initial SS-MEA;
- The biocompatibility testing of the SS-MEA;
- The development of a nano-edge over the micro-electrodes that was used to increase the signal resolution;
- The recorded neural activity and comparison with other existing devices;
- A demonstration of the different opportunities made possible with this new device, both in terms of neural activity pattern recognition and sub-threshold signaling detection;
- And finally, a computational simulation developed to better model the theory behind the nano-edge structure.

3.2 Fabrication of the SS-MEAs

As described in chapter 2 and in previous publications [89], the SS-MEA followed a standard photolithographic fabrication process where an electrode design was patterned on top of a substrate (49mm x 49mm soda lime glass, 1mm thick, figure 7, c). Rectangular pads located on the edge of the substrate allowed for connecting the SS-MEA to a recording system and each individual pad was then wired to a micro-electrode present at the center of the MEA. A glass ring was attached at the center of the SS-MEA using PDMS (polydimethylsiloxane), forming the "recording chamber" where cells could be cultured (Figure 7, a). At the center of the MEA, the shapes, sizes (30 µm), and disposition of the micro-electrodes were adjusted to form "multi-electrodes units" that would allow both pre- and post-synaptic cells to be plated (Figure 7, b). Groups of 4 and 6 electrodes were designed to accommodate different cell sizes.

a)

b)

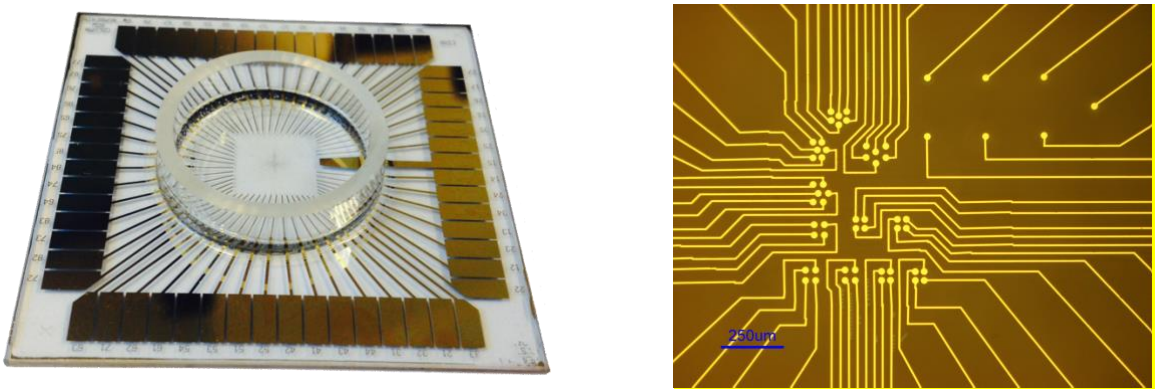

c)

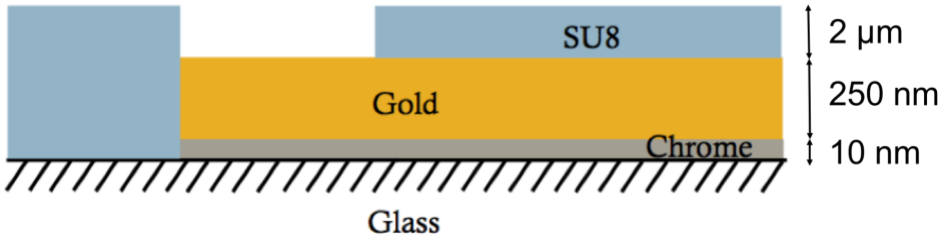

Figure 7: SS-MEA used for extracellular recording

SS-MEA used for extracellular recording [89]. a) macro view and b) microscope capture showing the electrode connecting traces terminating in groups of either 4 or 6 circular micro-electrodes, all 30 µm in diameter. The central electrode pattern is reconfigurable. c) Schematic of the glass, metals and photoresist layers created during the fabrication process.

3.3 Assessing the biocompatibility of our in-house fabricated MEAs

Biocompatibility can be defined as the quality of a system and its composed elements to be compatible with biological, living tissue or a living system, thus being non-toxic or non-injurious. For the new biomedical devices reported here, the materials were tested for biocompatibility to ensure that cells developed correctly, and that all experiments and data collected are indeed from biologically viable cells.

While most of the materials used during the fabrication process have been previously reported as biocompatible in the literature [79,89], it was important to determine if there was any remaining potential toxicity when neurons come in contact with the materials/coatings. Indeed, over an extended time period, individual materials used to create a device may be biocompatible in part, but the combination of various materials needed to be considered as they may cause a toxic reaction when present in the same environment. It was therefore essential to ensure that our fabrication process did not create an injurious environment to the cells.

To assess the biocompatibility of the new MEAs, three key aspects were considered; whether the neurons: a) exhibited neurite out-growth, c) maintained their intrinsic membrane properties, and d) developed synaptic connections.

3.3.1 Axonal growth

Axonal growth is typically the first indication of a growth-conducive environment and a biocompatibility validator of the extracellular milieu. Neurons are extremely sensitive to their extracellular milieu; a non-conducive environment compromises axonal and dendritic growth [52,100]. Sprouting neurons are indicative of a healthy environment, starting with neuronal adhesion, neurite outgrowth and the maintenance of intrinsic electrical membrane properties. It was therefore critical for all experiments that the chemical compounds used during the fabrication processes did not affect cellular adhesion or sprouting, and that the neurons exhibited characteristics similar to those seen on standard Poly-L-Lysine coated substrates or/and *in-vivo* [93].

To determine whether neurons cultured on the MEAs exhibited proper axonal growth, individually identified neurons Left Pedal Dorsal 1 (LPeD1) from the snail *Lymnaea* were plated onto Poly-L-Lysine coated SS-MEAs in the presence of brain Conditioned Medium (CM). For the purpose of this first experiment, it did not matter if the cells were cultured precisely on top of the MEA micro-electrodes, or adjacent to them. Indeed, even if a cell were to be displaced away from the electrode, its extracellular milieu would have remained the same thus allowing measurement of its cellular viability. Neurons were allowed to settle for 7 days, and images were taken every 24 hours after plating in order to measure the axonal and dendrites growth over time. Growth was then compared to standard poly-L-lysine coated glass dishes, commonly used for intracellular recording [93].

It was found that all cells (n=9) plated on the SS-MEAs exhibited extensive outgrowth, with neurons growing at a rate of up to 1mm per 24 hours (Figures 8), indicating a high degree of biocompatibility with the substrate materials used in the fabrication process. In addition, some neurons remained viable for at least a month, similar to what is seen on conventional coated glass coverslips, as long as the extracellular environment was regularly replaced with new CM. This endorses the first biocompatible pre-requisite and demonstrates that the MEAs offer a growth conducive environment for the cells.

a)

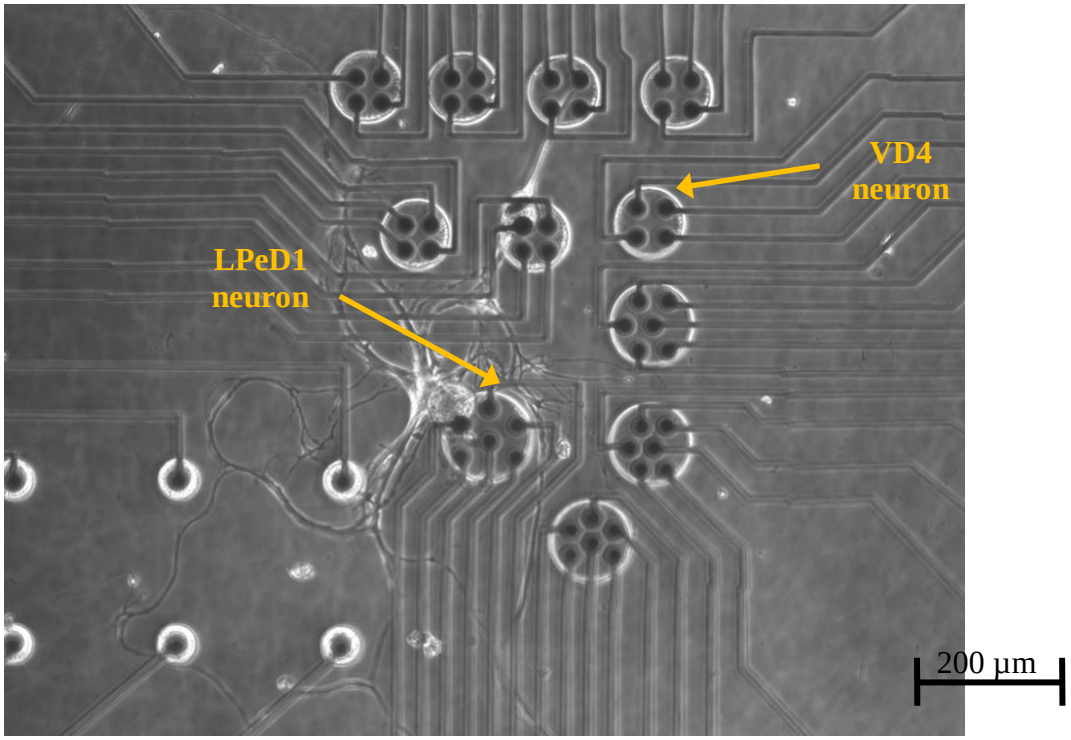

b)

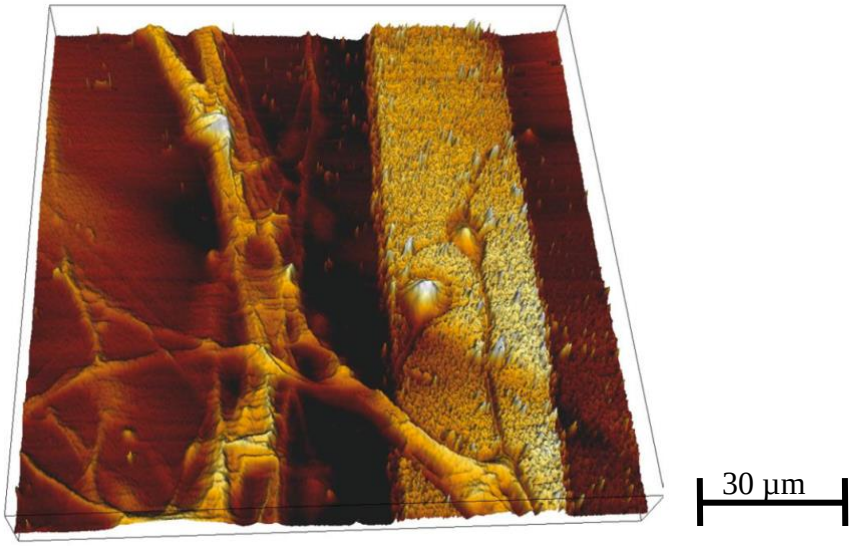

Figure 8: Neurons cultured on our customized SS-MEAs

Neurons cultured on our customized SS-MEAs exhibited extensive outgrowth. a) LPeD1 and VD4 cells displayed axonal growth on the SS-MEA even after 7 days. b) Three-dimensional rendering of an axon growing along a micro-electrode wire (10 µm wide) observed using an atomic force microscope.

3.3.2 Maintenance of intrinsic membrane properties

Following observation of the neural growth over a 7-day period, the electrophysiological properties of the cells, including the membrane potential, threshold potential and action potential amplitude, were tested using sharp intracellular micro-electrodes. To demonstrate that neurons maintain their intrinsic membrane properties, the voltage differential across the membrane was manipulated and action potentials triggered to assess the health status of neurons. In addition, due to the interest in evaluating the ability of the MEAs to record neural activity extracellularly, instances where the cells were in direct contact with the surface of a MEA micro-electrode were primarily focused upon.

It is important to note that when using commercially available MEAs, neurons do not often remain on top of the micro-electrodes for more than 1 to 2 days after culturing, strongly impacting the ability to record single cell activity for longer time-periods. Indeed, cultured single or paired cells generally have the tendency to move away from their original recording sites [75]. This natural phenomenon occurs when neurons grow and form neural processes during which the extending growth cones generate a mechanical stress along the axon and the cell membrane thus pulling the soma away from the electrode sites. To overcome this problem, other researchers erected, for example, cell-restraining pillars [70]. However, these had limited success as they were unable to maintain the cell's viability for more than two days. As described in the previous section, the SS-MEAs were designed to overcome this challenge: a neuron could be plated on a "multi-electrode unit" (Figure 8, b) and always be in the vicinity of an adjacent electrode, thus allowing activity to

be recorded over an extended time period even when the cells moved away from their original culture site.

The results presented in the figure 9 below show that activity could be reliably recorded from single cells over a period of weeks. In fact, all cells (100%, n = 20) were consistently able to do so at least 7 days post-culture. These results are comparable to those traditionally collected using standard Poly-L-Lysine coated glass dishes, thus validating the second biocompatible aspect of our in-house MEAs. The design of the multi-electrode unit also allowed the cells to move away from their original location, without suffering damage to their membranes, while remaining in contact with adjacent micro-electrodes (Figure 9, a). Thus, injecting a positive current to depolarize a neuron triggered action potentials that could also be recorded simultaneously by our SS-MEA (Figure 9, b and c). This design considerably simplified our ability to continuously record the activity from single neurons over much longer time periods as compared to standard commercially available 8 x8 MEAs.

a)

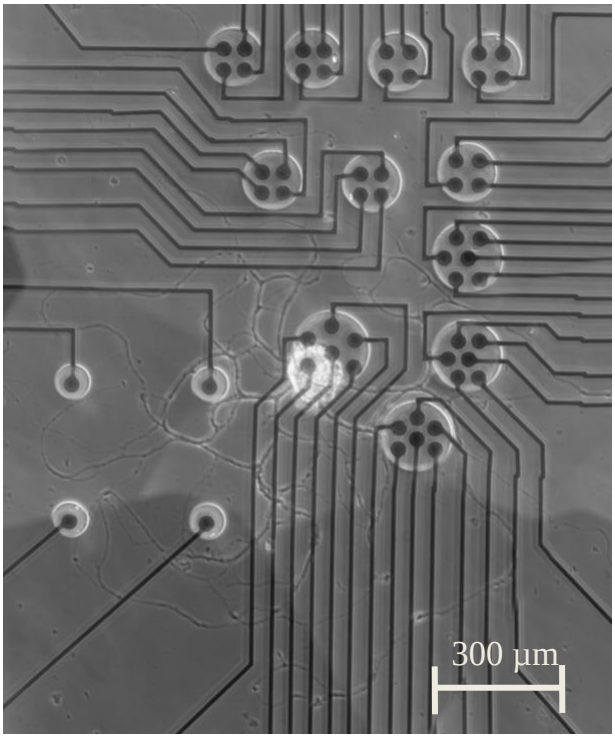

b)

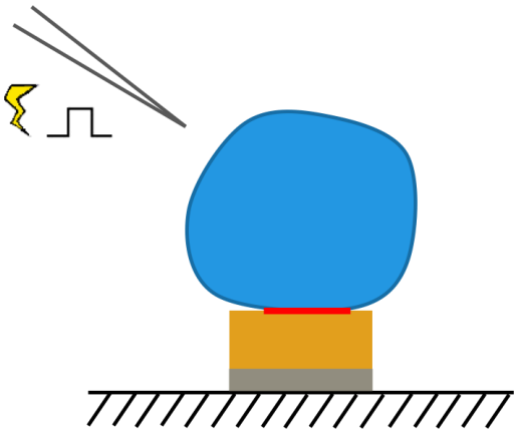

c)

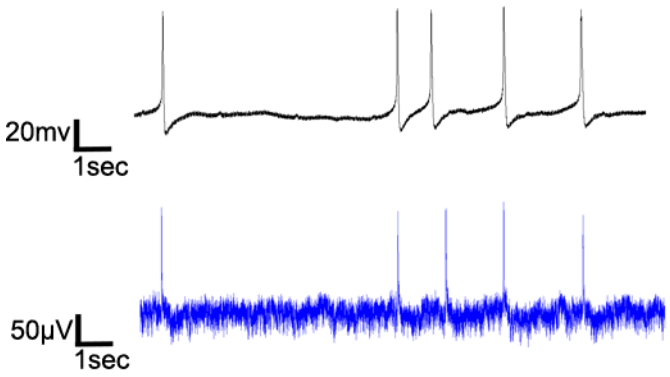

Figure 9: Recording neural activity with the SS-MEA

The SS-MEA design allowed neural activity recording after several days. a) LPeD1 neuron remained in contact with at least one recording site of the multi-electrode unit even 7 days after culture. While the cell was originally plated at the center of the multi-electrode unit, it could freely move around without disrupting its fragile membrane and remained interfaced with adjacent electrodes. b) Schematic of a cell being positioned on an extracellular gold micro-electrode and impaled with a sharp glass electrode. c) Depolarization of a LPeD1 neuron using sharp intra-cellular electrode (top) generated 1:1 action potentials that were also recorded extracellularly (bottom). The difference in signal amplitude between these two techniques is typical in the field of electrophysiology as they both have two different cell-coupling coefficient [75].

3.3.3 Presence of synaptic connections

Finally, I sought to determine whether, in addition to their intrinsic membrane properties, the neurons cultured on the new SS-MEAs could also develop and maintain their synaptic properties. While the naturally occurring neural growth and preservation of the neuron's intrinsic electrophysiological membrane properties had been demonstrated, synapses need an even higher degree of biocompatibility to form proper connections (i.e. as seen *in-vivo*).

Here, both pre- and post-synaptic neurons (VD4 and LPeD1, respectively) were cultured together in a soma-soma configuration in CM on Poly-L-Lysine coated SS-MEAs. For the purpose of this experiment, cells were not required to be specifically positioned on a multi-electrode unit as no extra-cellular recordings were conducted. Cells were then allowed to settle overnight in an incubator at room temperature (22°C, air composition) for 12 to 24 hours, the time usually required for a synapse between these two cells to form [91,93]. The following day, action potentials were triggered in VD4 using intracellular sharp electrodes, which elicited 1:1 Excitatory Post-Synaptic Potentials (EPSPs) of constant amplitude and latency when cultured on the SS-MEAs (95% of paired cells formed a synapse within 24 hours on the SS-MEAs, n = 20, Figure 10).

a) b)

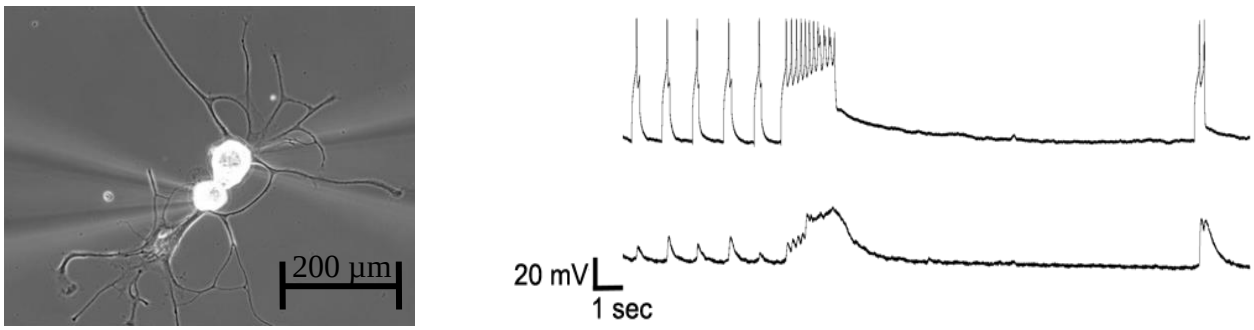

Figure 10: Biocompatible SS-MEAs allow synaptogenesis

Biocompatible SS-MEAs allow synaptogenesis. a) Pre- and post-synaptic neurons VD4 and LPeD1 juxtaposed in a soma-soma configuration and impaled with sharp glass electrodes 24h after culture. b) Action potentials elicited in VD4 (top) produced corresponding 1:1 EPSPs and PTPs (Post Tetanic Potentials) from LPeD1 (bottom) when recorded with intra-cellular sharp electrodes.

3.3.4 Biocompatibility summary

Meeting all criteria for cellular viability and compatibility pre-requisites, I was able to demonstrate that the in-house fabricated SS-MEAs were fully biocompatible after considering three neuron properties: neural growth, maintenance of intrinsic membrane properties, and natural development of synaptic connections between pre- and post-synaptic cells cultured in conditioned media. This high degree of biocompatibility was expected as materials that have been previously reported as safe in the literature were used [52–54,101,102]. However, this characteristic needed to be tested due to the customized fabrication processes used which may have introduced unanticipated biocompatibility issues. By using similar chemicals and compounds used in the MEA fabrication, the aim was then to develop micro-electrodes that could improve the recording resolution (signal-to-noise ratio) of the in-house SS-MEAs.

3.4 Developing a planar micro-electrode with nano-edges

To understand the most fundamental and critical aspects of the brain's basic functional units - the neurons - and their synapses, it is imperative that we design and develop novel MEAs that are biologically and physiologically compatible with cultured invertebrate and mammalian neurons [103,104]. The main scope of such an approach would be to perform better than traditional MEAs - both in terms of signal amplitude and recording length. As described in chapter 1, combining both advantages of the three-dimensional and planar micro-electrodes (i.e. high fidelity and long-term recordings) could offer new opportunities to monitor and record subtle aspects of neural brain activity [75,85]. Inspired by the structural attributes of a synaptic cleft, I designed and developed a planar micro-electrode arrays with nano-edges, to increase the sealing resistance, with the aim of obtaining long-term high fidelity neuronal activity recordings non-invasively that were better than commercially available micro-electrode arrays.

3.4.1 Design and analysis of the nano-edge micro-electrodes

The development of SS-MEAs allowed for the investigation of the effect of different fabrication steps on the sealing resistance. During this process the morphology of a synaptic cleft, whereby both pre- and post-synaptic neurons were juxtaposed and semi-encapsulated, was examined in detail. Specifically, developing micro-electrodes that "bio-mimic" the postsynaptic cleft were designed, with 'nano-edges' hopefully providing a tighter physical and di-electrical seal between the device and the neuron. This structural geometry was also anticipated to prevent the leakage of

current into the surrounding extracellular milieu, thus preserving and augmenting the functional integrity of chemical and electrical neuronal signal processing (Figure 11).

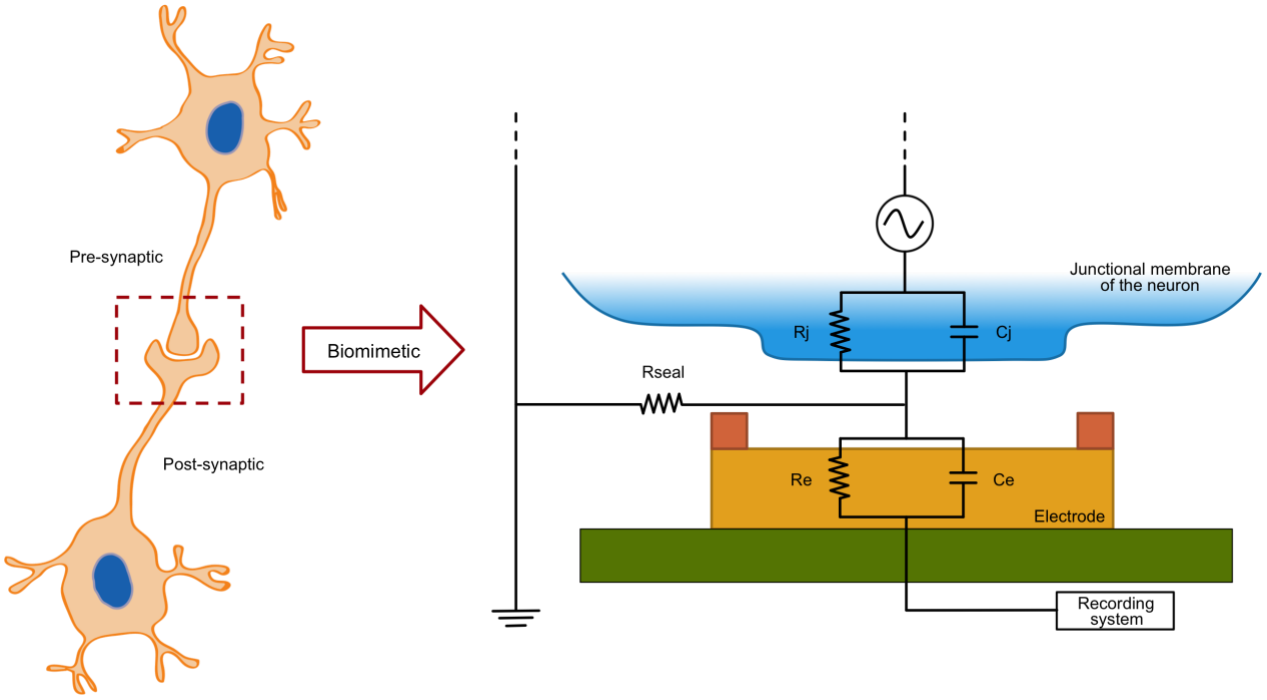
Pre-synaptic
Post-synaptic
Biomimetic
Junctional membrane
of the neuron
Rj
Cj
Rseal
Re
Ce
Electrode
Recording
system

Figure 11: Biomimetic nano-edge micro-electrode

Biomimetic nano-edge micro-electrode mimicking the morphological structure of a synaptic cleft. Left: Schematic representation of two synaptically connected neurons (the box depicts a chemical synapse between the cells). The post-synaptic terminal is shown as encapsulating the pre-synaptic terminal; thereby enhancing tight physical and di-electric coupling between the neurons. Right: Schematic layout developed further from *Spira and Hai, 2013* [75], illustrating an electrode-neuron interface with its analogue passive electrical circuit. Only the junctional membrane (part of the membrane in contact with the micro-electrode) of the cell body is represented here (blue) – depicted to be in close contact with the electrode (yellow) and its nano-edges (orange). The non-junctional membrane (not shown in this diagram) refers to the part of the membrane not juxtaposed against the electrode. The electrode was fabricated on a silicon dioxide substrate (green) and connected to a recording system (MEA1060; Multichannel Systems, Reutlingen, Germany). The junctional membrane resistance (Rj) and conductance (Cj) are represented in parallel, similar to the electrode resistance (Re) and impedance (Ce). The sealing resistance (R_{seal}) was enhanced due to the nano-edges implemented on the electrodes.

Gold planar nano-edge micro-electrodes followed a standard fabrication process as described in the methodology chapter. First, gold planar micro-electrodes were developed using a standard photolithography technique and lift off process. Electrode sizes, and distances between them, were adjusted according to our experimental needs by modifying the photomask designs, allowing us to keep the fabrication process relatively simple, economical and scalable. Once the planar micro-electrodes were fabricated, a nano-edge was added using a custom photolithography process. The nano-edge was also developed along the wire, and not limited to the circular area forming the micro-electrode, to increase the sealing resistance even when a neuron is not placed exactly on top of the micro-electrode. This configuration also increased the surface area of the micro-electrode that was in contact with the neuronal cell membrane (when bigger than 30µm in diameter). Following the fabrication, the morphological attributes of the nano-edge micro-electrodes were characterized and validated using atomic force microscopy to qualitatively confirm the presence of the nano-edges (Figure 12).

a)

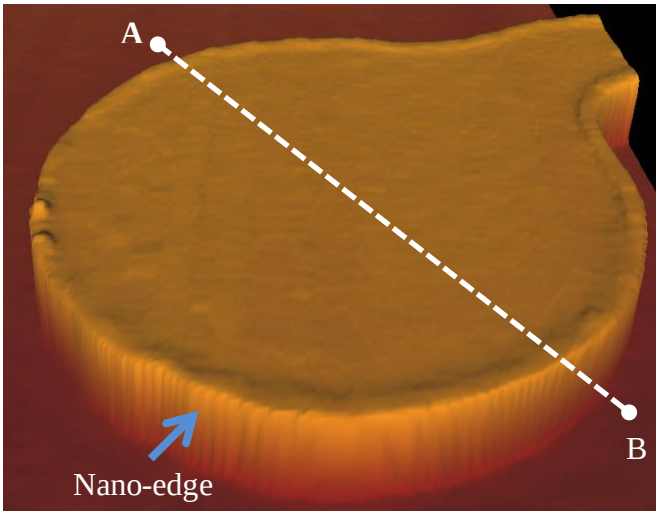
A
B
Nano-edge

b)

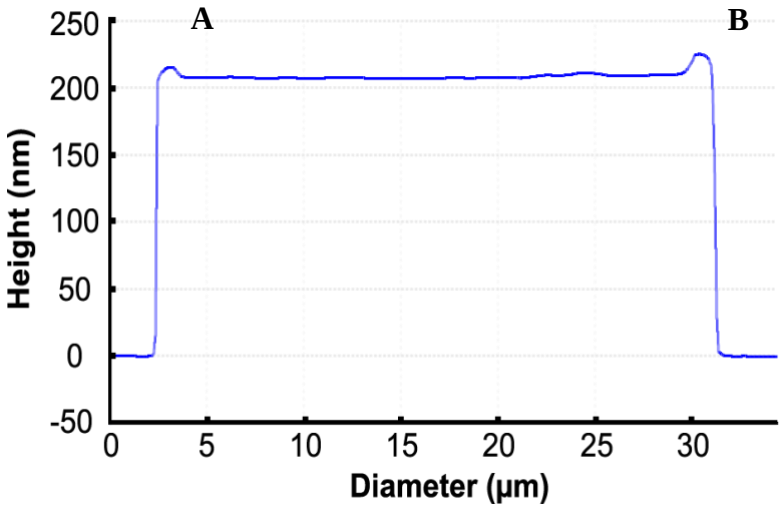
A
B
Height (nm)
250
200
150
100
50
0
-50
0
5
10
15
20
25
30
Diameter (μm)

Figure 12: Characterization of the nano-edge micro-electrodes

Characterization of the nano-edge micro-electrodes using atomic force microscopy. a) A three-dimensional representation of a 30µm micro-electrode with a 40° tilt is depicted. The nano-edge is discernable around the micro-electrode perimeter (blue arrow), and can be seen continuing along the connecting electrode wire (bottom right). b) Measured cross-section of the micro-electrode height showing the shape of the nano-edge. The micro-electrodes are 30 ±1µm in diameter, 200 ±15nm in height, and the nano-edges varied between 5 and 15nm in height and 2 to 3µm in width. Letters 'A' and 'B' refer to the location of the cross-section taken from Figure 12, a.

3.4.2 A higher recording resolution using the nano-edge micro-electrode

Using the nano-edge micro-electrodes developed on the SS-MEAs, the electrical activity of single LPeD1 and RPeD1 isolated neurons was investigated. These identified neurons from the mollusk *Lymnaea* were interfaced with the electrodes under sterile culture conditions in CM and spontaneous action potentials were recorded using the extra-cellular recording system. From the very first recordings (Figure 13, a), it was possible to record neural activity with an amplitude of 4.2 mV peak-to-peak and a noise level of 35 µV. The associated signal to noise ratio (120) was 7 times higher than similar commercially available planar microchips, as described in the literature [75]. I however quickly realized that the recorded action potentials were truncated due to the limitation of the recording software MC_Rack due to gain limitation (Figure 13, b), and that the resolution of the signal could still be optimized by tuning the gain.

a) b)

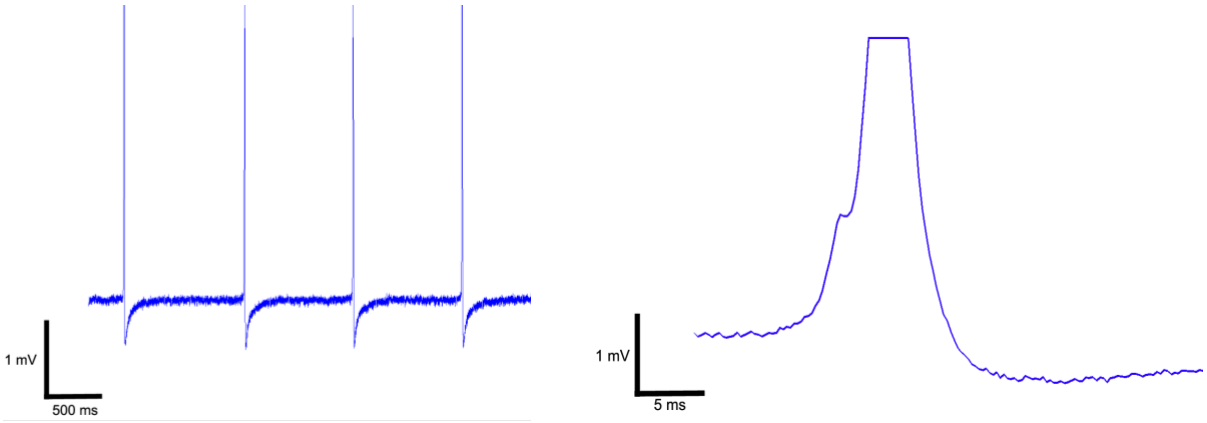

Figure 13: Initial action potentials recorded with the newly developed nano-edge micro-electrodes

Initial action potentials recorded with the newly developed nano-edge micro-electrodes, showing a peak to peak amplitude of 4,2mV. a) We consistently measured action potentials with a constant maximum amplitude. b) This intriguing feature was then understood after analyzing the action potentials more carefully and realizing that the signals were truncated due to a gain limitation.

After modifying software parameters from the recording system as recommended by the support team from Multichannel Systems (Reutlingen, Germany), I managed to overcome this challenge and determined the exact signal amplitude peak-to-peak. I was then able to record neural activity with a maximum amplitude of up to 10.6mV peak-to-peak (n=13; Average peak-to-peak amplitude = 4.44mV; Min and Max range peak-to-peak amplitude = 330µV-10.6mV, Standard deviation = 4.08µV) (Figure 14). These resolutions are significantly higher compared to other standards and commercially available devices with planar electrodes (typically ≤1mV [75,77,105,106]. To conduct this analysis, only those cells that completely covered at least 100% of one micro-electrode were considered.

a)

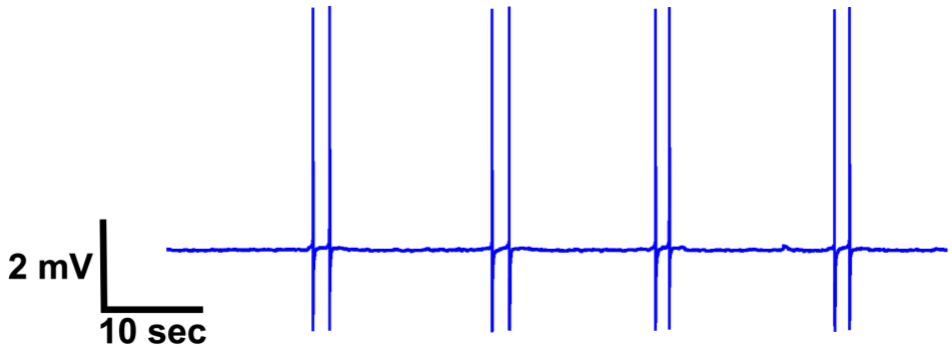

b)

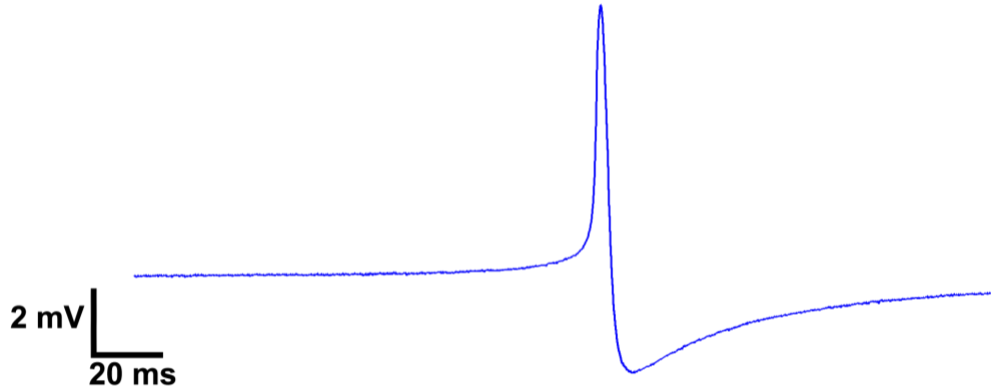

Figure 14: Unprecedented resolution using the nano-edge micro-electrodes

Nano-edge micro-electrodes permit unprecedented resolution and long-term neural recording at the single neuron level. a) Recording of action potentials from a single neuron showing distinguishable patterned activity from selected *Lymnaea* neurons [91]. b) Single action potential with clearly defined depolarization followed by rebound hyperpolarization. Average of the recorded action potentials amplitude was 4.44mV peak-to-peak (n=13) with a maximum measured value of 10.6 mV.

As demonstrated by the standard deviation, the observed variability can be due to numerous application specific factors. Chief among these are cell-specific variables such as the size of the neurons and the interfacing between their membrane and the electrode which enables the nano-edge to fully increase the sealing resistance.

I found that the neuronal coupling coefficient was 0.15, which is 15 times higher than what has been reported for traditional planar and resistor electrodes (0.001-0.01) [75,82], our novel nano-edge micro-electrodes recorded neural activity at a significantly higher resolution than any other traditional planar electrodes, and often better than most three-dimensional electrodes (ranging from 0.1 to 0.3) (Figure 15).

a)

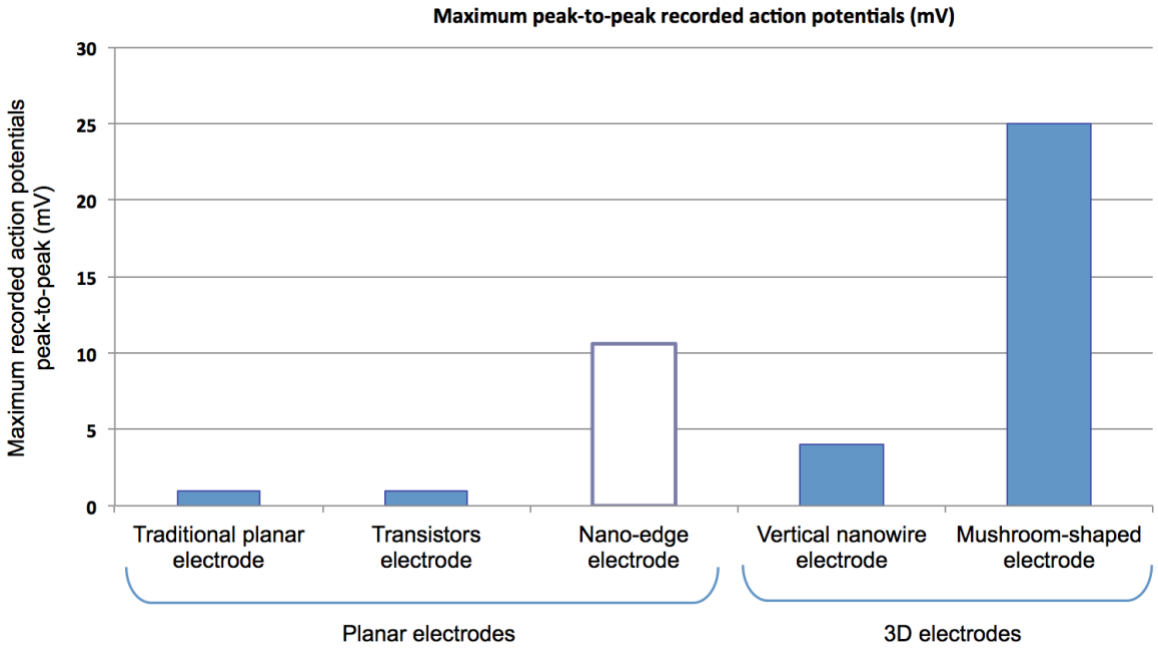
Maximum peak-to-peak recorded action potentials (mV)
Maximum recorded action potentials peak-to-peak (mV)
30
25
20
15
10
5
0
Traditional planar electrode
Transistors electrode
Nano-edge electrode
Vertical nanowire electrode
Mushroom-shaped electrode
Planar electrodes
3D electrodes

b)

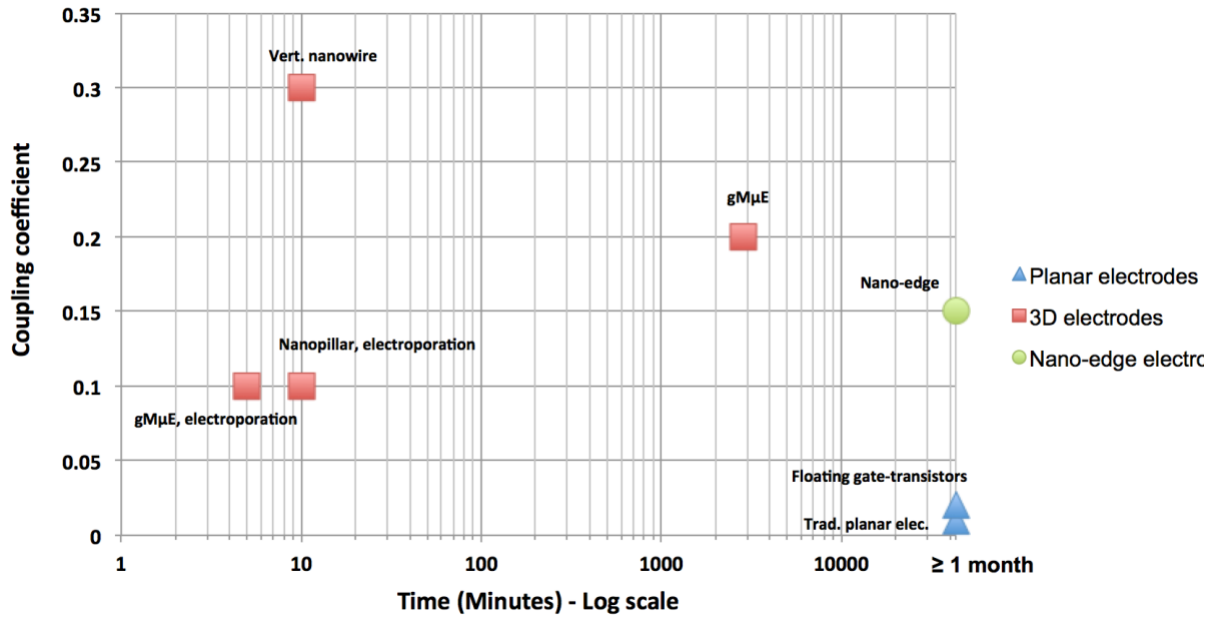
Coupling coefficient
0.35
0.3
0.25
0.2
0.15
0.1
0.05
0
Vert. nanowire
gMµE
Nano-edge
Nanopillar, electroporation
gMµE, electroporation
Floating gate-transistors
Trad. planar elec.
1
10
100
1000
10000
≥ 1 month
Time (Minutes) - Log scale
Planar electrodes
3D electrodes
Nano-edge electrc

Figure 15: Comparison of nano-edge micro-electrodes against other devices

Comparison of nano-edge micro-electrodes against other devices. a) Comparison of maximum-recorded peak-to-peak action potential between the nano-edge micro-electrodes compared with other types of extra-cellular electrode, showing that the nano-edge micro-electrodes record higher action potentials than all other planar micro-electrodes [75,107], including some three-dimensional ones (e.g. vertical nanowire [83,85], Mushroom shape electrode [84,87]. b) Comparison of the most commonly used micro-/nano-electrodes used to record neural activity *in-vitro*. The maximum coupling coefficient and the longest reported recording time were used to evaluate electrodes capabilities. Our nano-edge micro-electrodes (green circle) permits monitoring of action potentials with a coupling coefficient comparable to that of 3D electrodes (red square), and for a period of time equivalent to traditional planar micro-electrodes (blue triangles).

In addition, the planar nano-edge micro-electrodes did not limit neurons' movements, and subtly maintained the interface with the contact site, thus enabling stable neuronal recordings for at least two weeks (recordings were conducted arbitrarily for a minimum of two weeks in this case and then stopped intentionally as per the experimental paradigm). After these two weeks, it was assumed that electrodes could maintain this recording for an even longer period of time (>1 month), similar to traditional planar micro-electrodes [69]. Also, due to the presence of a nano-edge of 5 to 15 nm in height, the neuronal membrane integrity was not compromised nor did the cells migrated away from the electrode. This allowed for neurons to develop networks whose activity could be continuously monitored for extended time periods (Figure 16). In instances where neurons did migrate away from their initial site of electrode contact, high fidelity recordings were still acquired because of to the following reasons: First, the adjacent nano-edge micro-electrodes (grouped in multi-electrodes units) maintained the dielectric contact with the cell. Specifically, adjacent nano-edge micro-electrodes could be used as new monitoring sites and then the acquired data was merged at the end of the experiments using MC_Rack and MC_DataTools software. Secondly, to enable stable and high-resolution recordings over and above the background noise, a neuron must fully cover a typical planar electrode at all times. Any movement away from the recording site may thus render the signal undetectable. Since the signals recorded by the nano-edge micro-electrodes were significantly larger than traditional devices, the amplitude of the recorded action potentials remained easily discernable from the noise level throughout the course of an experiment, even if a cell was not fully covering the micro-electrode surface area.

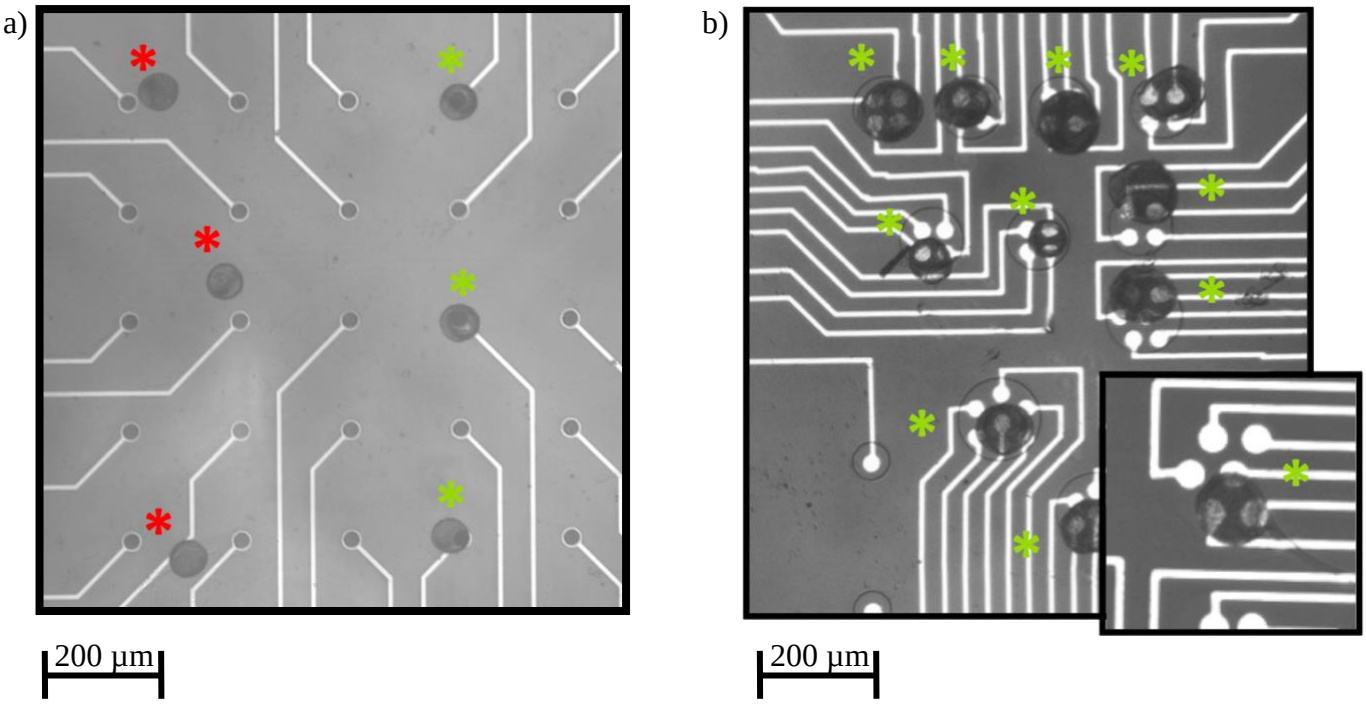

Figure 16: Comparing LPeD1 neurons movements

Comparing LPeD1 neurons movements between traditional 8 x 8 MEA and the customized SS-MEAs 24h after culture. Red stars mark neurons that are not interfaced with a micro-electrode anymore, while green stars mark those who still are. a) When cultured on a traditional 8 x 8 MEA, neurons rapidly move away from their original recording site, limiting the ability to conduct long-term recordings. b) Neurons were cultured on a custom designed SS-MEA with multiple nano-edge micro-electrodes grouped into clusters of 4 or 6 micro-electrodes per set. Neural activity could be continuously monitored, even if the cells had moved away from their initial culture site [108].

Taken together, I was able to demonstrate that our novel nano-edge design offers tremendous potential to study neural activity at a single neuron resolution. Indeed, while testing the potential of these new micro-electrodes, I was able to investigate the feasibility of two longer term projects:

1) These electrodes allowed the monitoring of changes in the patterned neural activity as the neuronal membrane and network properties mature over time [91], thus allowing the investigation of network connectivity and plasticity at a resolution never achieved before;
2) In addition, while the development of MEAs in the industry has been limited to standard fabrication processes with a limited number of electrode designs and placement, often not suited for our customized experiments, our fully biocompatible in-house SS-MEAs could offer new opportunities to record pre- and post-synaptic activity over extended periods of time. In turn, this innovative biomorphic design would allow researchers to better understand how neurons communicate over time and help identify neural activity signatures found in specific neurons.

3.4.2.1 Recording neural activity signature

The development of neuronal networks and the refinement of their connectivity require both molecular cues and highly coordinated patterns of electrical activity – the disruption of which could lead to dysfunction [109]. Decrypting patterned neuronal activity is therefore essential to better

understand brain functions and dysfunctions. As the new SS-MEAs with nano-edges allowed long-term monitoring of neuronal activity and connectivity through extra-cellular field potentials, they provided an excellent opportunity to decipher the unique neuronal activity signature of individual cells from the freshwater snail *Lymnaea stagnalis*.

Identified single LPeD1 (cardiac homeostasis) and RPeD1 (respiratory) neurons were isolated and cultured on our in-house fabricated SS-MEAs, as described in *Luk et al. 2015* [91]. After allowing the cells to settle for 1 hour on the micro-electrodes, their activity was recorded continuously for a period of 24 hours. Both neurons exhibit spontaneous, yet very distinct, activity patterns (Figure 17). Some of the main clues that I was able to identify, and which demonstrated the opportunity offered by the SS-MEAs to decipher patterned activity (n = 8) changes, are as follow:

- While RPeD1 neurons started to exhibit spontaneous activity 1 to 2 hours after recording (i.e. 2 to 3 hours after culture), LPeD1 neurons were firing immediately as the recording started.
- Over a period of 24 hours, LPeD1 neurons first exhibit short bursting patterns which transitioned to tonic activity, while RPeD1 neurons maintain phasic bursting patterns even after 24 hours – albeit the length of each burst was much longer.
- After 24 hours, LPeD1 neurons' interspike interval frequency (fISI) was 0.8±0.1Hz, and 0.6±0.1Hz for RPeD1 neurons (n)

- A coefficient defined by the frequency of action potentials and the Inter-Spike Interval (coefficient of 1 implies perfectly tonic firing) was 1±0.05 for LPeD1 neurons while RPeD1 never reached tonic firing.

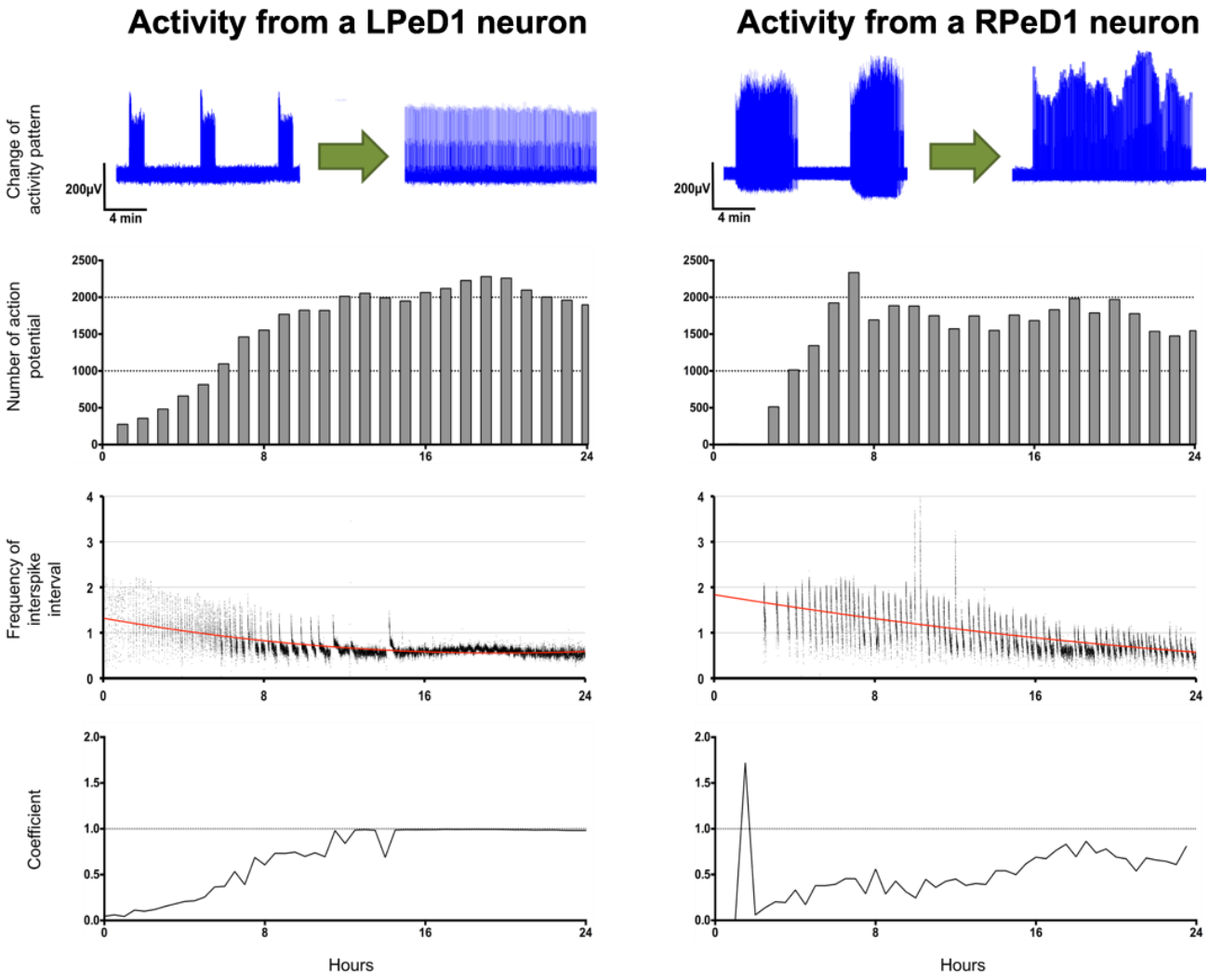
Activity from a LPeD1 neuron
Activity from a RPeD1 neuron
Change of activity pattern
200µV
4 min
Number of action potential
Frequency of interspike interval
Coefficient
Hours
Hours

Figure 17: Raw data showing distinctive spontaneous activity patterns

Raw data showing distinctive spontaneous activity patterns between LPeD1 and RPeD1 neurons in CM. Variables identified were the shape of the bursts (frequency and inter-burst intervales), number of action potentials, frequency of inter-spike intervals (fISI), and a coefficient function of the fISI and frequency of action potentials. No activity was seen in DM, as expected from Luk *et al., 2015* [91].

These experiments demonstrated that by maintaining long-term contact with the cells, our novel micro-electrodes allowed the deciphering of subtle differences between neural firing patterns.

3.4.2.2 Sub-threshold post-synaptic neural activity

The importance of synaptogenesis in the establishment of neural networks has been already well defined in the literature [20,21,110–112] and synaptic deregulation is known to cause many human neuro-degenerative diseases. It was therefore of interest to understand if the newly developed nano-edge micro-electrodes could also record EPSPs or PTPs , non-invasively. Not only would this allow us to better understand how sub-threshold currents between two cells take place and change over extended time periods, but also help understand many other aspects of synaptic plasticity and dysfunction.

Pre- and post-synaptic cells VD4 and LPeD1 were cultured in a soma-soma configuration on a multi-electrode unit from a SS-MEA with nano-edge in CM (Figure 18, a). As described previously, when plated side by side, these neurons naturally form a "soma-soma" synapse within several hours [20,93] in a biocompatible environment. Pairs were allowed to settle overnight, and the following day, both pre- and post-synaptic cells were impaled with intracellular sharp electrodes (Figure 18, b). The pre-synaptic cell (VD4) was electrically depolarized to trigger action potentials and resulting 1:1 excitatory postsynaptic potentials (EPSPs) in the post-synaptic cell (LPeD1) were recorded.

a)

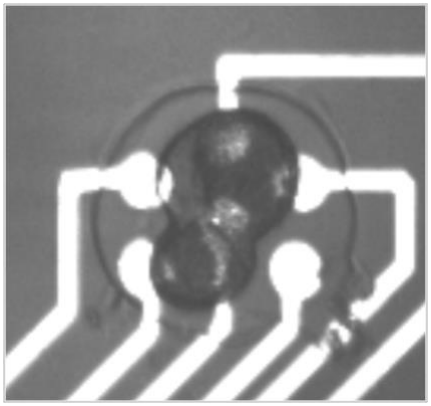

b)

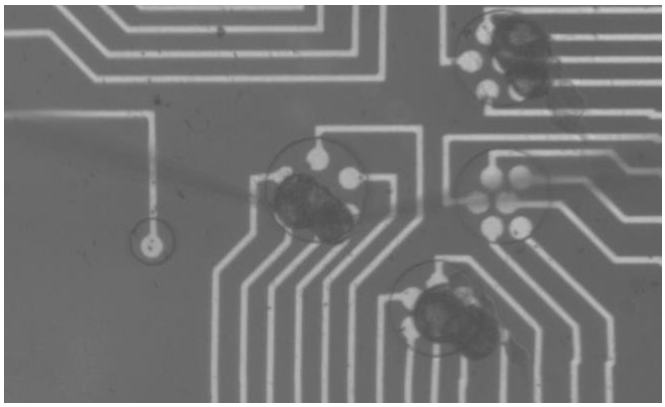

c)

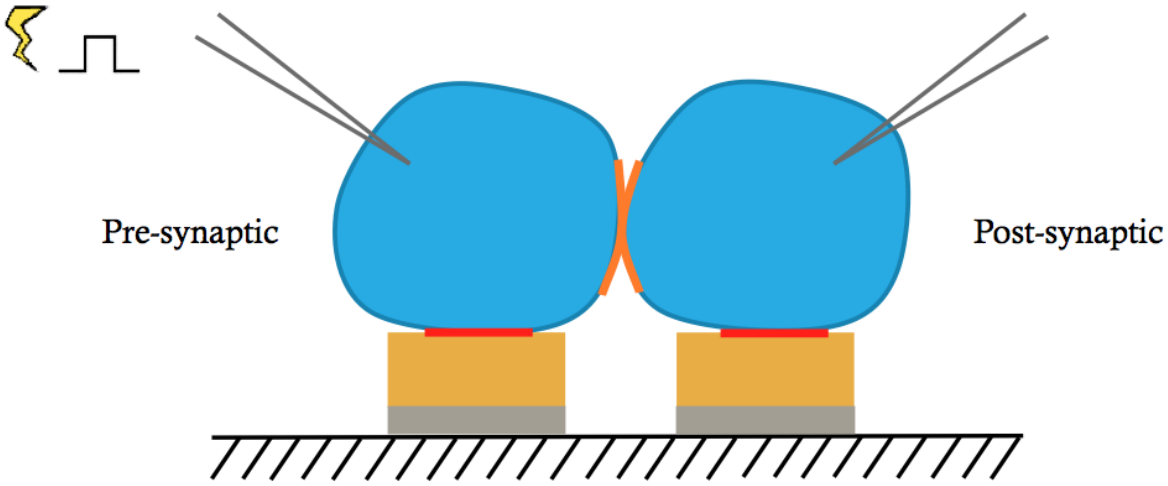

Figure 18: Culture in a soma-soma configuration

Culture in a soma-soma configuration a) Pre- and post-synaptic neurons, respectively VD4 and LPDe1, formed a soma-soma synapse on a multi-electrodes unit from our SS-MEA. b) Both neurons were impaled using sharp intracellular glass electrodes and the pre-synaptic cell (VD4) was depolarized. c) A schematic representation of the soma-soma configuration used to record neural activity from both the pre- and post-synaptic cells simultaneously, using intra and extra-cellular techniques. While the red lines depict the interface between each cell and their respective micro-electrode, the orange line represent the synapse location.

Results showed that action potentials triggered in VD4 using intracellular sharp electrodes elicited 1:1 EPSPs of constant amplitude and latency in LPeD1, and that this activity could also be simultaneously recorded extracellularly using the SS-MEAs (Figure 19). These post-synaptic potentials (PSPs) were similar in both their form (excitatory) and strength (10 mV in average) as those seen in standard Poly-L-Lysine coated plastic dishes. Interestingly, the EPSPs as monitored intracellularly had to be at least of 15mV ± 3 before they could also be detected by the extracellular SS-MEAs.

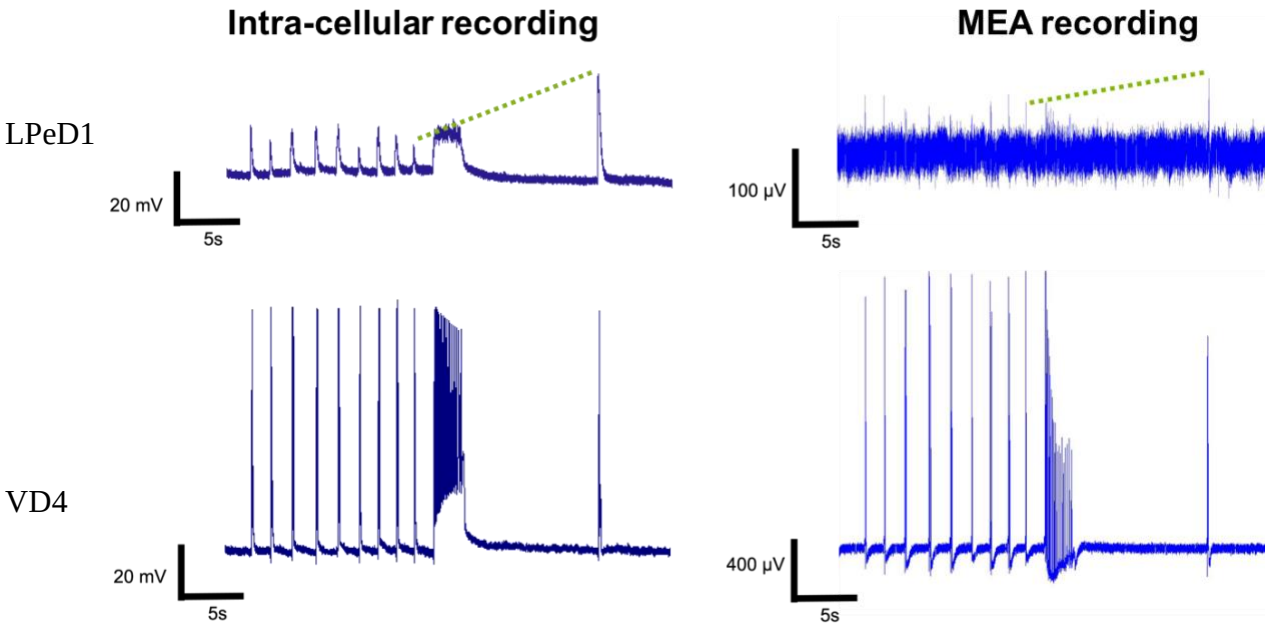

Figure 19: Extracellular synaptic potentials recorded by SS-MEA

Extracellular synaptic potentials recorded by SS-MEA were identical to those of gold standard intercellular electrodes. Example of resulting EPSPs and PTP from LPeD1 (top) following action potentials from VD4 (bottom) that were recorded simultaneously with intra-cellular sharp electrodes (left) and the nano-edge micro-electrodes present on the SS-MEA (right).

Comparing the activity recorded simultaneously using both intra- and extra-cellular techniques, it was also possible to demonstrate the presence of EPSPs and Post-Tetanic Potentials (PTPs) as their respective amplitudes were significantly different during every single experiment ($n = 27$, $p < 0.0001$ with Students t-test, Figure 20). More precisely, PTPs denote an increase in synaptic efficacy that occurs following a high-frequency tetanic stimulation (i.e. "burst" of EPSPs), and can be triggered by a lower-frequency, shorter-duration stimulation [113].

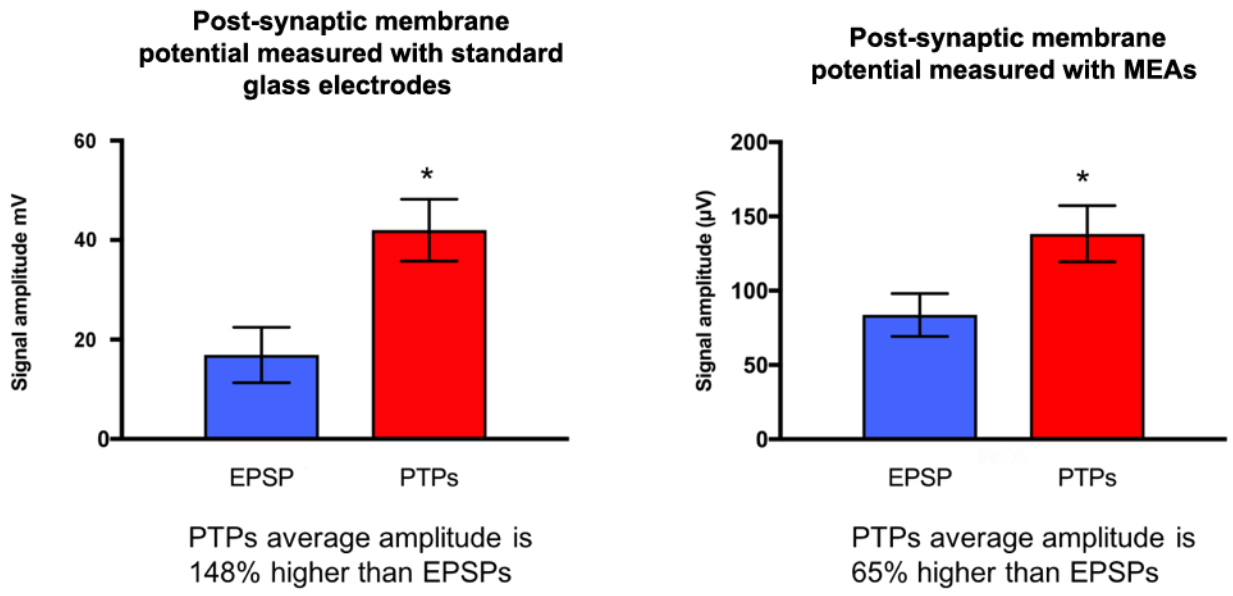

Figure 20: Statistical analysis of EPSPs and PTPs

Statistical analysis showed a significant difference between the amplitude of recorded EPSPs and PTPs, both intra and extracellularly ($n=27$, $p<0.0001$, Students *t* test). Note that the respective ratios are different (1:2.5 and 1:1.7) and can be attributed to the specificity of both intra- and extra-cellular recording techniques (respectively, recording of a potential difference between the inside of a cell and a reference ground placed in the extra-cellular milieu, versus the detection of ionic movements around the cells).

These experiments demonstrated that designing a nano-edge on top of the micro-electrodes proved to be successful in recording sub-threshold currents, like EPSPs and PTPs.

3.5 Computational simulation

To validate the functional efficacy of our nano-edge micro-electrodes, the software COMSOL was used to run computational simulations. From the information provided in chapter 1 and the results presented previously, the observed signal enhancement could be attributed to two main factors: either an increased sealing resistance or a decreased electrode impedance. In our case, as the materials and dimensions of the micro-electrode did not vary significantly from conventional planar gold electrodes [107], a decreased impedance was an unlikely reason. Thus, a change in the sealing resistance was likely the determining factor underlying higher amplitude signals.

To investigate this variable further, a neuron-electrode interface was modeled using the built in *Electric Currents* module in COMSOL Multiphysics (COMSOL Inc., Burlington MA). The goal of this simulation exercise was to improve on previous COMSOL models of neuron simulation [101,114], and also to determine the effect of the nano-edge on the sealing resistance, which is defined as the resistance that restricts current leakage through the gap between a neuron and the electrode.

3.5.1 Modelling the different domains

As shown in figure 21, the simulation model consists of several domains. Firstly, a glass substrate, which acts as an insulating layer, was modeled to form the basis for the MEA. The glass substrate was modeled with an infinite boundary for this simulation, meaning that the multi-physical

properties were preserved along the entire surface of the glass substrate. The micro-electrode was modeled above the glass using a gold cylinder with a diameter of 30μm, which reflects the size of our micro-electrodes. A thin layer of chrome was inserted in between the gold micro-electrode layer and the glass, which acted as an adhesive substrate between the two layers in the fabricated devices. However, no differences in the simulation results were observed when the chrome layer was added or removed from the model. Located 50nm above the electrode, to reflect the junctional gap in neuron-electrode interfaces [75,115,116], the neuron was modeled using a semi-circle (ranging from 5μm in diameter to 80μm, to reflect the variability of cell diameters found in vertebrate as well as invertebrate models). The boundaries and volume of this semi-circle acted as the membrane and intracellular fluid, respectively. A 2 μm wide nano-edge was added to the electrode via a ring of dielectric material around its upper edges. While the nano-edge height on our fabricated micro-electrode ranges between 5-15 nm, we simulated a nano-edge ranging from 0 nm (no nano-edge, similar to traditional planar electrodes) to 50nm (height at which the nano-edge completely fills the gap between the electrode and the neuron [117] to provide a better understanding of its effect. The remaining external space was filled with the extracellular fluid. Similar to the glass substrate, this domain of extracellular fluid was modeled as an infinite region. The table 1 below shows the values of electrical conductivity and relative permittivity used for the various materials.

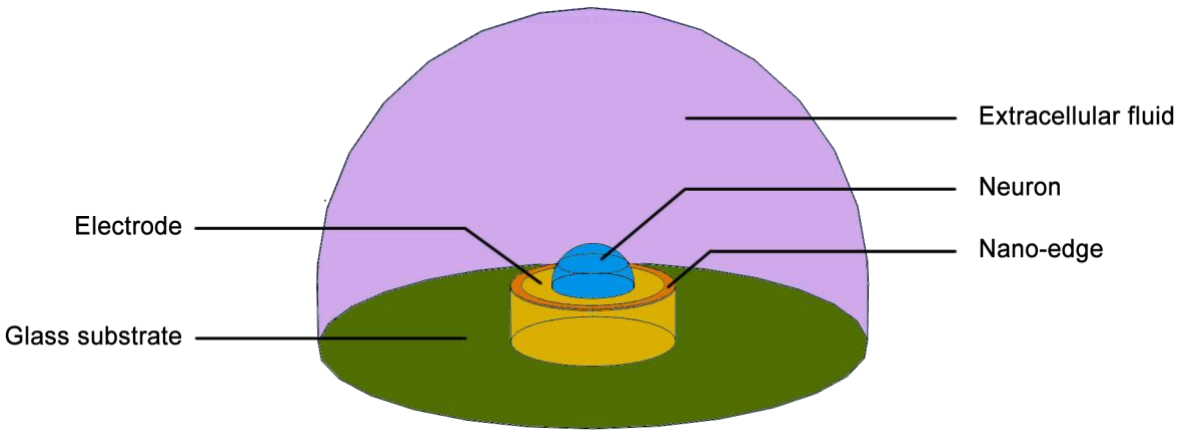

Figure 21: Schematic representation of the simulated elements

Schematic representation of the simulated elements using COMSOL Multiphysics and their physical characteristics. Both glass substrate and extracellular fluid were modeled as infinite boundaries. The micro-electrode height was set at 200nm and its width to 30µm as per our experimental needs. The neuron was positioned 50nm above the micro-electrodes to mimic the gap found at the neuron-electrode interfaces [75,115,116], and was modeled with diameters in the range of 5 to 80µm, which is representative of most vertebrate and invertebrate cell diameters. Finally, the nano-edge was modeled at various heights from 0 (no nano-edge, similar to traditional planar electrodes) to 50nm (same height as the cleft).

Materials	Electrical Conductivity	Relative Permittivity
Gold electrode	45.6e6 [18]	6.9 [18]
Cell Membrane	7.93e-8 [24]	5.6470 [25]
Extracellular Fluid	0.84 [26]	80 [26]
Intracellular Fluid	0.68 [26]	80 [26]
Dielectric nano-edge	3.5e-15 [27]	4.1 [27]

Table 1: Physical values of electrical conductivity and relative permittivity used to run the computational simulation.

Two specific meshes were used in the computational model to improve the outcomes and analysis [ref]. A standard free tetrahedral mesh was used for the neuron and the surrounding extracellular fluid. However, the free tetrahedral mesh was unable to mesh the smaller portions of the simulation due to computational limitations with regards to smaller elements, and therefore a free triangular swept mesh was implemented for these regions. This mesh was utilized for the glass substrate, gold electrode, and the thin layers in between the electrode and neuron. A swept mesh was found to be better for modeling thin layers and non-proportioned domain sizes by avoiding redundant mesh elements, which also decreased the computation time (by 80%, hours to minutes) and facilitated the collection of results. The mesh contained between 253,178 and 157,401 mesh elements. Increasing the mesh from 250,513 to 779,642 elements resulted in a very small change of 0.02MΩ to the sealing resistance, indicating that a larger mesh did not have an extensive impact on the results and a smaller mesh was therefore used to reduce computational time [118].

3.5.2 Simulation Results

When analyzing the sealing resistance values of planar micro-electrodes with no nano-edge, the results were in the same range to that of *Cohen et al. 2008* [76] when using transistor planar electrodes, which validated the accuracy of the simulation. The sealing resistances calculated using this model for the nano-edge micro-electrode of 30μm diameter ranged from 0.66MΩ to 8.71MΩ, depending on the height of the nano-edge and the size of the neuron simulated (Figure 22).

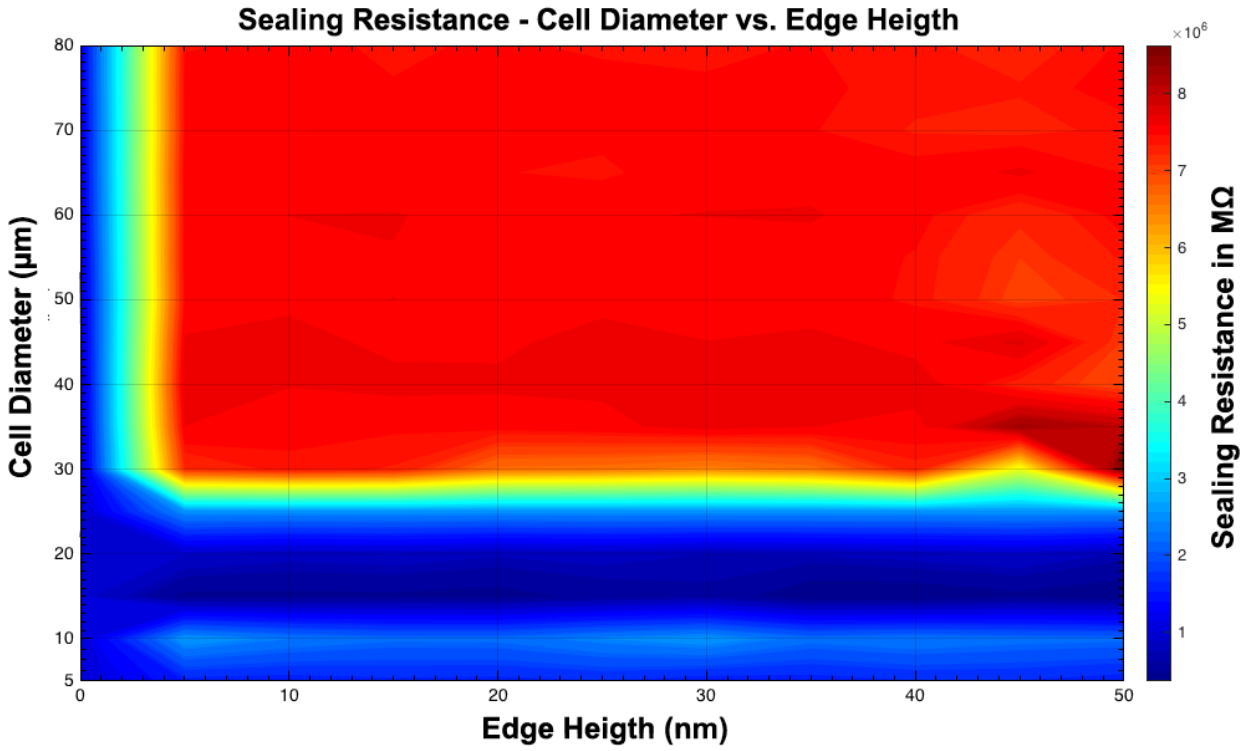

Figure 22: Graphical representation of the sealing resistance disparity

Graphical representation of the sealing resistance disparity when computationally varying the nano-edge height and the cell's diameter using a heat map, function of the cell's diameter and the nano-edge height. Note the rapid increase in sealing resistance when the nano-edge is present and the cell's diameter is equal or larger than the electrode (here 30µm in diameter).

Results of this simulation help draw two important conclusions: 1) The neuronal diameter is a determining factor underlying the sealing resistance value, which significantly increases as the diameter is equal to or larger than the circular micro-electrode diameter (30µm in our case). When a cell's diameter is smaller than the electrode, the sealing resistance values tend to vary due to current leakage. 2) As soon as the nano-edge is present (nano-edge ≥ 5nm in height) and that the neuronal diameter is equal to or larger than the electrode, the sealing resistance remains approximately the same, with an average of 7.49 ± 0.34 MΩ (standard deviation), no matter the height of the nano-edge. In the absence of the nano-edge, no significant difference in sealing resistance is observed (average of 1.03 ± 0.08 MΩ), no matter what the cell diameter is. These results are represented in figure 23 and 24.

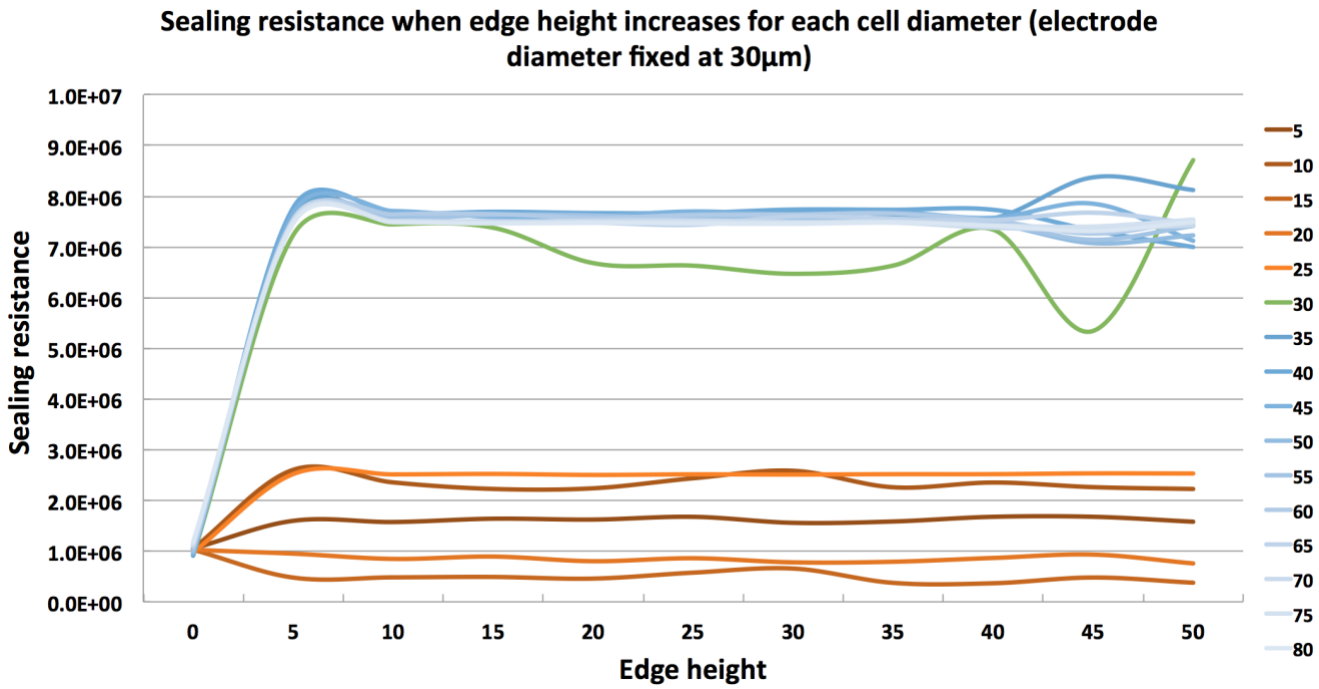

Figure 23: Variation of the sealing resistance for each cell diameter

Variation of the sealing resistance for each cell diameter when the nano-edge increases in height. When the cell's diameter reaches a diameter equal to or larger than the micro-electrode and that an edge is present, the sealing resistance reached a plateau of 7.49 ± 0.34 MΩ.

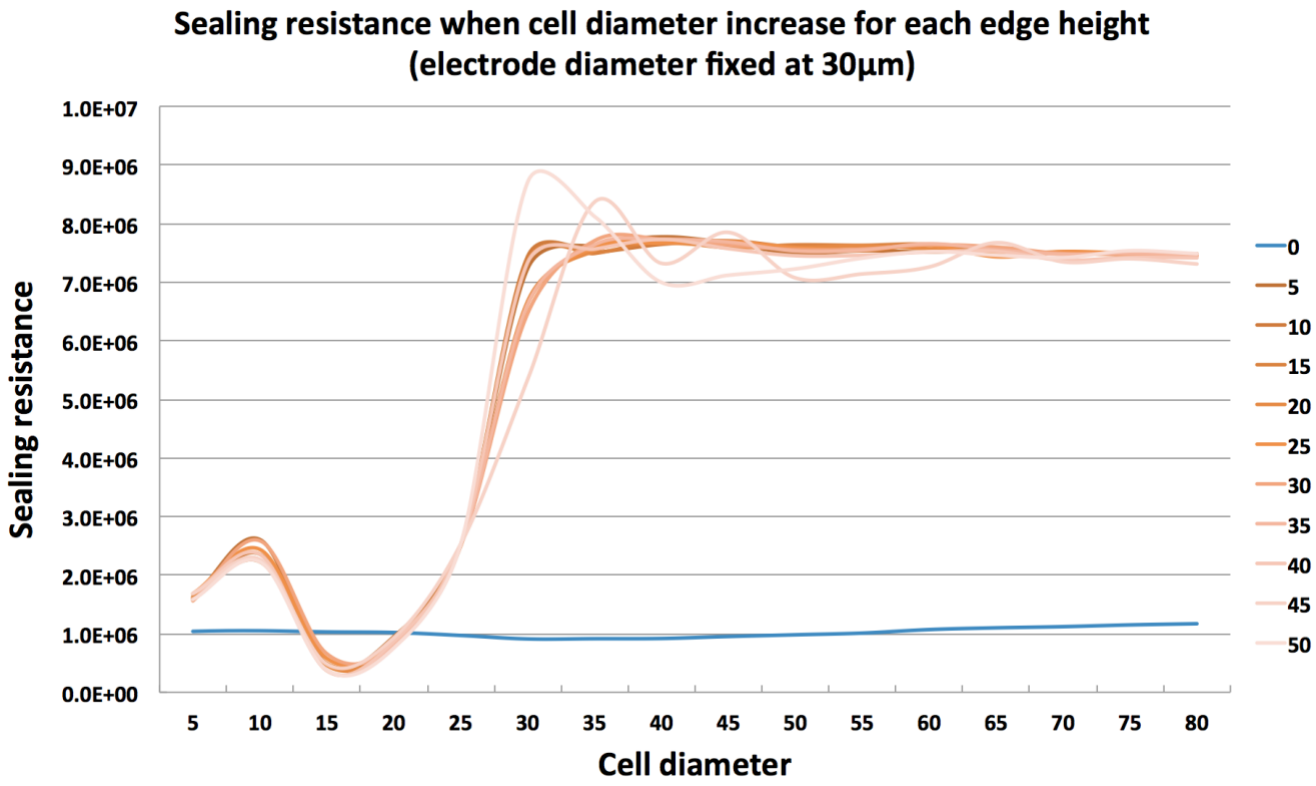

Figure 24: Variation of the sealing resistance for each nano-edge height

Variation of the sealing resistance for each nano-edge height when the cell diameters increases. A dip between 10 and 25µm can be attributed to current leakages happening when a cell's diameter is smaller than the electrode. A similar plateau as for Figure 23 can be seen.

3.6 Conclusion

In this chapter, I have demonstrated that relatively simple nano-scale structural modifications to a planar multi electrode array can significantly increase not only the cell-coupling coefficient (by a factor of 15), but also facilitate long-term recordings at the resolution of single neurons. By exploiting parameters such as the size and spatial pattern of the micro-electrodes, or the types and thickness of materials, recording potential can be optimized while maintaining a relatively simple, scalable fabrication process. These experimental data were also supported by a computational simulation model, that validated the reasons behind the nano-edge effect. An increase in the sealing resistance value was observed if the cell's diameter was at least equal to the electrode's diameter and only if there existed a nano-edge greater than 5nm. Overall, it was demonstrated that designing bio-compatible neuro-electronic devices that are based on natural cellular architecture could pay large dividends in the recording capabilities of bionic hybrids like MEAs.

The nano-edge micro-electrodes fill a large technological gap and provide a breakthrough in the field of neural recording by coupling the advantages of both planar and three-dimensional electrodes. Such attributes when combined together are necessary as they open up new opportunities to investigate advanced neural phenomena such as network formation, maturation, plasticity and dysfunction [14 of nano-edge paper]. Such high fidelity recording capability are beginning to allow the monitoring of sub-threshold synaptic events, that can also be distinguished from various spike patterns of bursting or tonically active neurons embedded in a complex network.

In addition, several modifications could be made in the future to further improve the recording resolution. For example, using conductive materials for the nano-edge; replacing the gold electrode with another metal or alloy coated with platinum black [119], or increasing the general roughness of the electrode surface may all enhance the quality of the recordings further. While the structural design of the micro-electrodes was the only modified variable, other parameters can still be adjusted to optimize the signal-to-noise ratio and obtain recordings with a similar resolution to what is obtain with intra-cellular electrodes. Ultimately, this novel technology will enable better understanding of brain function and offer tremendous opportunities towards the development of future bionic hybrids and drug discovery devices.

Chapter 4: The Multi-Well MEA, from single invertebrate cells to complex mammalian networks

The following chapter comprises sections described in the following patent:

- **Wijdenes P.**, Dalton C., Syed N.I. *Novel planar micro-electrodes with unique morphological structure for enhanced neural recording*. US 62277803 (2015) - Filled application, PCT Status

4.1 Introduction

The SS-MEAs helped me define fundamental parameters required for biocompatibility, and improve the Signal-to-Noise ratio and length of neural recordings by improving the sealing resistance. However, to expand this approach and enable recordings from mammalian neurons, additional changes to the electrode design were deemed necessary. Our computational simulation had predicted that a neuron would need to be at least of the same diameter as that of the nano-edge micro-electrode in order to acquire an ideal sealing resistance, thus providing higher signal resolution. Because mammalian neurons (6 to 25µm diameter on average) are smaller than their invertebrate counterparts (40 to 80µm diameter on average), the diameter of the micro-electrodes needed to be significantly reduced in order to achieve the desired outcome.

However, replicating the exact same design of the nano-edge micro-electrodes on a smaller scale with our current equipment appeared to be very difficult – if not impossible – due to technical limitations. While we could have reduced the diameter of the micro-electrodes down to 5-7µm in diameter, correctly developing the nano-edges for such smaller electrodes would have been challenging.

Furthermore, giant invertebrate neurons generate large electrical currents whereas mammalian neurons tend to exhibit smaller currents. While traditional planar micro-electrodes can record extra-cellular activity from mammalian neurons, their reported signals are however of lower

amplitudes as compared with their invertebrate counterparts [75]. This in turn reduces the probability of recording mammalian neurons' activity at a resolution of single cells.

The above two considerations (i.e. the fabrication limitation and lower probability to detect action potentials from mammalian neurons) were therefore carefully examined during the design and development of a second MEA for the purpose of recording higher resolution signals from mammalian cells: The Multi-well MEA (MW-MEA). Based on the above data, I hypothesized that this new device will allow better recording resolution of mammalian cells than standard commercialized MEAs, and likely maintain long-term recordings (> 2 weeks) of entire networks.

This chapter describes the development of the MW-MEA step by step:

- How we developed a similar biomimetic approach to fabricate micro-electrodes adapted to mammalian neurons' specificities;
- The analysis made to determine the quality of this new device and quantify our fabrication limitation in terms of structures resolution.
- How the recorded activity compared with other commercialized planar micro-electrodes.

4.2 Extending the computational simulation for mammalian neurons

MW-MEAs were designed for extracellular neuronal recordings of mammalian neurons. It used the same bio-mimetic principle as the planar nano-edge MEA by mimicking the postsynaptic cleft [108] with the aim of increasing the sealing resistance between neurons and electrode contact sites. Based on additional computational simulations using COMSOL Multiphysics and its *Electric Currents* module (Figure 25), the model described in Chapter 3 was adapted to estimate the increase of sealing resistance when using a mammalian cell. In the model, a cell of 10 µm in diameter was centered on a gold micro-electrode of 30 µm in diameter, and the nano-edge width was gradually modified from 0 µm (i.e. no edge) to a width of 15 µm (i.e. completely covering the 30 µm diameter micro-electrode). The sealing resistance was determined along these changes to understand the effect of the nano-edge width on a mammalian neuron and analysis was done with Microsoft Excel.

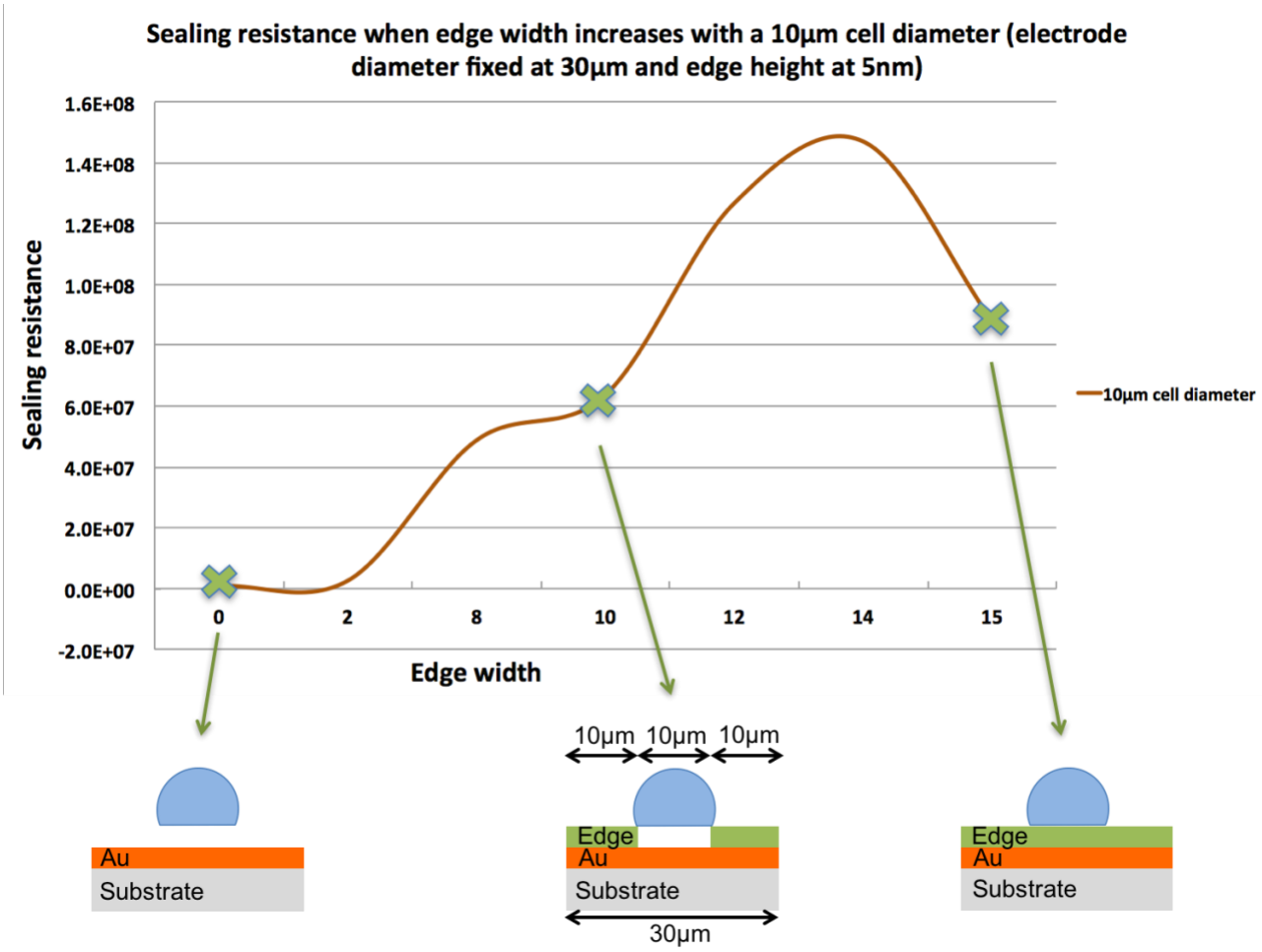

Figure 25: Simulation of a mammalian cell on a micro-electrode

Using a combination of COMSOL Multiphysics and its *Electric Currents* module, a 10 µm diameter cell was centered on a gold micro-electrode of 30 µm in diameter. The nano-edge width was increased gradually (from no edge to a width of 15 µm, i.e. completely covering the micro-electrode).

A higher sealing resistance value than the previous simulation perfomed with larger neurons in Chapter 3 was noticed. While a smaller value of the sealing resistance was expected because mammalian neurons generate smaller electrical events than their invertebrate counterparts, this was considered to be an artifact of the software COMSOL Multiphysics as it is not meant to work with elements of such a small scale. This simulation demonstrated two important aspects:

1) The sealing resistance increases significantly when the nano-edge width expands;
2) It is also possible to increase the sealing resistance using an edge width in the micro range. This second aspect considerably impacted the design of the following multi-well micro-electrodes presented in the following section. Indeed, it reduced the complexity of the fabrication design and allowed the application of more micro scale features.

4.3 Design and fabrication of the multi-well micro-electrodes

Based on the computational results, and as scaling of the planar nano-edge micro-electrode fabrication process down to a diameter of 6-25µm (average sizes of mammalian neurons) was considered unfeasible, a new design consisting of multiple wells with different sizes was developed. Here, six wells were created on each circular micro-electrode and two main variables were modified: the diameters of the wells (5 to 15 µm), and the distances side-to-side between each well (5 to 15 µm) (Figure 26). These ranges allowed for testing of the best wells and electrodes' dimensions to record neural activity, and informed on the fabrication limitations in term of structure resolution. In addition, the presence of multiple wells on each and every single planar micro-electrode would increase the probability that a proper seal forms at the interface between a neuron and the micro-electrode surface, thus allowing a higher recording resolution at multiple recording sites. The depth of the wells was also brought down to 500nm to allow the cells to grow and move freely without damaging their membranes.

The devices were then fabricated at the AMIF facility (University of Calgary) following a standard photolithography process as described in chapter 2 (Figure 27).

a)

Electrodes top

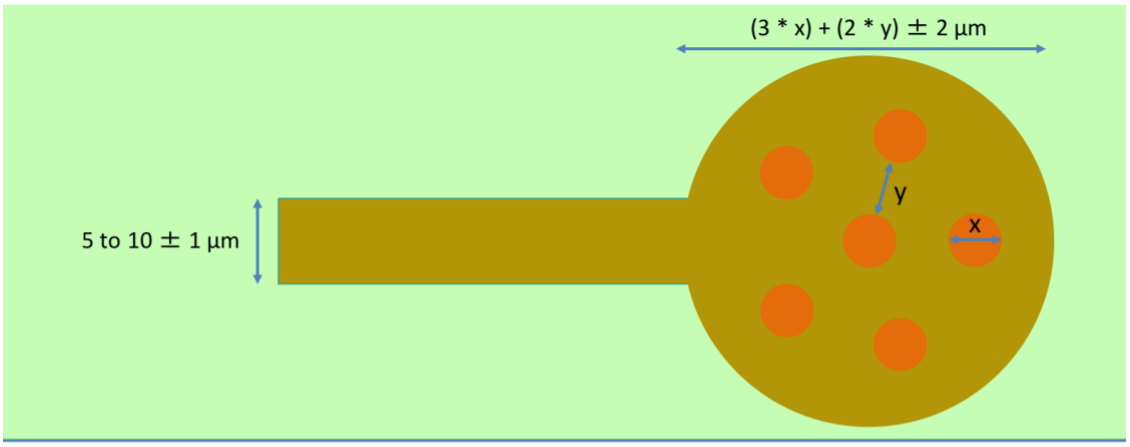

Electrodes side view

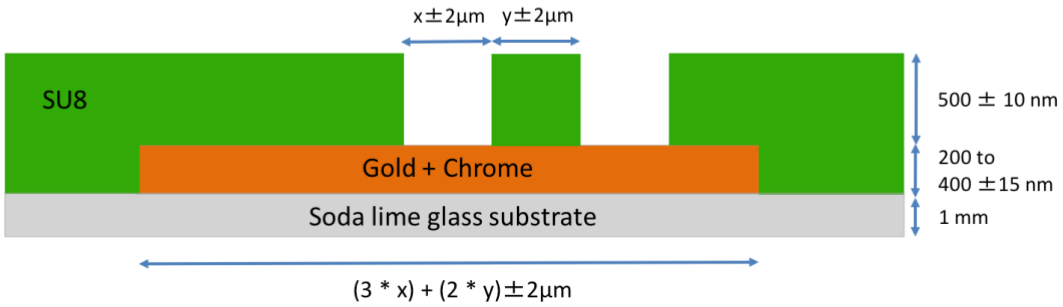

b)

Matrix of X and Y values with the associated electrodes' diameters (all in µm)

(5,5) Ø 35	(7,5) Ø 41	(9,5) Ø 47	(11,5) Ø 53	(13,5) Ø 59	(15,5) Ø 65
(5,7) Ø 43	(7,7) Ø 49	(9,7) Ø 55	(11,7) Ø 61	(13,7) Ø 67	(15,7) Ø 73
(5,9) Ø 51	(7,9) Ø 57	(9,9) Ø 63	(11,9) Ø 69	(13,9) Ø 75	(15,9) Ø 81
(5,11) Ø 59	(7,11) Ø 65	(9,11) Ø 71	(11,11) Ø 77	(13,11) Ø 83	(15,11) Ø 89
(5,13) Ø 67	(7,13) Ø 73	(9,13) Ø 79	(11,13) Ø 85	(13,13) Ø 91	(15,13) Ø 97
(5,15) Ø 75	(7,15) Ø 81	(9,15) Ø 87	(11,15) Ø 93	(13,15) Ø 99	(15,15) Ø 105

Figure 26: Schematics and dimensions of the planar multi-well micro-electrodes

a) Top and side views schematics of the planar multi-well micro-electrodes used to record activity from mammalian neurons. b) (X,Y) matrix describing the variations of the X (wells diameters) and Y (inter-well spacing) variables with corresponding overall micro-electrode diameters.

a) b)

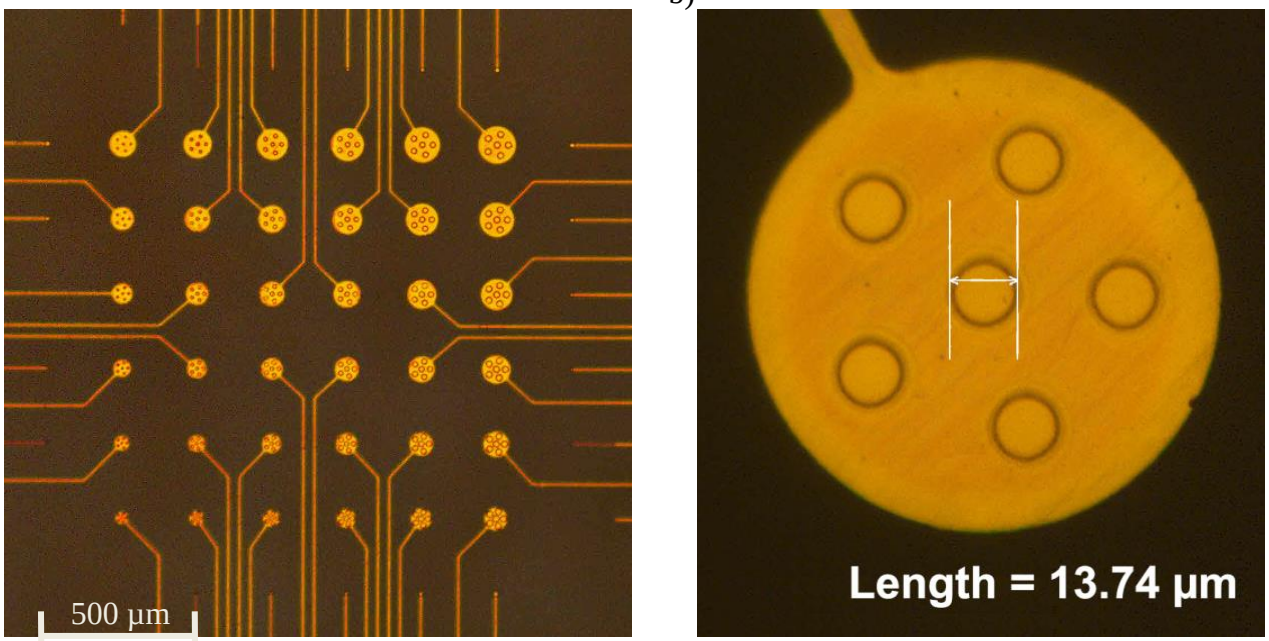

Figure 27: Optical image of an array of multi-well micro-electrodes

a) Top-down optical picture of an array of multi-well micro-electrodes. b) One multi-well micro-electrode with x = 13 µm and y = 15 µm. Initial measurements were performed with an optical microscope to identify structure and lengths defects.

4.4 Fabrication limitations

To determine which multi-well micro-electrodes were successfully fabricated according to the original design, each micro-electrode and its respective wells were imaged using Atomic Force Microscopy at the Microscopy and Imaging Facility (MIF, University of Calgary). Based on the generated three-dimensional rendering, the quality of these micro-electrodes was rated on a scale of 1 to 5, best to worst respectively, after analyzing the digital three-dimensional surface details. Factors that were considered in this quality rating included the following: (a) depth of the well, (b) amount of residue inside the well, and (c) maximum residue height. The table 2 below shows specific ratings metrics for all three factors. In addition, figure 28 shows example of digital three-dimensional surfaces obtained using AFM, associated with measured depths of the wells.

Rating	d, Well depth (nm)	Relative amount of residue	Max residue height (nm)
1	d > 400	Little to none	50
2	400 > d > 300	Little to Moderate	150
3	300 > d > 200	Moderate to High	200
4	200 > d > 100	High	200
5	100 > d	Very High	100

Table 2: Quality rating metrics used to qualitatively control the wells quality.

a)

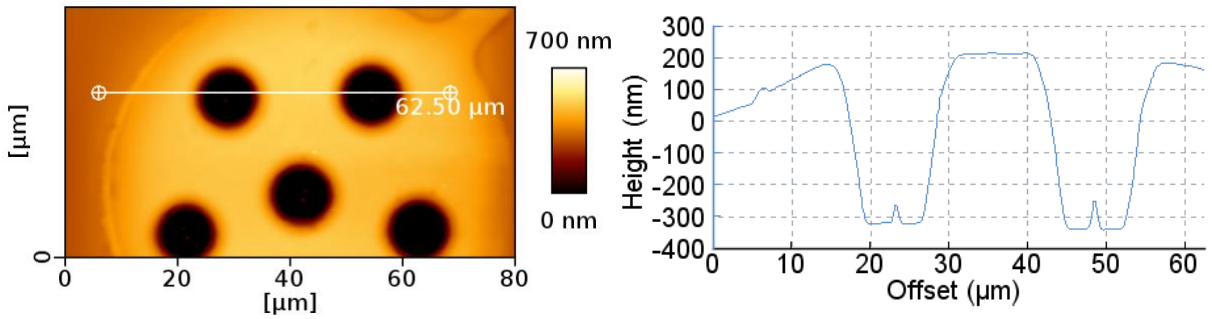
700 nm
0 nm
62.50 µm
[µm]
0
20
40
60
80
[µm]
300
200
100
0
-100
-200
-300
-400
Height (nm)
0
10
20
30
40
50
60
Offset (µm)

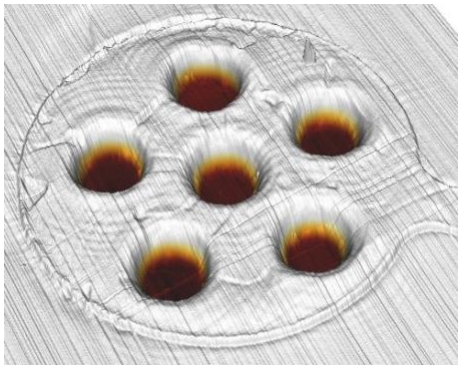

b)

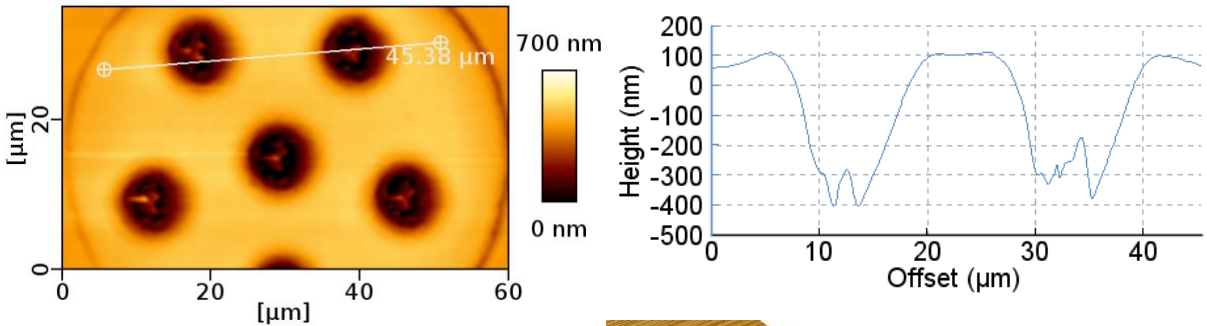
700 nm
0 nm
45.38 µm
[µm]
0
20
0
20
40
60
[µm]
200
100
0
-100
-200
-300
-400
-500
Height (nm)
0
10
20
30
40
Offset (µm)

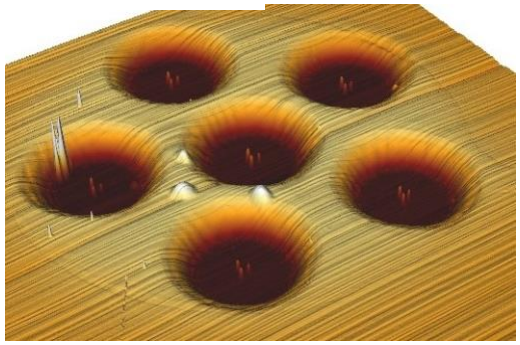

c)

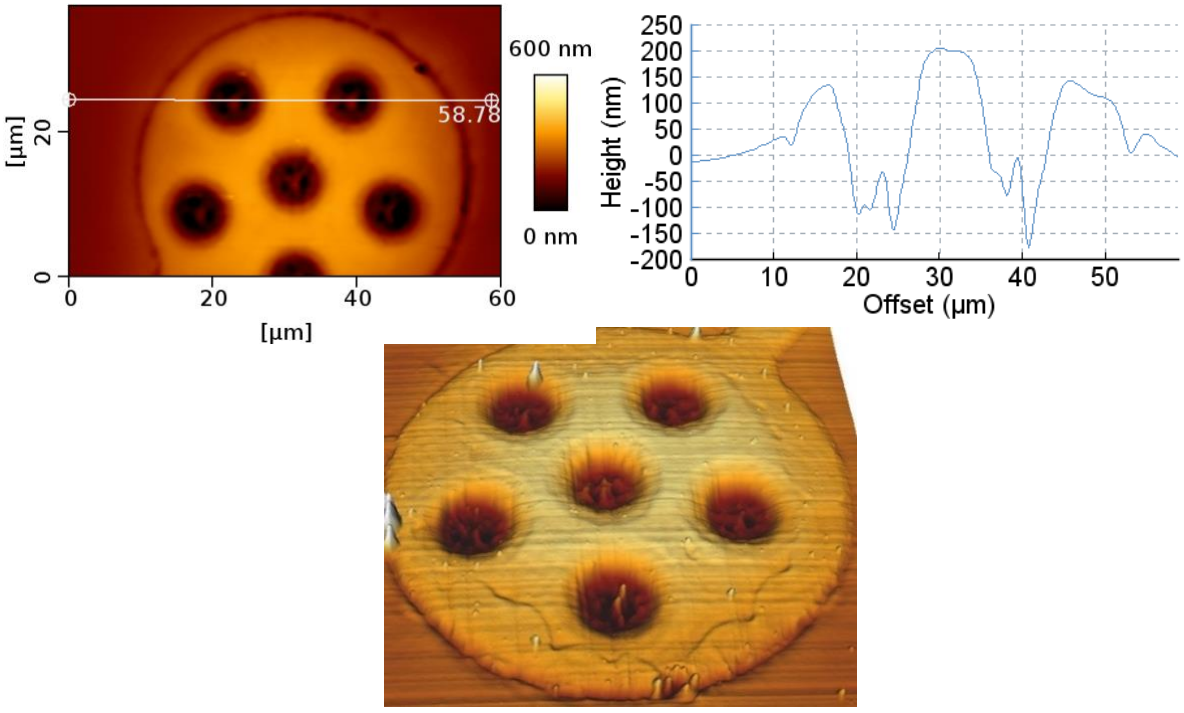

Figure 28: Digital representations of multi-well micro-electrode surfaces

Examples of the digital representations of multi-well micro-electrode surfaces using AFM to qualitatively determine the quality rating from 1 to 5, best to worst respectively. The white line shown on each two-dimensinal image (top-left) has an associated depth graph (top-right). (**a**) A micro-electrode with the best quality rating of 1. The well depth is approximately 500nm; no visible residues on the images; and the residue heights are <50nm as seen on the depth graph. (**b**) A micro-electrode where three spikes and some additional fabrication residues apear in the center of the wells. More specifically, the well depth is approximately 400 nm and residues heights are up to 150 nm in heigth. It was therefore given a quality rating of 2. (**c**) A micro-electrode with a quality rating of 3, as the well depth is approximately 250 nm and the residues heights are up to 175 nm.

Finally, heat maps were generated using MatLab by compiling the quality ratings of each micro-electrode in each MW-MEA into a 6 x 6 data matrix. To make the heat maps more continuous, a cubic interpolation was applied to the data from this matrix and a transformed 600 x 600 interpolated matrix was generated. Some examples are presented in figure 29. A red dashed line was also overlaid onto the heat maps indicating a quality rating of 1.5. This line indicates the estimated limits between multi-well micro-electrodes that have little or no debris (i.e. quality rating of 1) and all the other ones that have some debris and that could ultimately affect the recording resolution (i.e. quality rating of 2 to 5).

a)

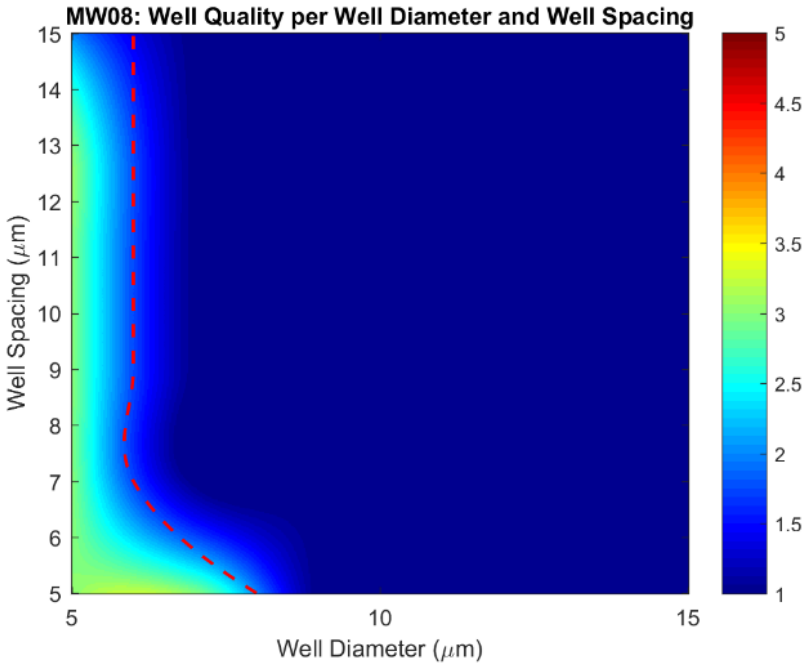
MW08: Well Quality per Well Diameter and Well Spacing
Well Spacing (μm)
Well Diameter (μm)
15
14
13
12
11
10
9
8
7
6
5
5
10
15
5
4.5
4
3.5
3
2.5
2
1.5
1

b)

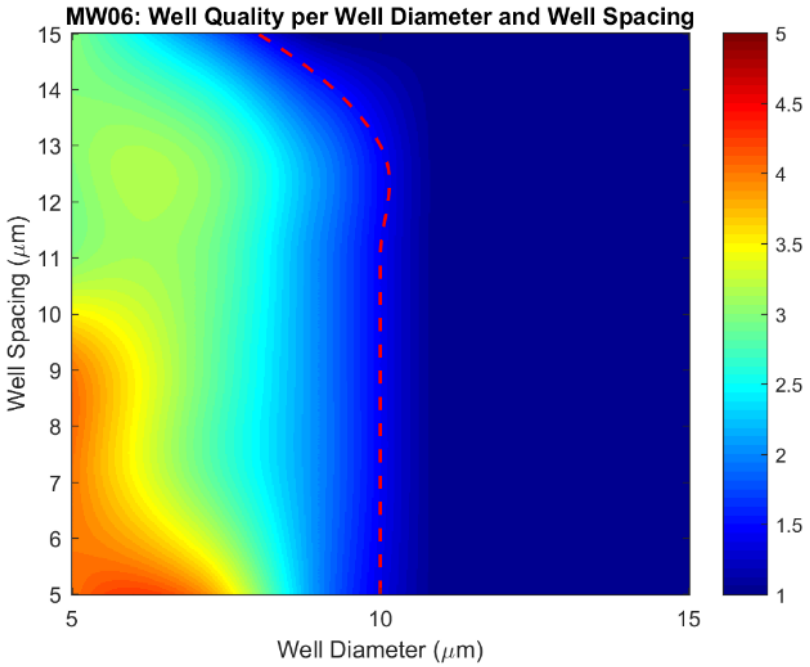
MW06: Well Quality per Well Diameter and Well Spacing
Well Spacing (μm)
Well Diameter (μm)
15
14
13
12
11
10
9
8
7
6
5
5
10
15
5
4.5
4
3.5
3
2.5
2
1.5
1

c)

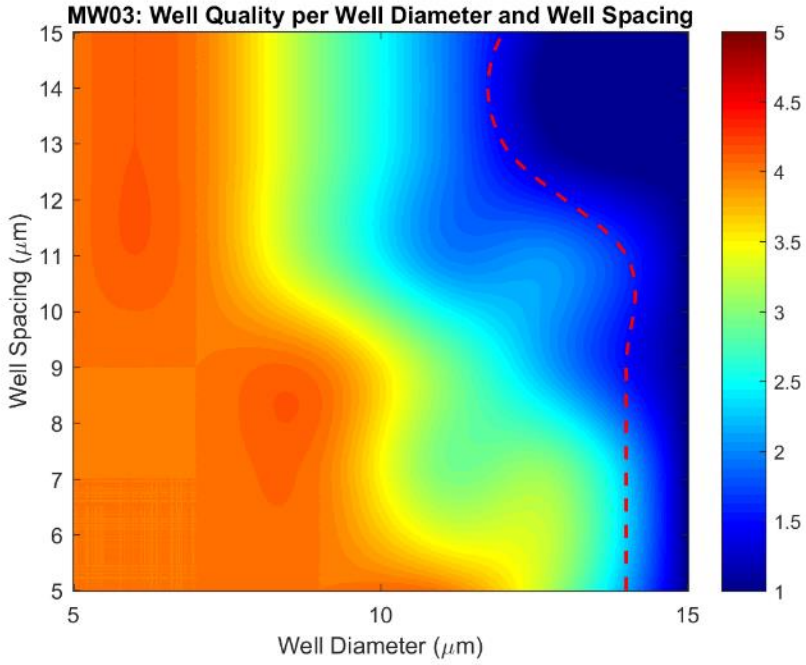

Figure 29: Heat maps showing the quality rating for different MW-MEAs

Examples of heat maps generated with 600 x 600 interpolated matrices showing the quality rating for different MW-MEAs. a) Most micro-electrodes have wells that are clear of debris, except when the well diameters are equal or smaller to 7 µm. b) Here, more debris are present in the wells of the micro-electrodes, especially in those with a well diameter smaller than 10 µm. c) This example shows an array of multi-well micro-electrodes were almost all the wells have some amount of debris, thus making this MW-MEA hardly usable.

Based on the analysis of the three-dimensional representation of the micro-electrodes' surfaces, the MW-MEA fabrication process was refined following an iterative process. It also informed on our fabrication limitations and how slight variations in identified fabrication steps could give rise to a wide range of variances with regards to electrode quality. This is very clearly represented in the above heat maps; the process used to create the MW-MEA in figure 29 (a) is far better than the process used to fabricate the MW-MEA in figure 29 (c).

Following the optimization of the fabrication process, the MW-MEAs were developed with a very limited number of micro-electrodes that had debris remaining in their wells (generally micro-electrodes with well diameters of 5 µm). This optimization allowed for better efficacy of the MW-MEAs by recording spontaneous electrical activity from mammalian neurons.

4.5 Recording mammalian neuronal activity with the multi-well micro-electrodes

Once fabricated, the MW-MEAs were cleaned, sterilized, and coated with a combination of PDL and Laminin to enhance the interfacing between the electrodes and the neurons (more details provided previously in chapter 2. Hippocampal or cortical neurons from Sprague Dawley rats (P0 to P1) were then cultured on the surface of the MW-MEAs and placed in an incubator (37°C, 5% CO_2) for 6 days. During this time, the culture media was regularly replaced and pictures were taken every 2 days to assess the development of the neural network. At day 7, MW-MEAs were positioned onto the extra-cellular recording system and spontaneous neural network activity was continuously recorded for 10 minutes, before the MW-MEAs were returned to the incubator. Recordings were conducted every one to two days until day 14 to evaluate electrical activity changes over time, both in terms of activated micro-electrodes and amplitude of signal recorded (Figure 30).

a)

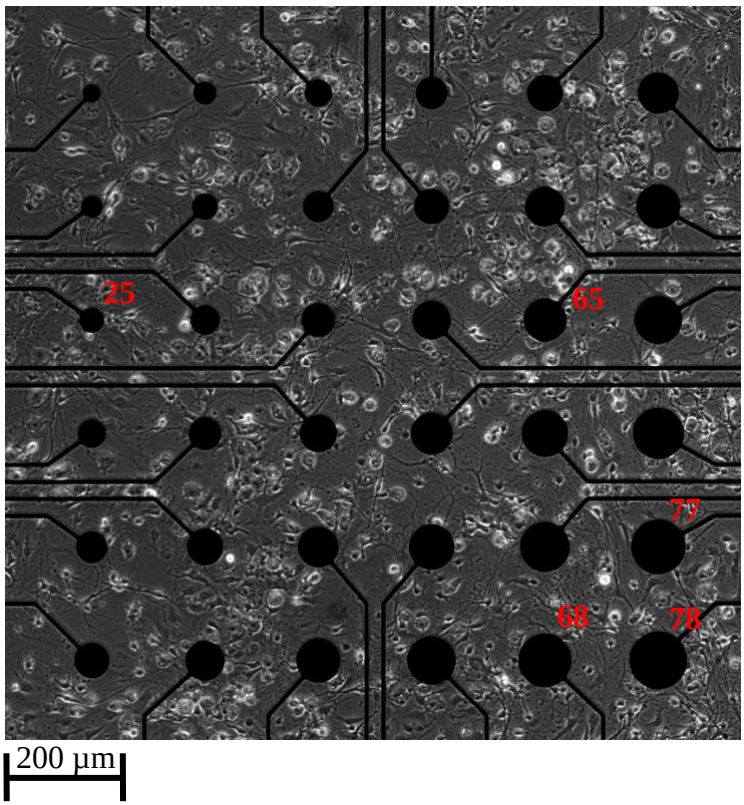

b)

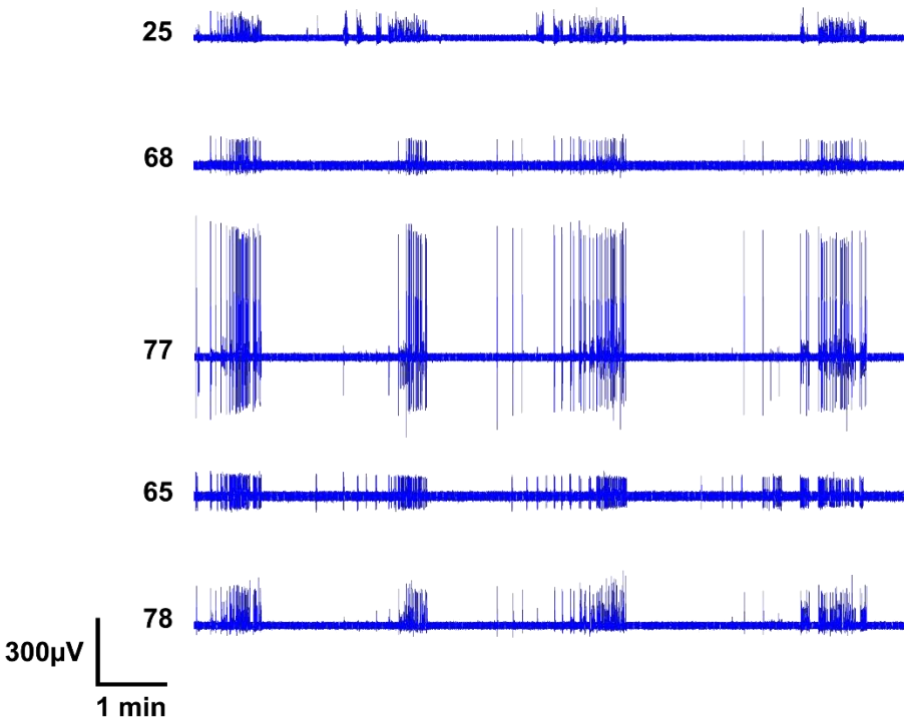

c)

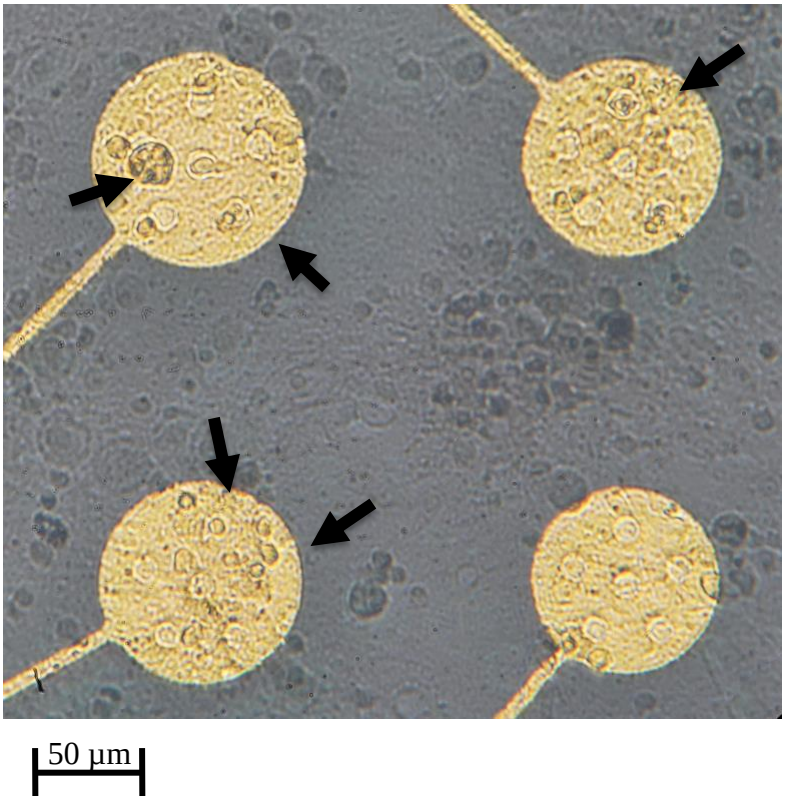

Figure 30: Neural network on the surface of a MW-MEA

Development of a neural network on the surface of a MW-MEA. a) 7 days after being cultured, hippocampal neurons from Sprague Dawley rats (P0 to P1) developed into a dense and healthy, well connected network (bottom up microscope image, electrodes appear as silhouettes). b) Spontaneous single action potentials and bursting events were recorded daily over several minutes and across the culture at different recording sites. Variations of signal amplitude is attributed biological and cell/electrode interfacing variabilities. c) Top-down optical picture shows four multi-well micro-electrodes with neurons of different sizes located inside the wells (black arrows).

Analysis of the recordings obtained demonstrated our ability to monitor neural network activity across multiple multi-well micro-electrodes simultaneously (Figure 30, b), with a maximum amplitude of up to 949 µV peak-to-peak (n = 34; Average peak-to-peak amplitude = 202 µV; Min and Max range peak-to-peak amplitude = 71 µV - 949 µV, Standard deviation = 166). The highest signal-to-noise ratio recorded was found to be 28.8. Note that for this analysis, only the activity with a signal-to-noise ratio superior or equal to 3 was considered. This arbitrary filtering was done to remove signals that were hardly distinguishable from the noise level, and were therefore susceptible to induce a misinterpretation of the results. Similar to the nano-edge micro-electrodes (chapter 3), the observed variability of recorded signal amplitudes is attributed to numerous application factors, mainly being cell-specific variables such as: 1) the size of the neurons and 2) the interfacing between their membrane and the micro-electrodes' well which can increase the sealing resistance.

Compared to other standards and commercially available devices used to monitor mammalian neurons, this resolution was significantly higher both in terms of maximum recorded amplitudes and signal-to-noise ratio (Figure 31). Indeed, and to best of our knowledge, whereas the maximum action potentials recorded with the MW-MEAs were approximately 450% higher than signals reported in the literature, the signal-to-noise ratio has also been improved by approximately 250%. These results also demonstrated our ability to reduce the recorded noise on average by 50% (29.9 µV, n = 50).

a)

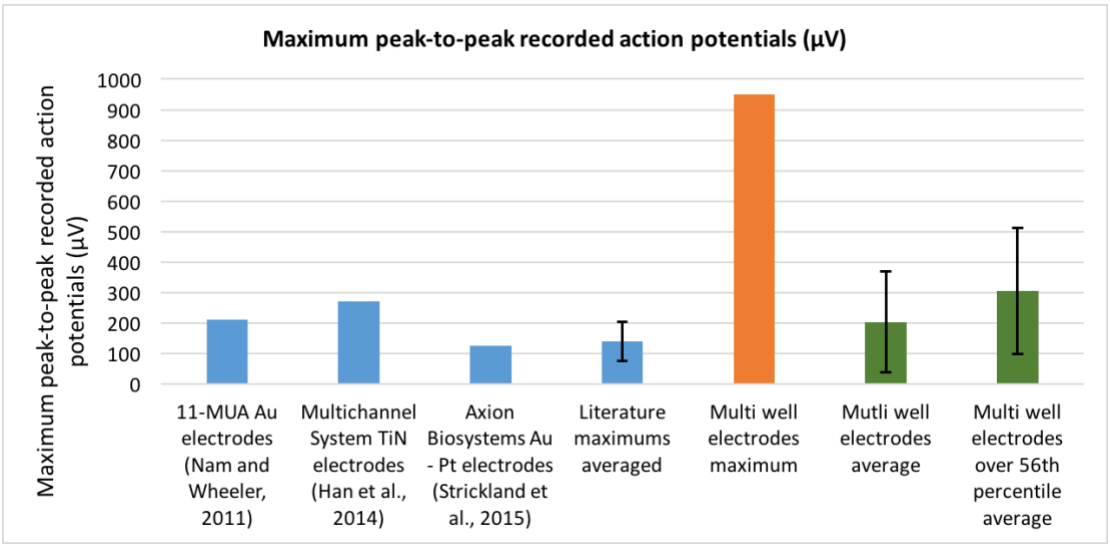
Maximum peak-to-peak recorded action potentials (µV)
Maximum peak-to-peak recorded action potentials (µV)
1000
900
800
700
600
500
400
300
200
100
0
11-MUA Au electrodes (Nam and Wheeler, 2011)
Multichannel System TiN electrodes (Han et al., 2014)
Axion Biosystems Au - Pt electrodes (Strickland et al., 2015)
Literature maximums averaged
Multi well electrodes maximum
Mutli well electrodes average
Multi well electrodes over 56th percentile average

b)

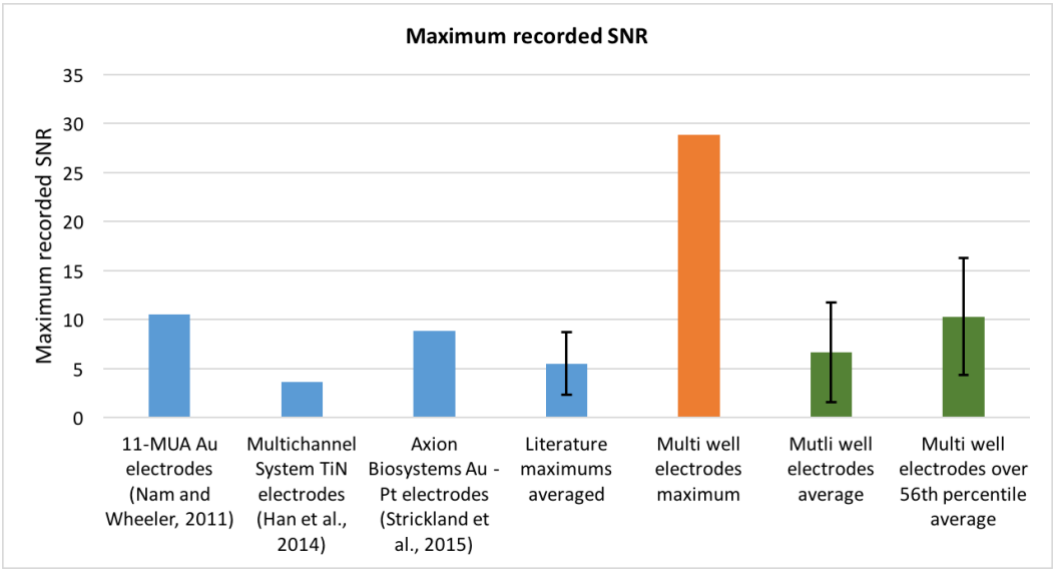
Maximum recorded SNR
Maximum recorded SNR
35
30
25
20
15
10
5
0
11-MUA Au electrodes (Nam and Wheeler, 2011)
Multichannel System TiN electrodes (Han et al., 2014)
Axion Biosystems Au - Pt electrodes (Strickland et al., 2015)
Literature maximums averaged
Multi well electrodes maximum
Mutli well electrodes average
Multi well electrodes over 56th percentile average

Figure 31: Comparison of the maximum reported peak-to-peak action potentials and SNR

Comparison of the maximum reported peak-to-peak action potentials (a) and signal-to-noise ratio (b) between the multi-well micro-electrodes and other planar micro-electrodes. Both the maximum amplitude (949 µV peak-to-peak) and SNR (28.8) recorded with the multi-well micro-electrodes are higher than other reported values.

4.6 Conclusion

Further to my the findings presented in Chapter 3, I was able to advance the design and develop the multi-well micro-electrodes for mammalian cells recording following an iterative fabrication process. Because of the increased sealing resistance, these new micro-electrodes could record neural activity from complex mammalian neural networks at the resolution of a single cell, which was higher than traditional devices, and at multiple sites simultaneously and over an extended time-period.

Interestingly, the resolution of recorded action potentials did not vary significantly between well diameters across MW-MEAs. This suggests that neither the overall micro-electrode diameters, nor their exposed surface areas (i.e. bottom of the wells) impacted the noise or signal levels. More specifically, we did not notice a significant difference in terms of signal-to-noise ratio between each specific multi-well micro-electrode (both in terms of X and Y variables, figure 32), suggesting that an improved sealing resistance was in effect at each micro-electrode sites (One-way ANOVA, $p = 0.899$). This implies that as long as a well is devoid of debris, any micro-electrode, no matter what the well diameter might be, had the potential to record activity with signal-to-noise ratios as high as any other micro-electrode. However, I did find a correlation between the number of recorded signal and the different well diameter, which were strongly correlated with the overall surface area of the wells (Spearman's correlation test, correlation coefficient = 0.986, figure 32). This suggests that the well diameters could be increased further (> 15µm in diameter) in a later version of the MW-MEAs to augment the probability of recorded

signals. Finally, in accordance with previous publications [94,120], an increase in the number of activated recording channels per MEAs between days 7 and 14 was noticed.

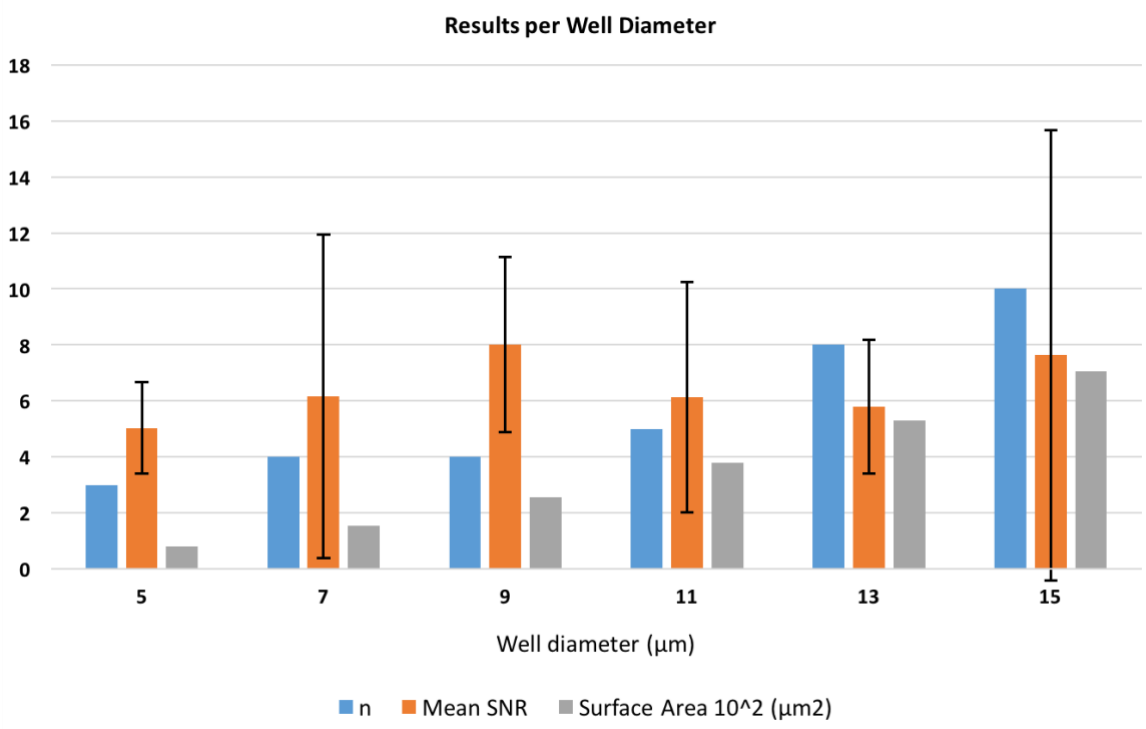

Figure 32: Analysis of the recorded activity using the MW-MEAs

Analysis of the recorded activity using the MW-MEAs per well diameters. No significant difference exists between the SNR recorded by each well diameter (orange). However, a correlation can be seen between the numbers of active micro-electrodes (blue) and their respective surface areas (grey).

This novel design will enable us to investigate synapse and network formation, as well as neuroplasticity over time. It is now possible to continuously record the spontaneous activity seen during network formation and to characterize it further to investigate network-associated phenomena (for example, the relationship and interdependence between axonal growth and synaptogenesis). By compiling data collected during neural network formation, the activity signature from single cells could be analyzed using a computational approach, thus further expanding our work presented in *Luk et al. 2015* [91]. Variables, mathematical coefficients and algorithms could then be created to help quantify and fully characterize the overall neural activity, differentiate various bursting patterns and understand the general network behaviors. These variables used to investigate the activity could for example include: the Inter-Spike Interval (ISI); the Frequency of Inter-Spike Interval (FISI); the Frequency of Action Potentials (FAP); the Frequency of Spikes per Cycle Period (FSCP) (Figure 33). Together, this new device and an appropriate computational analysis would allow researchers to better understand - and ultimately predict - the different stages associated with network formation (axonal growth, synaptogenesis, etc.) by looking at the electrical activity only. This to the best of my knowledge, has never been achieved in the field of neuro-development, especially with large inter-connected mammalian networks.

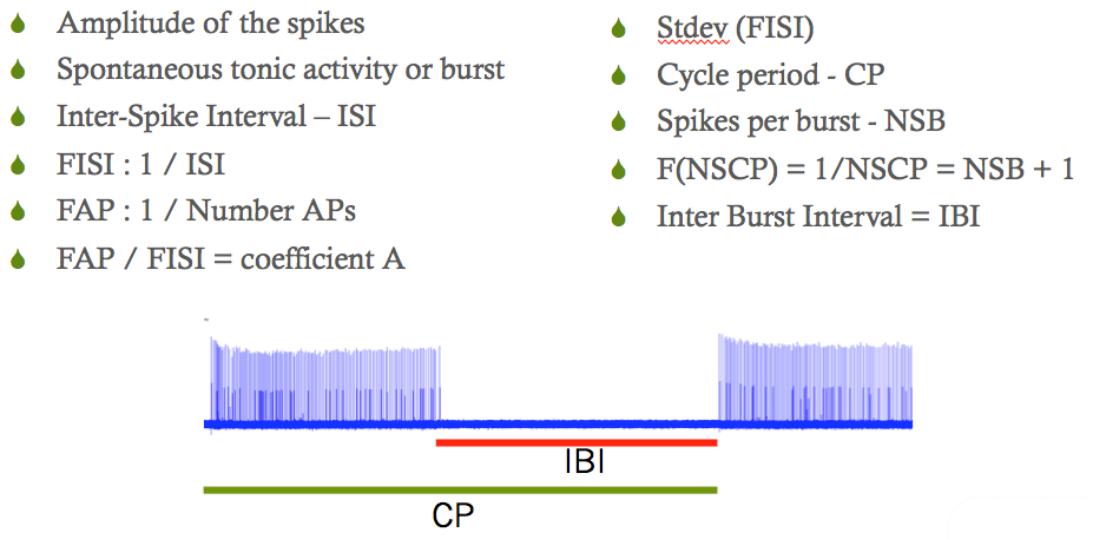

Figure 33: List of potential variables and coefficients for quantitative neural activity analysis

List of potential variables and coefficients that could be used to quantitatively analyze long-term neural activity at a single cell level.

In addition, this novel device could offer new opportunities to investigate aberrant network activity after applying extrinsic factors such as electrical stimulation or pharmacological compounds. For example, abnormal bursting events seen in epileptic patients undergoing seizures could be mimicked using a combination of 4-Aminopyridine, Bicuculline, high potassium or low sodium media, to trigger drug-induced seizure-like events *in-vitro* [121,122]. In turn, using a drug-screening approach, this induced aberrant activity could then be mitigated with anti-epileptic drugs or electrical stimulation, and lead to new approaches to discover more effective treatments for these patients.

Finally, because neural networks established in culture are 'artificial' and as such, the connectivity patterns studied in any given experiment may vary from preparation to preparation, many labs have opted to use multi-electrode arrays to record activity in intact brain slices [123–125]. I therefore decided to look into opportunities to develop another device that would answer the needs of recording from these more preserved networks that are seen *in-vivo* (e.g. brain slices).

.

Chapter 5: A novel three-dimensional micro-electrode chip that permits long-term neuronal recordings from intact brain slices.

The following chapter comprises sections published in the following manuscripts/patent or presented at conferences:

Manuscript:

- **Wijdenes P.**, Gavrilovici C., Lijnse T., Armstrong R., Rho J.M., Dalton C, Syed N.I. *Novel three-dimensional electrodes enable high-resolution brain slice recordings*. Manuscript submitted to a peer-reviewed journal.

Conferences:

- **Wijdenes P.**, Armstrong R., Gavrilovici C., Rho J.M., Syed N.I., Dalton C. *Novel 3-dimensional gold micro-electrodes allow high resolution neural network recording.* SPIE BiOS Photonics West, San Francisco, USA – Podium presentation (2017).

- **Wijdenes P.**, Gavrilovici C., Armstrong R., Dalton C., Rho J.M., Syed N.I. *High-resolution recording of seizure-like network activity using novel 3-dimensional gold electrodes*. American Epilepsy Society, Houston, USA – Poster presentation (2016).

Patent:

- **Wijdenes P.**, Dalton C. *Novel 3-dimensional micro-electrode arrays for enhanced neural recordings of tissues.* United States Provisional Patent Application No.62/481,473 filed April 4, 2017.

5.1 Introduction

The inability to monitor the activity of large neuronal ensembles over extended time periods undermines the potential to fully understand their function, and how best to repair damaged tissue following trauma, injury or neurodegenerative diseases [126–128]. This lack of fundamental knowledge partly stems from the lack of tools that would allow the monitoring of neural activity from complex, synaptically connected networks - at a higher, spatio-temporal resolution and over an extended time period. In this chapter, I set out to develop means of recording activity from an intact brain slice.

While useful in their utility to monitor neural activity at multiple sites, conventional MEAs with traditional planar micro-electrodes present some limitations [75,129]. Indeed, when interfaced with neural tissue, the signal-to-noise ratio (SNR) offered by these electrodes is often low and precludes longer-term recording of spontaneously active networks at a higher resolution. These limitations are due mainly to three factors: 1) traditional planar electrodes only record neural activity from the outer and "traumatized" layer of the brain slices, which harbor a larger population of either dead or dying cells [124]; 2) the tissue injured during slicing often releases proteases and ions - such as potassium and sodium - which in turn result in excitotoxicity of the adjacent area, thereby resulting in further tissue damage at the site of recording. Moreover, the released ions can also be detected by the electrodes in surrounding areas and generate signaling artifacts; 3) the perfusion system required to provide a continuous flow of nutrients and oxygen at a set temperature creates a flow of charged ions within the recording chamber and around the electrodes, thus

generating electrical noise (Figure 34). Thus, recording long-term activity from neurons embedded within a brain slice is therefore difficult when using planar micro-electrodes [130].

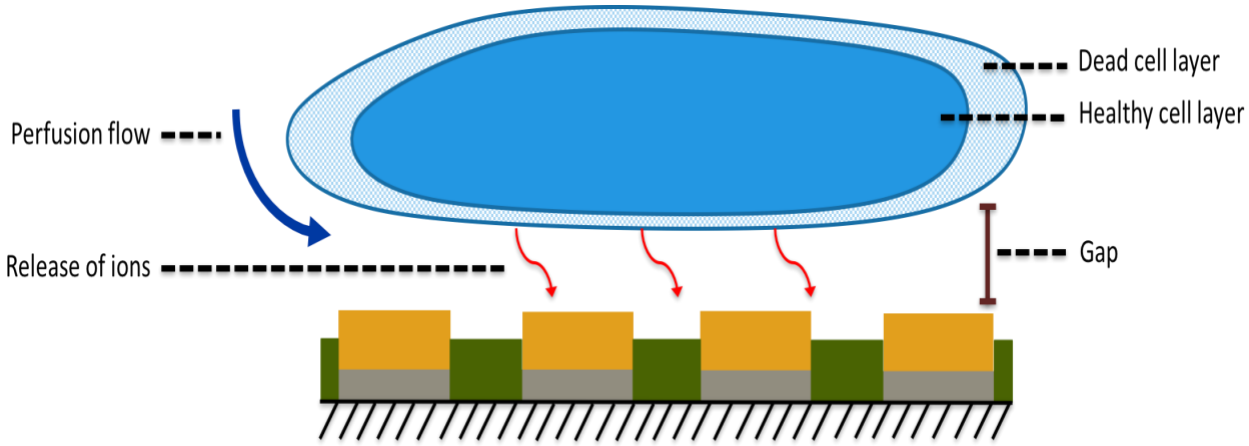

Figure 34: Schematic of a brain slice positioned on top of the traditional planar micro-electrodes

Schematic of a brain slice positioned on top of the traditional planar micro-electrodes, showing the inherent disadvantages, specifically the lack of electrical connection to the healthy cells located within the interior of the brain slice.

Even in those instances where recordings are possible, the above stated factors make data collection and interpretation inconsistent. While several types of protruding three-dimensional electrodes, like spine-shaped protrusion electrodes [117], carbon nanotube electrodes [85], metal-transfer-micromolded electrodes [130–132], have already been developed by research groups to record activity in brain slices, their efficacy in recording action potentials is often suboptimal due to low SNR [75]. I thus opted to develop a new MEA enabling slice penetration with minimal tissue invasion (i.e. that do not significantly damage brain slices to the same extent as compared to previously reported devices), as this would considerably enhance the quality of recordings by improving the cell-electrode interface.

This chapter presents the main results associated with the design and development of a novel MEA with three-dimensional gold micro-electrodes: the Neural Tissue MEA (NT-MEA). Based on my data presented above, I hypothesized that this new three-dimensional structure will allow the recording of healthy mammalian cells located inside the neural tissue, at a resolution higher than traditional planar micro-electrodes.

The following sections presented in this chapter describes:

- The iterative design and development process followed to fabricate the three-dimensional micro-electrodes;
- The recorded neural activity obtained with these three-dimensional micro-electrodes
- A comparison with other existing traditional planar micro-electrodes.

5.2 Over-coming the challenges of three-dimensional electrodes fabrication with an iterative fabrication process

From the observation that none of the existing three-dimensional micro-electrodes offer a very high SNR compared to traditional planar electrodes, we decided to develop an in-house fabrication technique exploring the potential of wire-bonders [133]. Traditionally, wire-bonders are used to interconnect different conductive elements present on integrated circuit or semiconductor devices and their packaging during the fabrication process. More specifically, using a ball-bonding method, a wire can be attached at both ends of the elements using a combination of downward pressure, ultrasonic energy, and in some cases heat (to make the metal softer), to create a weld caused by a so called thermosonic bonding process. It is generally considered the most cost-effective and flexible interconnect technology and is used to assemble a majority of electronic devices, including consumer-goods. This technique was therefore implemented on top of traditional planar micro-electrodes.

5.2.1 Three-dimensional gold micro-electrodes design

Similar to the previous chapters, planar electrodes in an 8x8 array configuration were fabricated using standard photolithography onto 49 x 49mm, 1mm thick glass. The glass was coated with ~300 nm gold, deposited on a ~50 nm chrome adhesion layer by sputter deposition. Sizes and intervals between the circular electrodes were adjusted according to experimental needs using

different photomasks in the photolithography process. For this first attempt, electrodes of 100µm diameter, with inter-electrode spacing of 500µm, were fabricated to fit the experimental requirements of recording from the hippocampal region of mice brain slices. An epoxy photoresist (SU8), was then spin coated over the entire electrode array, and the SU8 layer was patterned with a second photomask to leave the planar electrodes bare of SU8 insulator. At this stage, only the connecting wires were insulated (Figure 35).

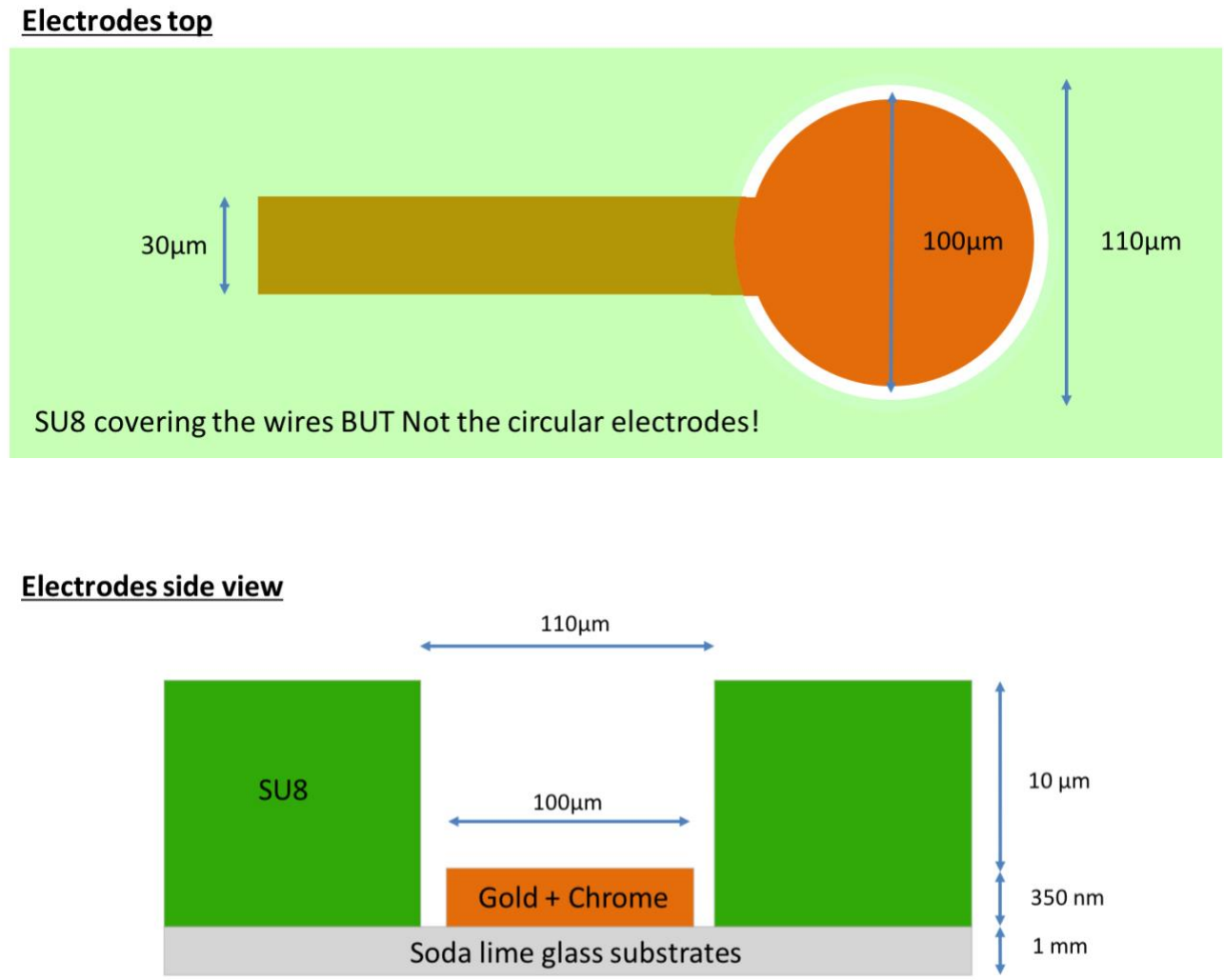

Figure 35: Schematic of the initial version of the planar micro-electrodes

Schematic of the initial version of the planar micro-electrodes used to create the base required to fabricate the three-dimensional micro-electrodes.

Spike-shaped three-dimensional gold electrodes were then added onto the surface of the planar electrodes using a manually programmable wire bonder (West-Bond model 454647E, West-Bond Inc., USA). These spikes were created by bonding gold wires onto the planar electrodes, manually extending the wires to a set height, and then cutting them with micro-scissors mounted on micro-manipulators (Figure 36).

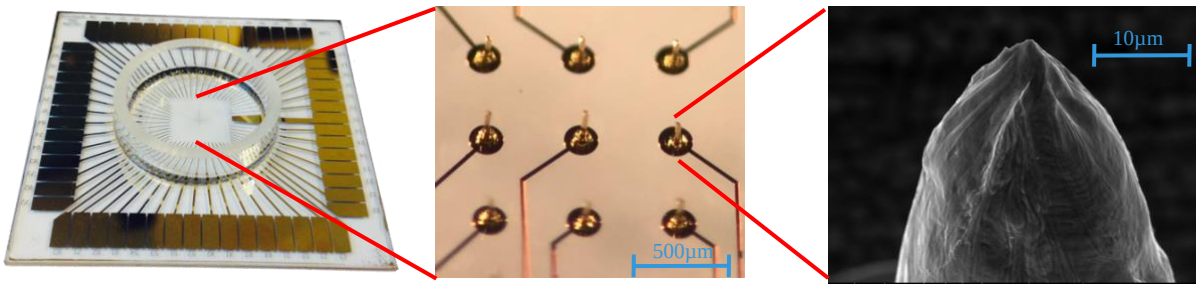

Figure 36: Images of the NT-MEA and its array of three-dimensional micro-electrodes

From left to right; Left: picture of the whole 49mm x 49mm square multi-electrode array chip. The rectangular gold pads on the four sides allow the connection between the recording setup and the 3-dimensional micro-electrodes present in the center. Middle: close up picture showing a section of the array of gold three-dimensional electrodes under an optical microscope. Each electrode is separated by a 500µm gap from each other. Right: picture of an uncoated tip from a three-dimensional electrode obtained with a Scanning Electron Microscope (SEM). The electrode diameter and the sharpness of the tip allows for optimal penetration within the brain slice, which limits the invasiveness.

However, it was noticed that at this stage of the fabrication process, the bonding process was not always successful. In fact, out of 59 micro-electrodes sites per MEA, an average of 31 (53%, n=4, standard deviation of 3.3) were correctly bonded. While different parameters were adjusted to maximize the reliability and strength of a wire bond (temperature, ultrasonic energy, speed, etc.), the inherent downward physical pressure created by the tip of the bonder on the planar micro-electrodes was often the cause of these damages, leaving the ends of the wires considerably impaired. To optimize the success rate of the wire bonding step, the design and fabrication parameters needed to be adjusted. The following parameters were considered:

- While wire-bonders are usually used to create interconnections between conductive domains of 1 to 3 µm thick, the thickness of our planar micro-electrodes was 350nm. This was probably one of the main reasons for having the circular planar micro-electrodes being ripped off;
- Most bonding techniques are employed in a clean room environment, thus preventing particles in the air affecting the bonding of the gold wires on the planar micro-electrodes;
- The ceramic tip that allowed the bonding-ball to be formed, and through which the gold wire was passing, was too wide and did not easily allow the ball to go through the well in which the planar micro-electrodes were located.

Based on this initial results, and following an iterative process, the NT-MEA was re-designed to prevent the planar micro-electrodes being ripped off during the bonding process. The modifications are presented in the following section.

5.2.2 Second design

Based on this initial experience, more robust planar micro-electrodes that could better handle the bonding process and not be damaged to such an extent were designed. Three major improvements were made (Figure 37):

- The thickness of the planar micro-electrodes was increased from 350 nm to 650 nm (50nm of Chrome covered by 600nm of Gold) to improve the probability of the bonding ball to stick correctly on the surface of the planar micro-electrodes.
- The overall diameter of the circular micro-electrodes was increased from 100 µm to 190 µm.
- The sides of the planar micro-electrodes were covered (40 µm on each side) with the insulating SU8, which brought more rigidity to the overall planar micro-electrodes.
- A thinner ceramic tip was chosen to permit the gold bonding-balls to go through the wells in which the planar micro-electrodes were located.

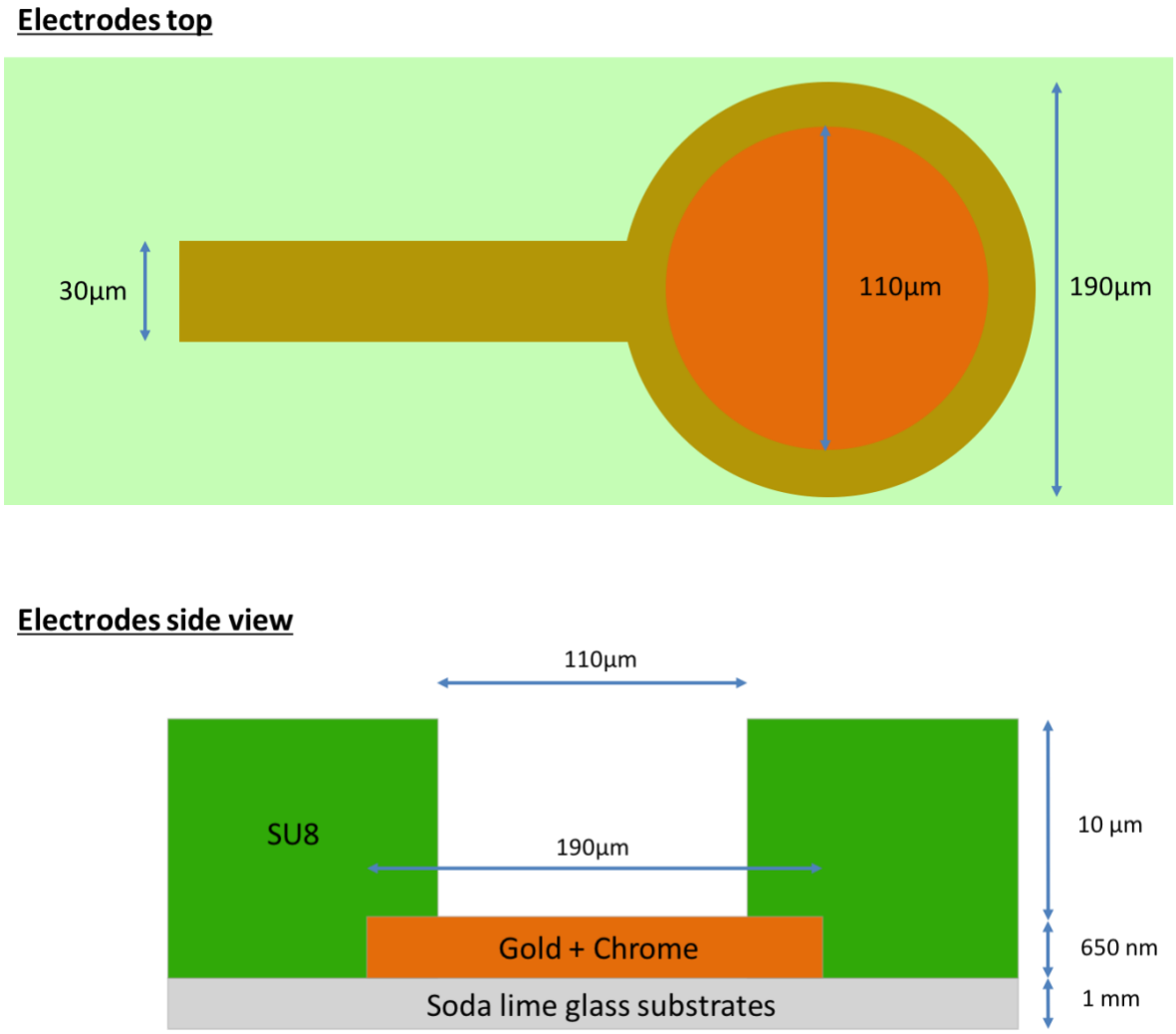

Figure 37: Schematic of the second version of the planar micro-electrodes

Schematic of the second version of the planar micro-electrodes used to create a more robust base needed to fabricate the three-dimensional gold micro-electrodes. Both the diameter and thickness of the planar micro-electrodes were increased to add more rigidity to their overall structure and facilitate the bonding process.

Overall, this method yielded full control and flexibility in the size (diameter of the gold wires used and their heights) of each single three-dimensional electrode, inter-electrode spacing, and materials used (gold, palladium, platinum, etc.). The electrodes were individually fabricated and were individually electronically addressable. For example, the three-dimensional gold electrodes reported here were fabricated with controlled heights ranging from 50µm to 400µm and a diameter of 25 to 15µm depending on the bonder wires used (Figure 39). These heights, spacing and materials were chosen specifically for recording from 400µm thick acute brain slices of mice, and can be adjusted individually to suit other experimental or clinical needs.

Following the fabrication of this second design, three-dimensional micro-electrodes were individually created on the top of the more robust planar micro-electrodes. This time, out of 59 micro-electrodes sites per MEA, an average of 51 (86%, n=4, standard deviation of 3.6) were correctly bonded. This new design therefore improved significantly the number of three-dimensional spikes that could be successfully created (two tailed p value = 0.0002, Student's t-test, figure below 38)

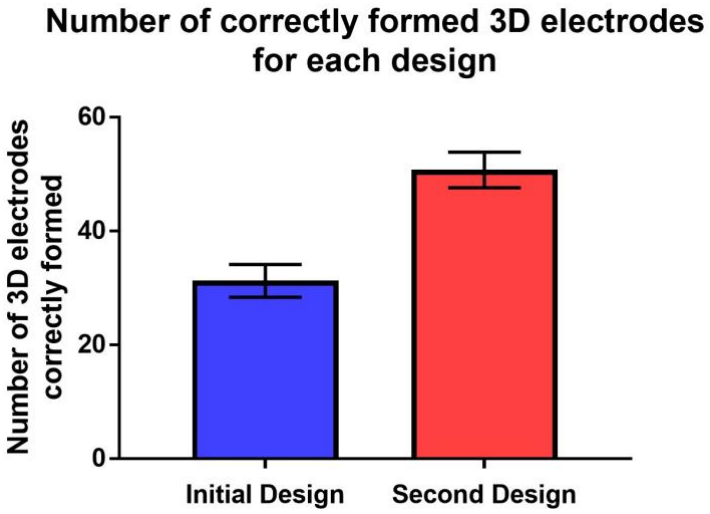

Figure 38: Statistical analysis of the number of correctly formed three-dimensional micro-electrodes

Number of three-dimensional spikes that could be successfully created on top of the planar micro-electrodes (two tailed p value = 0.0002)

5.2.3 Insulating the base of the three-dimensional micro-electrodes

Finally, a second insulating layer (the same photoresist used previously, SU8) was locally deposited on the bases and edges of the newly formed three-dimensional electrodes using a sharp glass micropipette (fabricated with a Vertical Pipette Puller, Model 700C, David Kopf Instruments, USA; and thin-wall glass tubes, TW150F-6, World Precision Instrument Inc., USA) with a 30µm tip opening whose positioning was accurately controlled using a 3-axis micromanipulator (M3301R, World Precision Instrument Inc., USA). The micropipette was connected through a tube to a syringe containing the SU8 photoresist, which was itself mounted on a syringe micro-pump to control the flow (Dual infusion/withdrawal pump model 942, Harvard Apparatus Co., Dover, MA, USA). See figure 39 for details. The photoresist SU8 was only deposited at the base and trunk of the three-dimensional micro-electrodes, leaving the tips bare of insulator and ensuring a direct contact with the healthy neurons located inside the brain slices (Figure 40, f).

a) b)

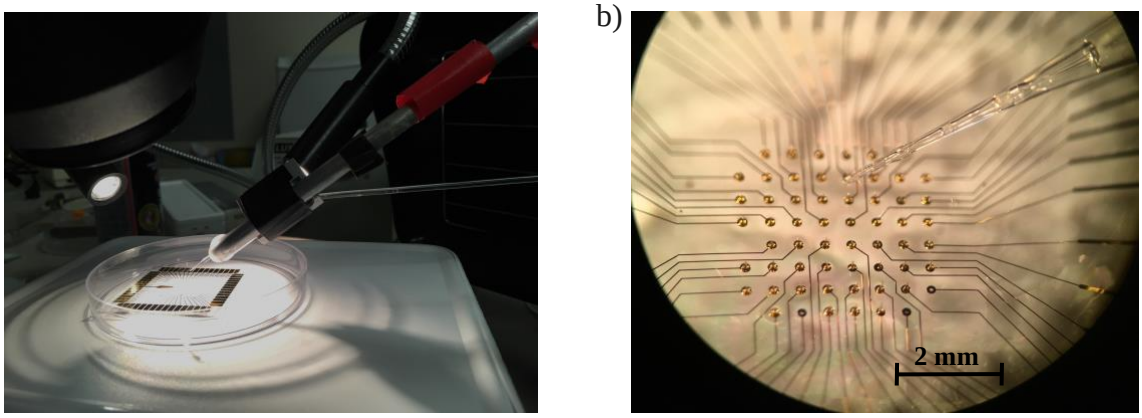

Figure 39: Deposition of the SU8 on the surface of the NT-MEAs

Deposition of the SU8 on the surface of the NT-MEAs. a) The sharp glass micropipette with an opening of 30 µm is mounted on the arm of the micromanipulator and carefully positioned on top of the NT-MEA under the microscope. b) Under the optical microscope, the tip of the sharp glass micropipette filed with liquid SU8 is approached to the surface of NT-MEA and locally disposed at the base of the three-dimensional micro-electrodes.

Once correctly deposited, the liquid SU8 was cured with broad spectrum Ultra-Violet (UV) light. This custom designed process allowed the three dimensional electrode tips to be left bare of insulator for the last few µm, so that they would be in direct contact with the healthy neural cells inside the brain slice (see figure 40 for a schematic describing the overall fabrication process). Using this highly customizable process, the amount of surface area in direct contact with the cells (bare of insulator) could be adjusted depending on experimental needs. Finally, a glass ring surrounding the electrode area was placed on the device to form the recording chamber, and sealed in place with PDMS.

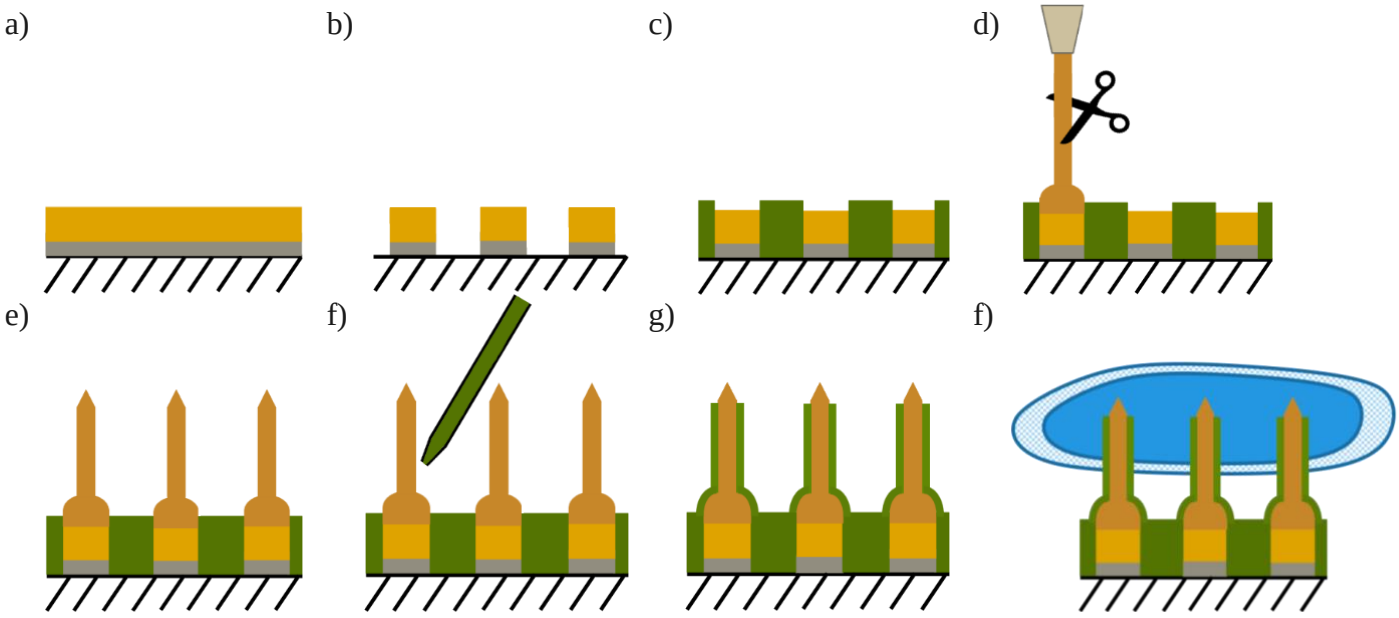

Figure 40: Schematic of the fabrication process of the three dimensional gold micro-electrodes

Schematic of the fabrication process of the three dimensional gold micro-electrodes: a) to c), metal electrode deposition and patterning; d) and e), Three-dimensional spike electrode fabrication onto planar electrodes; f) and g), insulation layer deposition and f), schematic showing only the bare tips of the electrodes directly interfacing with neural cells located inside the brain slice, i.e. within the remaining healthy tissue.

5.3 Brain slice recording using the NT-MEA

Following the fabrication process described previously, and after cleaning and sterilizing the MEAs, Poly-D-Lysine was used as a coating material to enhance the interfacing between the electrodes and the neurons (see chapter 2 for more details). Acute hippocampal brain slices (400µm thick) from wild-type mice littermates (P35) were then positioned with the help of an optical microscope in the recording chamber and anchored onto the electrode arrays by means of a mesh (or "harp", SHD-26H/2, Warner Instruments, USA) (Figure 41 b). The mesh was used to prevent any movement of the brain slice and to facilitate the penetration of the three-dimensional electrodes onto the tissue. Using a temperature controller connected to a perfusion system, both the temperature (33.0°C) and the oxygenated media (5% CO_2, 95% O_2) were controlled in the recording chamber of the NT-MEA's (Figure 41 a).

a)

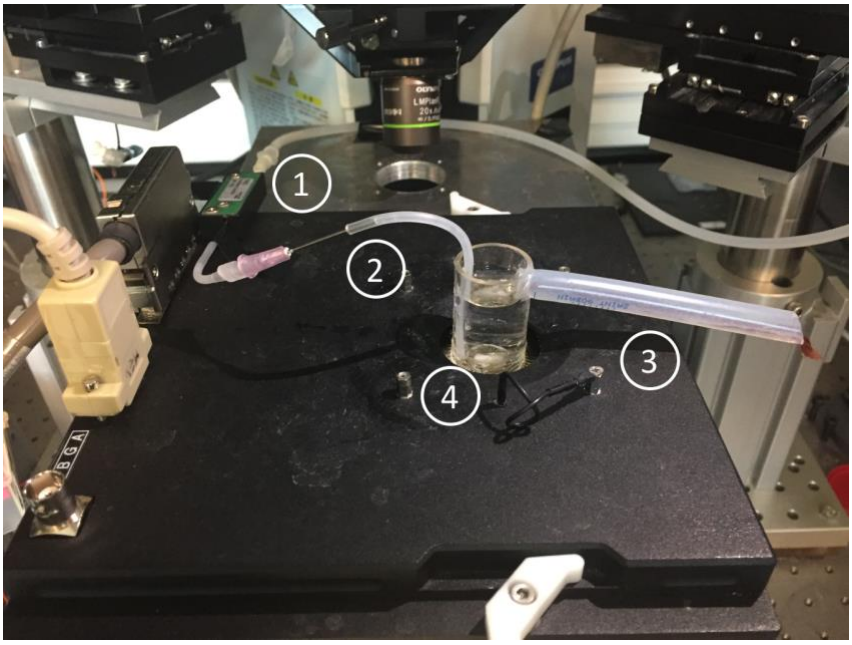

b)

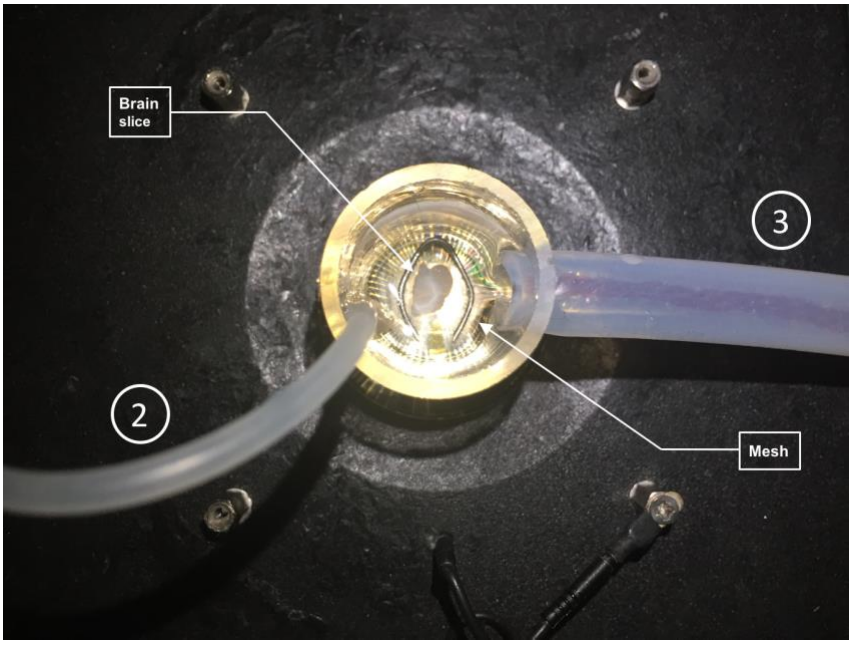

Figure 41: Recording of an acute hippocampal brain slice using the NT-MEA

NT-MEA positioned into the recording system with an acute hippocampal brain slice positioned at the center of the recording chamber (4). a) aCSF saturated with carbogen at a temperature of 33.0°C (1, heated cannula) was perfused inside the chamber (2, left tube) and sucked out at the bath level interface (3, right tube). b) A mesh was placed on top of the brain slice to prevent any movement and facilitate the penetration of the three-dimensional electrodes into the slice.

To test the recording capabilities of these new electrodes under specific experimental conditions that trigger spontaneous neural activity at the network level, the chamber was perfused with either one of three types of aCSF: "normal" or control aCSF, 0mM Mg^{2+} aCSF, high 8.5mM K^{+} aCSF (all at ~32°C, with 5% CO2, 95% O2). These changes in ionic concentration allowed spontaneous neural activity to occur within the brain slices and are well-known strategies used to induce spontaneous seizure-like activity [125,134,135]. As could be expected, no activity was recorded in "normal" aCSF.

However, shortly after positioning the acute hippocampal brain slice over the electrodes in an activity triggering aCSF (0mM Mg^{2+} or high 8.5mM K^{+}), spontaneous neural activity was consistently recorded (n = 55, 98% of the time) *in-vitro* at multiple electrode sites and across the different channels. The recorded neural activity could be tracked within the entire brain slice and patterns of propagation were identified (Figure 42). This activity consisted of bursting pre-ictal and ictal events, either localized or spread across different areas of the brain slices, with high frequency activity (80 Hz) often seen in mammalian brain systems undergoing seizures [136–138]. For example, while it was anticipated that we could record neural activity mostly within the well-studied region of the hippocampus, we also recorded high-frequency bursting activity in the mid-brain and thalamus regions simultaneously.

a)

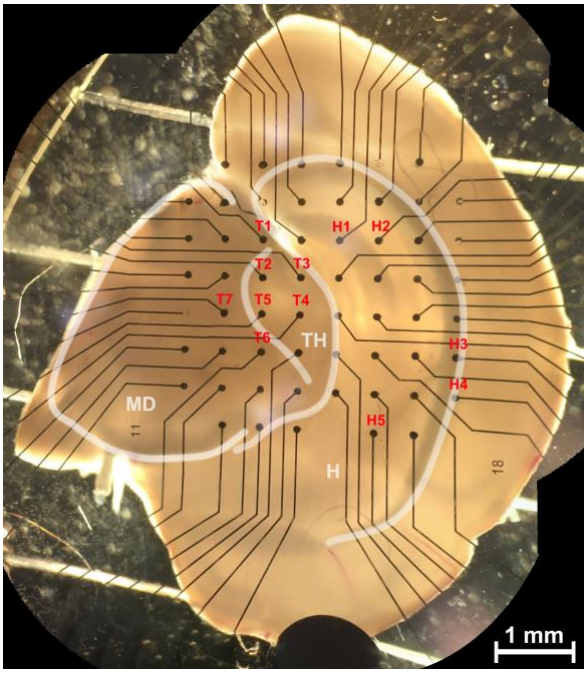
T1
H1
H2
T2
T3
T7
T5
T4
T6
TH
H3
H4
MD
H5
H
1 mm

b)

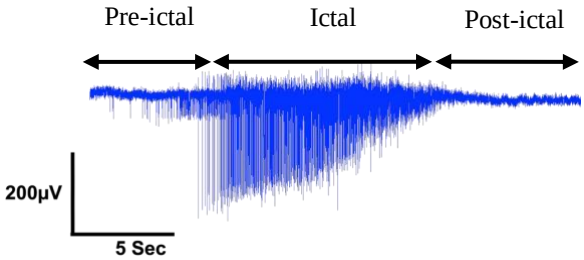
Pre-ictal
Ictal
Post-ictal
200μV
5 Sec

c)

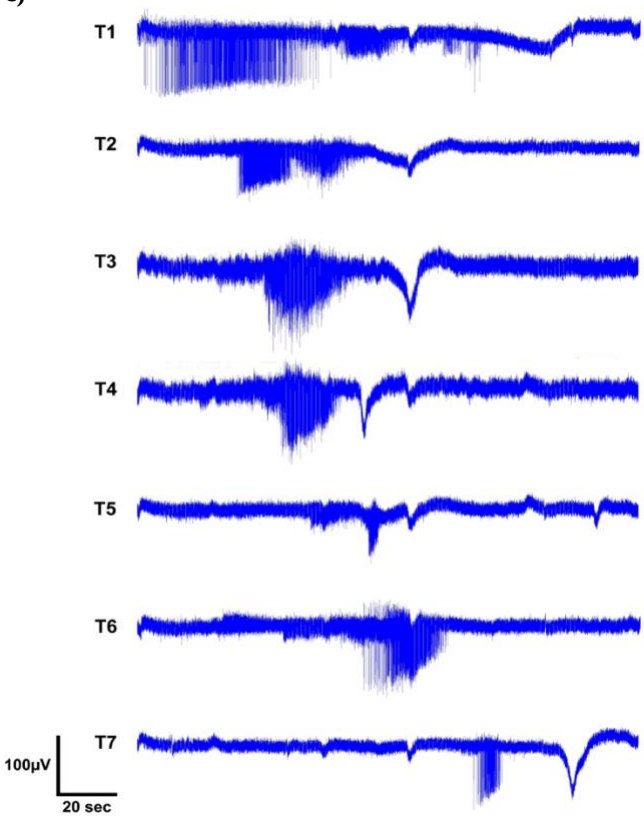
T1
T2
T3
T4
T5
T6
T7
100μV
20 sec

d)

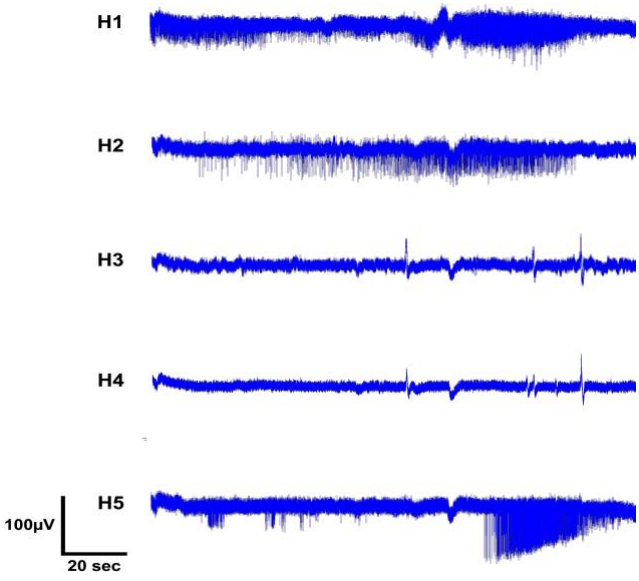
H1
H2
H3
H4
H5
100μV
20 sec

Figure 42: Image and recordings of an acute hippocampal brain slice

a) Picture of an acute hippocampal brain slice positioned on an array of electrodes taken with an optical microscope. Areas such as the mid-brain (MD), thalamus (TH) and hippocampus (H) are clearly visible. b) Example of bursting neural field potential recorded with the three-dimensional gold micro-electrodes (high 8.5mM K^+). Various type of activity were recorded, including pre-ictal and ictal-like events. c) Activity recorded within the thalamus and mid-brain from the same brain slice a). d) Simultaneously, activity was recorded within the hippocampus (CA1, CA2 and pyramidal layer)

The Signal-to-Noise Ratio of these gold three-dimensional micro-electrodes was then compared with earlier reported devices. While, to the best of my knowledge, the SNR of other three-dimensional electrode is not reported, traditional planar micro-electrodes have been more often used by various research groups, including ours, and are therefore well characterized [75,91,108]. Our novel three-dimensional gold micro-electrodes offered a reduced average noise of 20-30μV (compared to 50-70μV for traditional planar micro-electrodes [108]) which we attribute to the insulating coating present at the bases and edges of the spikes. Also, the highest recorded field potential activity peak-to-peak was in the mV range (3.2 mV, compared with signals of < 1mV with traditional planar micro-electrodes [75]). Overall, these new electrodes offer a significantly higher signal-to-noise ratio (> 300% better) than previously reported devices using traditional planar micro-electrodes.

Finally, as the bases and edges of the electrodes were insulated, we recorded activity from within the brain slice where most electrically active cells remain viable [124], thus enabling continuous recordings over 30 minutes (n = 9), sometimes over several hours (n = 4) at a resolution higher than traditional planar micro-electrode MEAs [75]. It is worth noting that the cured SU8 on the electrodes edges also provided strong structural support, which reduced the physical degradation of the three-dimensional electrodes over time; these made our NT-MEAs reusable (average of 10 times per MEA).

5.4 Conclusion

Following an iterative design process allowing the refinement of their morphological structures, the three-dimensional insulated gold micro-electrodes fabricated here offered several unique opportunities to record and monitor neural network phenomena both across and within intact brain slices (i.e. not from the traumatized outer layer). In addition, using an appropriate coating deposition method, the Signal-to-Noise Ratio was increased compared to traditional planar micro-electrodes, thus enabling the analysis of neural networks events (including seizure-like events) at a higher signal resolution, with less electrical noise, and sometimes for more than 1 hour. Compared to traditional planar micro-electrodes, this device offers new opportunities to investigate the effect of extrinsic factors on mammalian neural tissues.

Indeed, several research groups around the world have attempted to analyze seizure-like activity using neural networks from mouse or rat brain slices [89-91]. However, these studies commonly used commercially available planar electrodes or in-house developed devices that hardly permit a computational analysis of epileptic phenomena due to poor signal-to-noise resolution [26]. With the aid of this new technology, it is now possible to further explore spontaneous activity from complex and intact networks, as well as synaptic plasticity (e.g., long-term potentiation, etc.), over an extended time period. This new device will also allow monitoring of both spontaneous and induced seizures in slices obtained from genetically-engineered mouse models (e.g. Kcna1-null littermate mouse brain slices), as well as tissues surgically resected from

human epileptic patients, and serve as a powerful tool for drug screening in functionally connected neural networks. Also, drugs known to induce seizure-like activity (4-Aminopirydine, Bicuculline) could be used to trigger abnormal bursting activity patterns, that could then be mitigated using a combination of different AEDs or electrical stimulations. Such an approach would help researchers and clinicians to understand the cellular mechanisms underlying such pharmacological treatments.

Finally, these three-dimensional micro-electrodes could also offer a significant opportunity to envisage implantable electrodes positioned on a flexible membrane (e.g. silicon), to either record or stimulate brain activity *in-vivo*. This relatively simple and adaptable fabrication method allows the development of sharp micro-electrodes as thin as 15µm in diameter (limited by the metal wire diameters used in the wire-bonding process), which minimizes tissue damage and/or scar formation[139]. These results would then need to be compared with other existing implantable devices that are often considered too invasive[140,141,142].

Chapter 6: General conclusion and discussion

Progress in the field of neurosciences is generally hampered because of the lack of appropriate electrophysiological tools that permit concurrent monitoring and analysis of large networks of brain cells. In this study, I have attempted to either build upon existing technology or to develop novel and highly sensitive electrophysiology tools that permit the analysis of neuronal activities from single cells to complex neural networks contained in rat brain slices. The research presented here thus resulted in several proof of concepts, and the opportunities arising from this body of work harnesses the power of technology to further understand brain function in normal to pathological tissues.

6.1 Summary of Findings

Using an iterative design and fabrication process, as well as several animal model systems, I was able to develop and validate three state-of-the-art brain chip technologies that allow long-term neural recordings at a resolution higher than traditional commercially available devices provide (Figure 43).

First, establishing the biocompatibility status of the SS-MEA, I demonstrated that simple nano-scale, structural modifications to planar micro-electrodes could significantly increase the signal-to-noise ratio of recordings from single invertebrate cells. More specifically, the physical

changes that I made to planar micro-electrodes resulted in the generation of nano-edges which functioned as “bio-mimickery” of the synaptic structure. These electrode design changes resulted in increasing the sealing resistance and allowing for higher action potential amplitudes to be recorded. The functional efficacy of this chip and the interpretation of our conclusions drawn from the data was further backed up by computational simulation, which also highlighted the potentials and limitations of the nano-edge design.

With the ultimate goal that the tools developed and refined to record from snail neurons must also be appropriate and sufficient to monitor neural activities from vertebrate neurons, I applied these initial findings to more commonly used cultured mammalian neurons. Thus the physical principle behind the sealing resistance increase was applied into the design and development of micro-electrodes with multiple micro wells, thus creating a novel MEA (MW-MEA). I demonstrated that these novel microelectrodes could record neural activity from single cells embedded in complex mammalian neural networks with higher resolution than traditional devices available to date.

Finally, the three-dimensional, insulated gold microelectrodes were fabricated on a third MEA (NT-MEA) that offered unique opportunities to record and monitor neural network phenomena both across and within the intact brain slices. Again, the signal-to-noise ratio was significantly increased compared to traditional planar micro-electrodes. This chip enabled the analysis of neural activity events exhibited by more complex and intact networks - with a higher signal-to-noise resolution.

Overall, I demonstrated that designing bio-compatible neuro-electronic devices that are based on natural cellular architecture could pay large dividends in the recording capabilities of bionic hybrids like MEAs. These approaches will not only revolutionize the field of brain science, but also enable novel technology development, commercialization, and in a longer term, improve the quality of life for those affected by brain pathology.

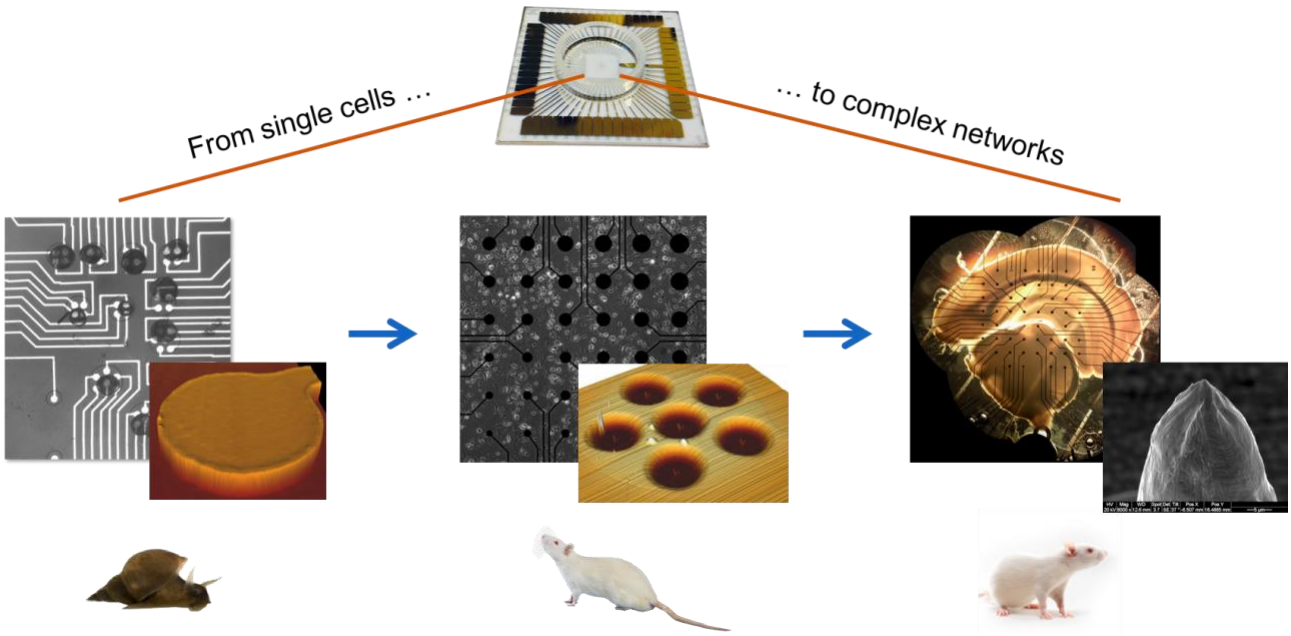

Figure 43: Summary of the research project

From single cells using the fresh water snail Lymnaea stagnalis, to cultured mammalian neurons using Sprague Dawley rats, and acute hippocampal brain slices from wild-type mice. Three MEAs were developed to record neural activity from single cells and more complex networks.

6.2 Limitations and Caveats

While the work presented here shows significant advancements in our ability to record neural activity at a higher resolution than conventional devices, further milestones need to be reached to make these technologies relevant in a clinical environment. The priority areas for advancement are:

a. The ability to record activity at an even higher signal-to-noise ratio (i.e. close to traditional intracellular recording, the gold standard in the field of electrophysiology) and with a denser spatial resolution (i.e. placement of additional electrodes in MEAs that can record simultaneously from more neurons). This is especially true when recording activity from neural networks. While a recent trend in MEA research is to fabricate microelectrodes with reduced size leading to an increased number of electrode sites on one array [143–145], these strategies also increase the electrode impedance and recording noise [81].

b. The electrodes developed during this research are mostly made of gold, a very conductive metal that is best suited for recording, but less so for stimulation purposes. Indeed, ions naturally present in the recording media tend to build-up after repetitive stimulations, which diminishes the potential for both recording and stimulating efficiently over time [81].

c. The development of filters to reduce the background noise and computational

methodologies to enhance signal processing that would manage and interpret the extracted data. From single cells to large networks, a main issue is the collection of large amounts of data and their analysis. Thus specific algorithms would need to be developed to interpret various patterns of neuronal activity. It is also important to understand the limits of the data obtained as well as kinks in the process when unwanted biological variability is introduced [146]. Thus, the neuroscience community needs to be better engaged and supported in exploiting the increasing array of data collected.

6.3 Recommendations and future prospects

While this research demonstrated the potential of new fabrication techniques for micro-electrodes, many more avenues should be explored to translate these advances into clinical applications. Based on the remaining general limitations presented in the previous section, further recommendations presented here highlight the potential offered by additional hardware and computational developments.

6.3.1 Further developments of the planar micro-electrode structures

For planar micro-electrodes, in addition to the nano-edge, several modifications of proven technologies could be made in the future to further improve the recording resolution. For example, using conductive materials for the nano-edge, replacing the gold electrode with another metal or alloy coated with platinum black [119], increasing the general roughness or active surface area of the electrodes [60]. Using different coatings and MEA substrates [79] in combination may enhance the quality of the recordings further. While the structural design of the micro-electrodes was the only modified variable, other parameters can still be adjusted to optimize the signal-to-noise ratio and hopefully obtain recordings with resolution closer to what is obtain with intra-cellular electrodes.

In addition, enabling a reliable extracellular stimulation would be a prerequisite for creating feedback loop systems, where an MEA could be used to simultaneously record and stimulate neural networks. However, a safe stimulation of the cells must be achieved (i.e. without causing cellular damages), as standard stimulation protocols have the risk of undesired electrochemical reactions [147–149] or irremediable electroporation [147,150–152]. To avoid these stimulating limitations, the use of capacitive currents has been reported to offer encouraging new stimulation capabilities [153]. Following a similar design as in chapter 3 and 4, a novel capacitive micro-electrode could be developed to stimulate single neurons (invertebrate or vertebrate). A tentative schematic is presented in the figure 44. More specifically, based on the work from the Fromherz group [154], a capacitor with adjusted electrode dimensions and with a "well" surface could be fabricated on a glass substrate. Titanium dioxide (TiO_2) would serve as an insulator between the cell and the electrode [155,156]. In addition, platinum black could be tested as a coating to increase the overall stimulating surface area in contact with the cellular membrane; thus, limiting the range of current required to initiate ionic displacements and generate action potentials.

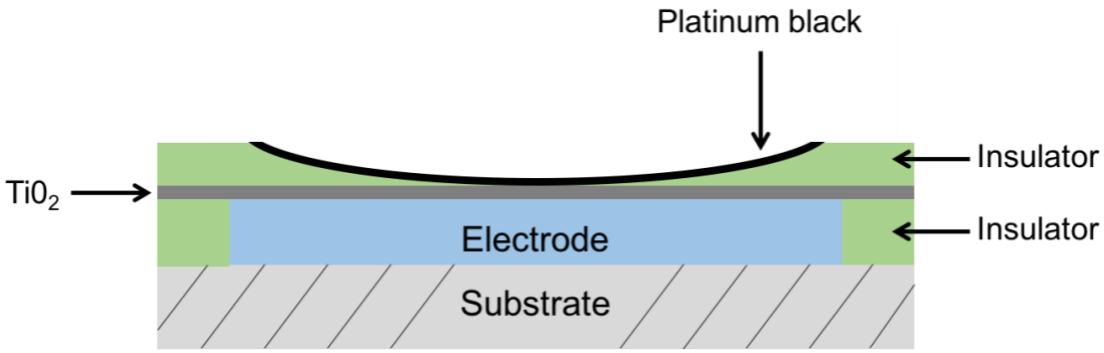

Figure 44: Tentative design of a novel capacitive micro-electrode

Tentative design of a novel capacitive micro-electrode with a "well" surface for stimulation (not on scale). An electrode (different materials to be tested, e.g.: gold, titanium, titanium/iridium alloy) is insulated with TiO_2. A well is then fabricated on top of the electrode and coated with platinum black to increase the overall stimulating surface area in contact with the cellular membrane.

6.3.2 From in-vitro to in-vivo

The fabrication of three-dimensional electrodes could also be further developed to envisage implantable electrodes positioned on a flexible membrane [74]. This implant could then be positioned in animal models or humans to record (or stimulate) neural activity *in-vivo* from the brain, the heart, or parts of the peripheral nervous system, including the vagus nerve to treat epilepsy symptoms. Indeed, the relatively simple and adaptable fabrication method presented in chapter 5 allowed for the development of sharp micro-electrodes as thin as 15µm in diameter (limited by the metal wire diameters used in the wire-bonding process), which could minimize tissue damage and/or scar formation following implantation [139]. The results from these implantations would then be compared with other existing implantable devices that are often considered invasive[140,141,142].

6.3.3 Neural activity analysis and machine learning

These novel custom MEAs, combined with a tractable model system, may allow for the deciphering of unique activity patterns between individual neurons integrated into dense networks. In the longer term, this opportunity will allow a better understanding of the impact of activity signatures on network formation and refinement, as well as how activity dysfunction can lead to neurological disorders, such as epilepsy [157]. Further experiments will also enable the prediction of neuron specific behaviours such as growth, connectivity, and synaptic plasticity by analyzing their

unique patterned activity signature and developing an appropriate computational evaluation method**.**

Finally, using a combination of signal filters, data mining, machine learning and artificial intelligence, the spatio-temporal dynamics of neural networks could be correlated to specific dysfunctional activity patterns seen in neurological disorders [158,159]. Thus the analyzed data could be better exploited and interpreted when studying interactions between different cell populations that undergo distinct extra-cellular conditions. In turn, this would support the neuroscience community with tools to allow: 1) more precise and efficient drug-screening systems, 2) better treatment paradigms (pharmacological or electrical) that could be implemented in a controlled feedback loop system to mitigate abnormal activity.

Ultimately, these approaches would enhance our knowledge of fundamental and clinical aspects of neuroscience; enabling the scientific community to better understand neural network related disease, and more importantly, facilitate the discovery of more appropriate therapeutic approaches for patients suffering from neurological disorders.

6.4 Beyond research, applications and economic impact of microelectrodes

The neuro-technology field is an emerging industry, and while several of my publications are now published in peer-reviewed journals, I am interested in the commercialization value of this research. Indeed, I quickly realized through my research that even the greatest technologies would have no significant impact if researchers do not expand on their accomplishments. To further this entrepreneurial passion of mine, I jointly filed two patents and a licensing opportunity is being negotiated with a growing company in North America. Below is a description of the economic potential of micro-electrode technologies.

6.4.1 General overview of the medical bionics market

The recent technological developments made in the miniaturization of microchips and integrated electrical circuits for the mobile phone market have been exploited to greatly improve our ability to record and stimulate the nervous system using similar semiconductor devices. By taking advantage of this opportunity, some very early firms in the neuro-technology field have been very successful in building and commercializing neuro-electronic devices. With the support of government and private research funding, it is anticipated that this century will see the development of more defined and cost-effective neuro-technologies.

Despite the fact that most neuro-technology devices are still under development, going through clinical trials or waiting for regulatory approval, several have already reached the market and are being used for the treatment of medical disorders and diseases. The neuro-technology industry can be segmented into the following subdivisions depending on their field of application: heart management (cardiac bionics), neuro-modulation using deep brain stimulation (neural/brain bionics), cochlear implant (ear bionics), artificial retina (vision bionics), prosthetics limbs (orthopedic bionics), and Brain Computer Interfaces or BCI. Their respective market shares in 2017 is represented in figure 45.

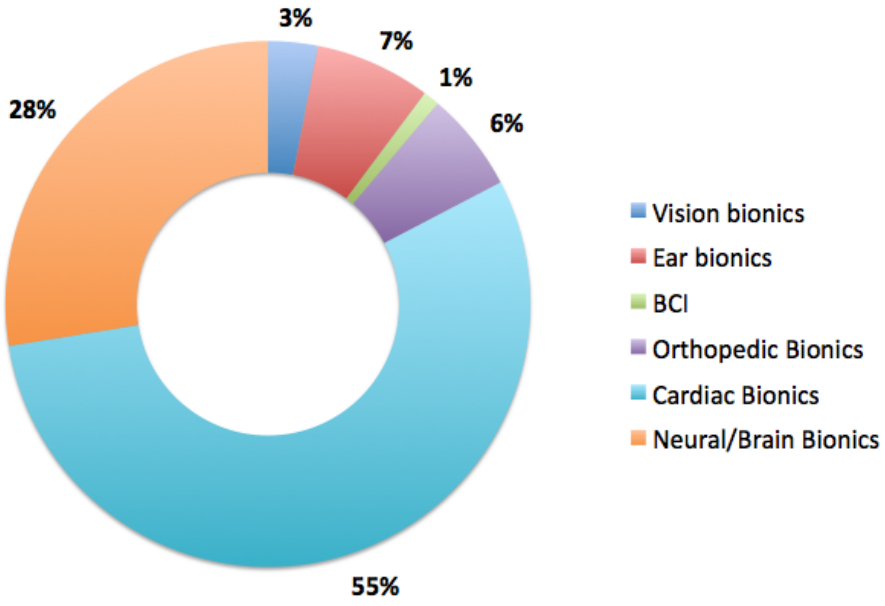

Figure 45: Global medical bionics implant/artificial organs market share, by products, in 2017

Global medical bionics implant/artificial organs market share, by products, in 2017. Behind cardiac bionics, neural and brain bionics represent more than a quarter of the market share and is deemed to increase. This figure was adapted from *Medical Bionic Implant /Artificial Organs Market***,** Report Summary [160].

The global market for medical bionic devices is expected to rise from 17.5 billion USD in 2013 to 38.75 billion USD by 2020, with an expected compound annual growth rate (CAGR) of 9.3% from 2014 to 2020 [161]. Within this market, the neuro-technology industry – which already holds the largest share of revenue above 8.8 billion USD in 2013 [160] – is likely going to grow at an estimated CAGR of 40% during the same period, making it by far one of the most important and profitable sub-market.

6.4.2 Cardiac bionics

Cardiac bionics is a field of treatment in cardiology aimed at managing arrhythmias (abnormal heart rhythm) using implanted electronic devices. It usually involves artificial cardioverter-defibrillator and/or pacemakers, which are basic battery-powered electrical impulse generators. While the first one will detect abnormal heart rhythms and deliver a jolt of electricity in patients at risk for sudden cardiac death to restore the mechanical sequence of ventricular activation and contraction, the second will stimulate the phrenic nerve responsible for transmitting the nerve impulses to the diaphragm, and therefore facilitate breathing. These devices are proven effective treatments for selected patients suffering from conditions such as heart failure-induced conduction disturbances, ventricular dysynchrony, permanent or severe hypoventilation, congestive heart failure, and bradycardia.

Heart bionics accounts for the largest share in the bionics market, primarily due to an increasing global population suffering from heart disease. The market was approximately 12.1 billion USD globally in 2012 with an average CAGR growth of 3-4% annually during the last decade [28]. This revenue is expected to reach 14.7 billion USD by 2017

6.4.3 Neural/brain bionics

Recent developments in neuro-engineering and brain bionics now allow the use of medical device-based therapy to modulate the brain's activity and its functions. Specifically, one leading technology within this field is deep brain stimulation (DBS). DBS refers to a neurosurgical technique involving the implantation of an electronic device called a neural or brain pacemaker on the surface of a patient's brain or cortex. Composed of multiple implanted electrodes connected to a pulse generator, this implant sends electrical impulses to specific parts of the brain for the treatment of different emotional and movement disorders. The stimulation appears to block and/or activate brain areas responsible for motor functions or hormonal production. Management of the pulses can be automated or activated by the patient using an external controller, depending of the type and severity of the pathology. The use of DBS in the past decade has provided tremendous therapeutic benefits for patients suffering from Parkinson's disease, muscular tremor, chronic pain, dystonia and epilepsy, but also mood disorders such as severe depression and obsessive-compulsive disorders. Currently this treatment is reserved for patients that are drug treatment-

resistant, however recent studies suggest that DBS could have a similar if not better efficiency than pharmacological approaches.

Growth of the DBS device market has been triggered by a number of factors including a rise in the world's aging population, a growing number of patients living with neuro-degenerative disease, ineffectiveness of current pharmaceuticals and a general awareness about mental health disorders. Thus, DBS is rapidly becoming an effective and financially acceptable technology. Its global market was estimated at 634.1 million USD in 2012, representing an increase of 6.7% from 2010 [162]. This revenue is expected to reach 927 million USD by 2017

6.4.4 Ear bionics

Within the field of neuro-prosthetics, the cochlear implant is a novel surgically implanted electronic device that provides patients suffering from a severe loss of hearing or deafness. Patients who receive such implantation are deaf because of damage to sensory hair cells in their cochlea. To bypass these non-functional cells, the implant is composed of two components: 1) an external component which includes a microphone, a sound processor and the external transmitter; 2) a surgically implanted component composed of the internal receiver and an electrode array placed in the cochlea. Sounds recorded by the microphone are analyzed and transformed by the sound processor and the resulting coded signal is transmitted to the internal receiver by and external transmitter. The signal is then converted to electrical impulses delivered to the auditory nerve

through the electrode array. Following the implantation, a rehabilitation program focusing on the development of hearing skills is necessary to achieve full benefit. Despite the quality of sound being different from natural hearing (less sound information is processed by the brain), this strategy offers most patients the ability to hear and understand speech and environmental sounds.

Because many of the key manufacturing companies are not in the public domain and do not all reveal financial information, it appears impossible to have accurate data indicating the global market revenue. However, the global cochlear implants market is expected to grow at a CAGR of 14.77% over the period 2013-2018 [163] and the two major competitors in this space, Sonova Holding and Cochlear Ltd, saw their revenues respectively increase in 2014 to 1.35 billion USD (+8,1% compared to 2013) and 805 million USD (+6,9% compared to 2013).

6.4.5 Vision bionics

Visual prosthesis, also called bionic eye or artificial retina, is one of the most recent innovations and radical technologies in the neuro-technology industry, bringing tremendous hope for patients suffering from partial or total blindness. Several prototypes have been developed (usually modeled on cochlear implant devices discussed previously) and while only one has been commercialized, most of them are going through clinical trials. Preliminary results reveal that patients tolerate the surgical procedure well and do have improved visual perception which improves their mobility and performance under daily-life conditions [45,46]. The principle is based on using electrical

stimulations to physiologically excite retinal nerve cells which will in turn activate the visual cortex and create a perception of light in blind subjects suffering from retinitis pigmentosa (RP). Retinal implants are composed of three separate components: 1) an external image detector (camera) record what is in front of the patient and an image processor encoding the images into an array of discreet pixels and sending the data to a transmitter; 2) an implanted receiver/decoder/stimulator hermetically sealed within a capsule and fixed within the eye of the patient such that it may receive the information from the external component, decode the signal and generate electrical pulses sent to an electrode array; 3) a flexible electrode array implanted on the surface of the retina which stimulate the retinal nerve cells.

References

1. Martinez, D. *et al.* High-fidelity patch-clamp recordings from neurons cultured on a polymer microchip. *Biomed. Microdevices* **12,** 977–985 (2010).

2. Martina, M. *et al.* Recordings of cultured neurons and synaptic activity using patch-clamp chips. *J. Neural Eng.* **8,** 34002 (2011).

3. Py, C. *et al.* A novel silicon patch-clamp chip permits high-fidelity recording of ion channel activity from functionally defined neurons. *Biotechnol. Bioeng.* **107,** 593–600 (2010).

4. Kaul, R. A., Syed, N. I. & Fromherz, P. Neuron-Semiconductor Chip with Chemical Synapse between Identified Neurons. *Phys. Rev. Lett.* **92,** 38102 (2004).

5. Lebedev, M. A. & Nicolelis, M. A. L. Brain-machine interfaces: past, present and future. *Trends in Neurosciences* **29,** 536–546 (2006).

6. Cipriani, C. *et al.* A Novel Concept for a Prosthetic Hand With a Bidirectional Interface: A Feasibility Study. *IEEE Trans. Biomed. Eng.* **56,** 2739–2743 (2009).

7. Konrad, P. & Shanks, T. Implantable brain computer interface: Challenges to neurotechnology translation. *Neurobiology of Disease* **38,** 369–375 (2010).

8. Donoghue, J. P., Nurmikko, A., Black, M. & Hochberg, L. R. Assistive technology and robotic control using motor cortex ensemble-based neural interface systems in humans with tetraplegia. *J. Physiol.* **579,** 603–611 (2007).

9. Frontiers Research Foundation., R. M. *Frontiers in neuroengineering. Frontiers in Neuroengineering* **3,** (Frontiers Research Foundation, 2008).

10. Azevedo, F. A. C. *et al.* Equal numbers of neuronal and nonneuronal cells make the human brain an isometrically scaled-up primate brain. *J. Comp. Neurol.* **513,** 532–541 (2009).

11. Herculano-Houzel, S. *et al.* The elephant brain in numbers. *Front. Neuroanat.* **8,** 46 (2014).

12. Drachman, D. A. Do we have brain to spare? *Neurology* **64,** 2004–2005 (2006).

13. Kandel, E. R., Schwartz, J. H., Jessell, T. M., Siegelbaum, S. A. & Hudspeth, A. J. *Principles of Neural Science, Fifth Edition*. *Neurology* **3,** (2014).

14. Afifi, A. K. & Bergman, R. A. (Ronald A. *Functional neuroanatomy : text and atlas*. (McGraw-Hill, Health Professions Division, 1998).

15. Hodgkin, A. L. & Huxley, A. F. *Hodgkin, Huxley - 1952 - Currents carried by sodium and potassium ions through the membrane of the giant axon of Loligo.pdf*. *The Journal of physiology* (1952). doi:10.1113/jphysiol.1952.sp004717

16. Robichaux, M. A. & Cowan, C. W. Signaling mechanisms of axon guidance and early synaptogenesis. *Curr. Top. Behav. Neurosci.* **16,** 19–48 (2014).

17. Colón-Ramos, D. A. Chapter 2 Synapse Formation in Developing Neural Circuits. in 53–79 (2009). doi:10.1016/S0070-2153(09)01202-2

18. Lai, K.-O. & Ip, N. Y. Central synapse and neuromuscular junction: same players, different roles. *Trends Genet.* **19,** 395–402 (2003).

19. Lai, K.-O. & Ip, N. Y. Postsynaptic signaling of new players at the neuromuscular junction. *J. Neurocytol.* **32,** 727–741 (2003).

20. Munno, D. W. & Syed, N. I. Synaptogenesis in the CNS: an odyssey from wiring together to firing together. *J. Physiol.* **552,** 1–11 (2003).

21. Meems, R., Munno, D., van Minnen, J. & Syed, N. I. Synapse formation between isolated axons requires presynaptic soma and redistribution of postsynaptic AChRs. *J. Neurophysiol.* **89,** 2611–9 (2003).

22. Waites, C. L., Craig, A. M. & Garner, C. C. Mechanisms of Vertebrate Synaptogenesis. *Annu. Rev. Neurosci.* **28,** 251–274 (2005).

23. Vitureira, N., Letellier, M. & Goda, Y. Homeostatic synaptic plasticity: From single synapses to neural circuits. *Current Opinion in Neurobiology* **22,** 516–521 (2012).

24. Regehr, W. G. Short-term presynaptic plasticity. *Cold Spring Harb. Perspect. Biol.* **4,** 1–19 (2012).

25. Yang, Y. & Calakos, N. Presynaptic long-term plasticity. *Frontiers in Synaptic Neuroscience* **5,** (2013).

26. Faingold, C. L. & Blumenfeld, H. Chapter 1 - Introduction to Neuronal Networks of the Brain BT - Neuronal Networks in Brain Function, CNS Disorders, and Therapeutics. in

1–10 (Academic Press, 2014). doi:https://doi.org/10.1016/B978-0-12-415804-7.00001-0

27. Hölscher, C. Functional roles of theta and gamma oscillations in the association and dissociation of neuronal networks in primates and rodents. in *Information Processing by Neuronal Populations* (eds. Holscher, C. & Munk, M.) 151–173 (Cambridge University Press). doi:10.1017/CBO9780511541650.007

28. Joseph, J. E. *et al.* The changing landscape of functional brain networks for face processing in typical development. *Neuroimage* **63,** 1223–1236 (2012).

29. Schneider-Mizell, C. M., Parent, J. M., Ben-Jacob, E., Zochowski, M. R. & Sander, L. M. From network structure to network reorganization: implications for adult neurogenesis. *Phys. Biol.* **7,** 46008 (2010).

30. Parent, J. M. & Murphy, G. G. Mechanisms and functional significance of aberrant seizure-induced hippocampal neurogenesis. *Epilepsia* **49,** 19–25 (2008).

31. Kuruba, R., Hattiangady, B., Shetty, A. K. & al., et. Hippocampal neurogenesis and neural stem cells in temporal lobe epilepsy. *Epilepsy Behav.* **14 Suppl 1,** 65–73 (2009).

32. Lynch, M. & Sutula, T. Recurrent excitatory connectivity in the dentate gyrus of kindled and kainic acid-treated rats. *J. Neurophysiol.* **83,** 693–704 (2000).

33. Rakhade, S. N. & Jensen, F. E. Epileptogenesis in the immature brain: emerging mechanisms. *Nat. Rev. Neurol.* **5,** 380–391 (2009).

34. Dudek, F. E. & Sutula, T. P. Epileptogenesis in the dentate gyrus: a critical perspective. in

755–773 (2007). doi:10.1016/S0079-6123(07)63041-6

35. WHO. *Neurological disorders. : Public Health Challenges*. (World Health Organization, 2006).

36. United Nations. Department of International Economic and Social Affairs. Population Division. *World population ageing, 2013*.

37. United Nations. Department of Economic and Social Affairs. Population Division. *World population ageing, 1950-2050*. (United Nations, 2002).

38. Snowball, A., Tachtsidis, I., Popescu, T. & Thompson, J. Long-Term Enhancement of Brain Function and Cognition Using Cognitive Training and Brain Stimulation. *Curr. Biol.* **23,** 987–992 (6AD).

39. McDermott, H. J. Music perception with cochlear implants: a review. *Trends Amplif.* **8,** 49–82 (2004).

40. Martins, M. B. B. *et al.* Cochlear implants: Our experience and literature review. *Int. Arch. Otorhinolaryngol.* **16,** 476–481 (2012).

41. Okun, M. S. Deep-Brain Stimulation for Parkinson's Disease. *N. Engl. J. Med.* **367,** 1529–1538 (2012).

42. Parkinson's disease: deep brain stimulation helps Parkinson's disease patients drive. **80,** 98 (2014).

43. Loddenkemper, T. & Pan, a. Deep brain stimulation in epilepsy. *J. Clin. Neurophysiol.*

116, 217–34 (2001).

44. Nagel, S. J. & Najm, I. M. Deep brain stimulation for epilepsy. *Neuromodulation* **12,** 270–279 (2009).

45. Sahel, J. A. *et al.* Subjects Blind From Outer Retinal Dystrophies Are Able To Consistently Read Short Sentences Using The ArgusTM Ii Retinal Prosthesis System. *ARVO Meet. Abstr.* **52,** 3420 (2011).

46. Humayun, M. S. *et al.* Interim results from the international trial of second sight's visual prosthesis. *Ophthalmology* **119,** 779–788 (2012).

47. Leo, A. De, Primiani, V. M., Russo, P., Moglie, F. & Cerri, G. Safety Investigation of a Magnetic Pulse Applicator for Heart Stimulation. *IEEE Transactions on Magnetics* **50,** 1–8 (2014).

48. Sugimachi, M. & Sunagawa, K. Bionic cardiovascular medicine. in *IEEE Engineering in Medicine and Biology Magazine* **24,** 24–31 (2005).

49. Noort, M. van den, Lim, S. & Bosch, P. Recognizing the risks of brain stimulation. *Science (80-.).* **346,** 1307 LP-1307 (2014).

50. Walsh, V. Q. & Walsh, V. Q. Ethics and Social Risks in Brain Stimulation. *Brain Stimul.* **6,** 715–717 (9AD).

51. Pasqualotto, A., Kobanbay, B. & Proulx, M. J. Neural stimulation has a long-term effect on foreign vocabulary acquisition. *Neural Plast.* **2015,** (2015).

52. Bae, S. H. *et al.* In vitro biocompatibility of various polymer-based microelectrode arrays for retinal prosthesis. *Investig. Ophthalmol. Vis. Sci.* **53,** 2653–2657 (2012).

53. Yu, W. *et al.* Biocompatibility of subretinal parylene-based Ti/Pt microelectrode array in rabbit for further artificial vision studies. *J. Ocul. Biol. Dis. Infor.* **2,** 33–36 (2009).

54. Jiang, X. *et al.* In vitro and in vivo evaluation of a photosensitive polyimide thin-film microelectrode array suitable for epiretinal stimulation. *J. Neuroeng. Rehabil.* **10,** 48 (2013).

55. Ribeiro, D. A., Marques, M. E. A. & Salvadori, D. M. F. Biocompatibility of glass-ionomer cements using mouse lymphoma cells in vitro. *J. Oral Rehabil.* **33,** 912–917 (2006).

56. Thomas, C. A., Springer, P. A., Loeb, G. E., Berwald-Netter, Y. & Okun, L. M. A miniature microelectrode array to monitor the bioelectric activity of cultured cells. *Exp. Cell Res.* **74,** 61–66 (1972).

57. Gross, G. W., Rieske, E., Kreutzberg, G. W. & Meyer, A. A new fixed-array multi-microelectrode system designed for long-term monitoring of extracellular single unit neuronal activity in vitro. *Neurosci. Lett.* **6,** 101–105 (1977).

58. Gross, G. W. Simultaneous Single Unit Recording in vitro with a Photoetched Laser Deinsulated Gold Multimicroelectrode Surface. *IEEE Trans. Biomed. Eng.* **BME-26,** 273–279 (1979).

59. Jobling, D. T., Smith, J. G. & Wheal, H. V. Active microelectrode array to record from the

mammalian central nervous system in vitro. *Med. Biol. Eng. Comput.* **19,** 553 (9AD).

60. Pine, J. Recording action potentials from cultured neurons with extracellular microcircuit electrodes. *J. Neurosci. Methods* **2,** 19–31 (1980).

61. Fromherz, P., Offenhäusser, A., Vetter, T. & Weis, J. A Neuron-Silicon Junction: A Retzius Cell of the Leech on an Insulated-Gate Field-Effect Transistor. *Science (80-.).* **252,** 1290–1293 (1991).

62. Droge, M. H., Gross, G. W., Hightower, M. H. & Czisny, L. E. Multielectrode analysis of coordinated, multisite, rhythmic bursting in cultured CNS monolayer networks. *J. Neurosci.* **6,** 1583–1592 (1986).

63. Novak, J. L. & Wheeler, B. C. Multisite hippocampal slice recording and stimulation using a 32 element microelectrode array. *J. Neurosci. Methods* **23,** 149–159 (1988).

64. Wheeler, B. C. & Novak, J. L. Current Source Density Estimation Using Microelectrode Array Data from the Hippocampal Slice Preparation. *IEEE Trans. Biomed. Eng.* **33,** 1204–1212 (1986).

65. Meister, M., Pine, J. & Baylor, D. A. Multi-neuronal signals from the retina: acquisition and analysis. *J. Neurosci. Methods* **51,** 95–106 (1994).

66. Oka, H., Shimono, K., Ogawa, R., Sugihara, H. & Taketani, M. A new planar multielectrode array for extracellular recording: Application to hippocampal acute slice. *J. Neurosci. Methods* **93,** 61–67 (1999).

67. Maeda, E., Robinson, H. P. & Kawana, A. The mechanisms of generation and propagation of synchronized bursting in developing networks of cortical neurons. *J. Neurosci.* **15,** 6834–45 (1995).

68. Jimbo, Y., Kawana, A., Parodi, P. & Torre, V. The dynamics of a neuronal culture of dissociated cortical neurons of neonatal rats. *Biol. Cybern.* **83,** 1–20 (2000).

69. Potter, S. M. & DeMarse, T. B. A new approach to neural cell culture for long-term studies. *J. Neurosci. Methods* **110,** 17–24 (2001).

70. Zeck, G. & Fromherz, P. Noninvasive neuroelectronic interfacing with synaptically connected snail neurons immobilized on a semiconductor chip. *Proc. Natl. Acad. Sci. U. S. A.* **98,** 10457–10462 (2001).

71. Giachello, C. N., Montarolo, P. G. & Ghirardi, M. Synaptic functions of invertebrate varicosities: what molecular mechanisms lie beneath. *Neural Plast* **2012,** (2012).

72. Massobrio, P., Giachello, C. N. G., Ghirardi, M. & Martinoia, S. Selective modulation of chemical and electrical synapses of Helix neuronal networks during in vitro development. *BMC Neurosci.* **14,** 22 (2013).

73. Stett, A. *et al.* Biological application of microelectrode arrays in drug discovery and basic research. *Analytical and Bioanalytical Chemistry* **377,** 486–495 (2003).

74. Hosp, J. A. *et al.* Thin-film epidural microelectrode arrays for somatosensory and motor cortex mapping in rat. *J. Neurosci. Methods* **172,** 255–262 (2008).

75. Spira, M. E. & Hai, A. Multi-electrode array technologies for neuroscience and cardiology. *Nat. Nanotechnol.* **8,** 83–94 (2013).

76. Cohen, A., Shappir, J., Yitzchaik, S. & Spira, M. E. Reversible transition of extracellular field potential recordings to intracellular recordings of action potentials generated by neurons grown on transistors. *Biosens. Bioelectron.* **23,** 811–819 (2008).

77. Brüggemann, D. *et al.* Nanostructured gold microelectrodes for extracellular recording from electrogenic cells. *Nanotechnology* **22,** 265104 (2011).

78. Prinz, A. a & Fromherz, P. Effect of neuritic cables on conductance estimates for remote electrical synapses. *J. Neurophysiol.* **89,** 2215–2224 (2003).

79. Taketani, M. & Baudry, M. *Advances in network electrophysiology: Using multi-electrode arrays*. *Advances in Network Electrophysiology: Using Multi-Electrode Arrays* (2006). doi:10.1007/b136263

80. Jones, I. L. *et al.* The potential of microelectrode arrays and microelectronics for biomedical research and diagnostics. *Analytical and Bioanalytical Chemistry* **399,** 2313–2329 (2011).

81. Cogan, S. F. Neural stimulation and recording electrodes. *Annu. Rev. Biomed. Eng.* **10,** 275–309 (2008).

82. Waser, R. *Nanoelectronics and Information Technology*. *Nanoelectronics and Information Technology* (2012). doi:10.1017/CBO9781107415324.004

83. Robinson, J. T. *et al.* Vertical nanowire electrode arrays as a scalable platform for intracellular interfacing to neuronal circuits. *Nat. Nanotechnol.* **7,** 180–184 (2012).

84. Xie, C., Lin, Z., Hanson, L., Cui, Y. & Cui, B. Intracellular recording of action potentials by nanopillar electroporation. *Nat. Nanotechnol.* **7,** 185–90 (2012).

85. Suzuki, I., Fukuda, M., Shirakawa, K., Jiko, H. & Gotoh, M. Carbon nanotube multi-electrode array chips for noninvasive real-time measurement of dopamine, action potentials, and postsynaptic potentials. *Biosens. Bioelectron.* **49,** 1–6 (2013).

86. Fromherz, P. & Stett, A. Silicon-neuron junction: Capacitive stimulation of an individual neuron on a silicon chip. *Phys. Rev. Lett.* **75,** 1670–1673 (1995).

87. Hai, A., Shappir, J. & Spira, M. E. In-cell recordings by extracellular microelectrodes. *Nat. Methods* **7,** 200–2 (2010).

88. Chen, C. & Folch, A. A high-performance elastomeric patch clamp chip. *Lab Chip* **6,** 1338 (2006).

89. Wijdenes, P., Dalton, C., Armstrong, R., Zaidi, W. & Syed, N. I. Development of a planar microelectrode array offering long-term, high-resolution neuronal recordings. in *IFMBE Proceedings* **51,** (2015).

90. Syed, N. I., Zaidi, H. & Lovell, P. In Vitro Reconstruction of Neuronal Circuits: A Simple Model System Approach BT - Modern Techniques in Neuroscience Research. in (eds. Windhorst, U. & Johansson, H.) 361–377 (Springer Berlin Heidelberg, 1999). doi:10.1007/978-3-642-58552-4_12

91. Luk, C. C. *et al.* Trophic Factor-Induced Activity 'Signature' Regulates the Functional Expression of Postsynaptic Excitatory Acetylcholine Receptors Required for Synaptogenesis. *Sci. Rep.* **5,** (2015).

92. Bulloch, A. G. M. & Syed, N. I. Reconstruction of neuronal networks in culture. *Trends Neurosci* **15,** (1992).

93. Schmold, N. & Syed, N. I. Molluscan neurons in culture: Shedding light on synapse formation and plasticity. *Journal of Molecular Histology* **43,** 383–399 (2012).

94. Biffi, E., Regalia, G., Menegon, A., Ferrigno, G. & Pedrocchi, A. The influence of neuronal density and maturation on network activity of hippocampal cell cultures: A methodological study. *PLoS One* **8,** (2013).

95. Simeone, T. A., Simeone, K. A., Samson, K. K., Kim, D. Y. & Rho, J. M. Loss of the Kv1.1 potassium channel promotes pathologic sharp waves and high frequency oscillations in in vitro hippocampal slices. *Neurobiol. Dis.* **54,** 68–81 (2013).

96. Gavrilovici, C., Pollock, E., Everest, M. & Poulter, M. O. The loss of interneuron functional diversity in the piriform cortex after induction of experimental epilepsy. *Neurobiol. Dis.* **48,** 317–328 (2012).

97. Gavrilovici, C., D'Alfonso, S., Dann, M. & Poulter, M. O. Kindling-induced alterations in GABAA receptor-mediated inhibition and neurosteroid activity in the rat piriform cortex. *Eur. J. Neurosci.* **24,** 1373–1384 (2006).

98. Gonzalez-Sulser, A. Mechanisms behind the GABA-mediated field potential in

hippocampus in the in vitro 4-aminopyridine model of epilepsy . (2012).

99. Giovangrandi, L., Gilchrist, K. H., Whittington, R. H. & Kovacs, G. T. A. Low-cost microelectrode array with integrated heater for extracellular recording of cardiomyocyte cultures using commercial flexible printed circuit technology. *Sensors Actuators, B Chem.* **113,** 545–554 (2006).

100. Graham, A. H. D., Bowen, C. R., Taylor, J. & Robbins, J. Neuronal cell biocompatibility and adhesion to modified CMOS electrodes. *Biomed. Microdevices* **11,** 1091–1101 (2009).

101. Ghazavi, A. *et al.* Effect of planar microelectrode geometry on neuron stimulation: Finite element modeling and experimental validation of the efficient electrode shape. *J. Neurosci. Methods* **248,** (2015).

102. Purdy, M. T., Wijdenes, P., Zaidi, W., Syed, N. I. & Dalton, C. Accelerating neurite outgrowth through electric field manipulation. in *IFMBE Proceedings* **51,** (2015).

103. Volkov, A. G. *Plant electrophysiology: Methods and cell electrophysiology*. *Plant Electrophysiology: Methods and Cell Electrophysiology* (2012). doi:10.1007/978-3-642-29119-7

104. Kaplan, P. W. & Nguyen, T. *Clinical Electrophysiology: A Handbook for Neurologists*. *Clinical Electrophysiology: A Handbook for Neurologists* (2010). doi:10.1002/9781444322972

105. Merz, M. & Fromherz, P. Silicon chip interfaced with a geometrically defined net of snail

neurons. *Adv. Funct. Mater.* **15,** 739–744 (2005).

106. Cohen, A., Shappir, J., Yitzchaik, S. & Spira, M. E. Reversible transition of extracellular field potential recordings to intracellular recordings of action potentials generated by neurons grown on transistors. *Biosens. Bioelectron.* **23,** 811–819 (2008).

107. Fromherz, P. Three levels of neuroelectronic interfacing: Silicon chips with ion channels, nerve cells, and brain tissue. in *Annals of the New York Academy of Sciences* **1093,** 143–160 (2006).

108. Wijdenes, P. *et al.* A novel bio-mimicking, planar nano-edge microelectrode enables enhanced long-term neural recording. *Sci. Rep.* **6,** (2016).

109. Hanganu-Opatz, I. L. Between molecules and experience: Role of early patterns of coordinated activity for the development of cortical maps and sensory abilities. *Brain Res. Rev.* **64,** 160–176 (2010).

110. Wiersma-Meems, R., Van Minnen, J. & Syed, N. I. Synapse formation and plasticity: the roles of local protein synthesis. *neuroscientist* **11,** 228–237 (2005).

111. Flight, M. H. Synaptogenesis: Switching to learn. *Nat Rev Neurosci* **12,** 248–249 (2011).

112. Feng, Z. P., Hasan, S. U., Lukowiak, K. & Syed, N. I. Target cell contact suppresses neurite outgrowth from soma-soma paired Lymnaea neurons. *J. Neurobiol.* **42,** 357–369 (2000).

113. Zucker, R. S. & Regehr, W. G. Short-Term Synaptic Plasticity. *Annu. Rev. Physiol.* **64,**

355–405 (2002).

114. Buitenweg, J., Rutten, W. & Marani, E. Finite element modeling of the neuron-electrode interface. *Eng. Med. Biol. Mag. IEEE* **19,** 46–52 (2000).

115. Gleixner, R. & Fromherz, P. The extracellular electrical resistivity in cell adhesion. *Biophys. J.* **90,** 2600–2611 (2006).

116. Wrobel, G. *et al.* Transmission electron microscopy study of the cell-sensor interface. *J. R. Soc. Interface* **5,** 213–22 (2008).

117. Hai, A. *et al.* Spine-shaped gold protrusions improve the adherence and electrical coupling of neurons with the surface of micro-electronic devices. *J. R. Soc. Interface* **6,** 1153–65 (2009).

118. Lavacchi, A. *et al.* Cyclic voltammetry simulation at microelectrode arrays with COMSOL Multiphysics?? *J. Appl. Electrochem.* **39,** 2159–2163 (2009).

119. Desai, S. A., Rolston, J. D., Guo, L. & Potter, S. M. Improving impedance of implantable microwire multi-electrode arrays by ultrasonic electroplating of durable platinum black. *Front. Neuroeng.* **3,** 5 (2010).

120. Charlesworth, P., Cotterill, E., Morton, A., Grant, S. G. & Eglen, S. J. Quantitative differences in developmental profiles of spontaneous activity in cortical and hippocampal cultures. *Neural Dev* **10,** 1 (2015).

121. Gonzalez-Sulser, A. *et al.* The 4-aminopyridine in vitro epilepsy model analyzed with a

perforated multi-electrode array. *Neuropharmacology* **60,** 1142–1153 (2011).

122. Johnstone, A. F. M. *et al.* Microelectrode arrays: A physiologically based neurotoxicity testing platform for the 21st century. *NeuroToxicology* **31,** 331–350 (2010).

123. Gong, X. W., Li, J. B., Lu, Q. C., Liang, P. J. & Zhang, P. M. Effective connectivity of hippocampal neural network and its alteration in Mg2+-free epilepsy model. *PLoS One* **9,** (2014).

124. Steidl, E. M., Neveu, E., Bertrand, D. & Buisson, B. The adult rat hippocampal slice revisited with multi-electrode arrays. *Brain Res.* **1096,** 70–84 (2006).

125. Hill, A. J., Jones, N. A., Williams, C. M., Stephens, G. J. & Whalley, B. J. Development of multi-electrode array screening for anticonvulsants in acute rat brain slices. *J. Neurosci. Methods* **185,** 246–256 (2010).

126. McNeill, A. S. Neurodegeneration : theory, disorders, and treatments. (2011).

127. Markram, H. Seven challenges for neuroscience. *Functional neurology* **28,** 145–151 (2013).

128. Brodie, M. J. Medical therapy of epilepsy: When to initiate treatment and when to combine? *J. Neurol.* **252,** 125–130 (2005).

129. Fromherz, P. Neuroelectronic Interfacing: Semiconductor Chips with Ion Channels, Nerve Cells, and Brain. *Nanoelectron. Inf. Technol.* **16,** 781–810 (2003).

130. Heuschkel, M. O., Fejtl, M., Raggenbass, M., Bertrand, D. & Renaud, P. A three-

dimensional multi-electrode array for multi-site stimulation and recording in acute brain slices. *J. Neurosci. Methods* **114,** 135–148 (2002).

131. Rajaraman, S., Bragg, J. a, Ross, J. D. & Allen, M. G. Micromachined three-dimensional electrode arrays for transcutaneous nerve tracking. *J. Micromechanics Microengineering* **21,** 85014 (2011).

132. Rajaraman, S. *et al.* Metal-transfer-micromolded three-dimensional microelectrode arrays for in-vitro brain-slice recordings. *J. Microelectromechanical Syst.* **20,** 396–409 (2011).

133. Aziz, J. N. Y., Genov, R., Bardakjian, B. L., Derchansky, M. & Carlen, P. L. Brain-silicon interface for high-resolution in vitro neural recording. *IEEE Trans. Biomed. Circuits Syst.* **1,** 56–62 (2007).

134. Filatov, G., Krishnan, G. P., Rulkov, N. F. & Bazhenov, M. Dynamics of epileptiform activity in mouse hippocampal slices. *J. Biol. Phys.* **37,** 347–360 (2011).

135. Jones, N. A. *et al.* Cannabidiol Displays Antiepileptiform and Antiseizure Properties In Vitro and In Vivo. *J. Pharmacol. Exp. Ther.* **332,** 569–577 (2010).

136. Hill, A. J., Jones, N. A., Williams, C. M., Stephens, G. J. & Whalley, B. J. Development of multi-electrode array screening for anticonvulsants in acute rat brain slices. *J. Neurosci. Methods* **185,** 246–256 (2010).

137. Simeone, T. A., Simeone, K. A., Samson, K. K., Kim, D. Y. & Rho, J. M. Loss of the Kv1.1 potassium channel promotes pathologic sharp waves and high frequency

oscillations in in vitro hippocampal slices. *Neurobiol. Dis.* **54,** 68–81 (2013).

138. Gavrilovici, C., Pollock, E., Everest, M. & Poulter, M. O. The loss of interneuron functional diversity in the piriform cortex after induction of experimental epilepsy. *Neurobiol. Dis.* **48,** 317–328 (2012).

139. Polikov, V. S., Tresco, P. A. & Reichert, W. M. Response of brain tissue to chronically implanted neural electrodes. *Journal of Neuroscience Methods* **148,** 1–18 (2005).

140. Christensen Pearce, S.M., Ledbetter, N.M., Warren, D.J., Clark, G.A., Tresco, P.A., M. B. The foreign body response to penetrating electrode arrays in the cat sciatic nerve. *Pre-Publication* **10,** 4650–4660 (2011).

141. Christensen, M. B., Wark, H. A. C. & Hutchinson, D. T. A histological analysis of human median and ulnar nerves following implantation of Utah slanted electrode arrays. *Biomaterials* **77,** 235–242 (2016).

142. Wark, H. A. C., Mathews, K. S., Normann, R. A. & Fernandez, E. Behavioral and cellular consequences of high-electrode count Utah Arrays chronically implanted in rat sciatic nerve. *J. Neural Eng.* **11,** 46027 (2014).

143. Frey, U., Egert, U., Heer, F., Hafizovic, S. & Hierlemann, A. Microelectronic system for high-resolution mapping of extracellular electric fields applied to brain slices. *Biosens. Bioelectron.* **24,** 2191–2198 (2009).

144. Charvet, G. *et al.* BioMEA: A versatile high-density 3D microelectrode array system using integrated electronics. *Biosens. Bioelectron.* **25,** 1889–1896 (2010).

145. Berdondini, L. *et al.* Active pixel sensor array for high spatio-temporal resolution electrophysiological recordings from single cell to large scale neuronal networks. *Lab Chip* **9,** 2644–51 (2009).

146. Akil, H., Martone, M. E. & Van Essen, D. C. Challenges and Opportunities in Mining Neuroscience Data. *Science (80-.).* **331,** 708–712 (2011).

147. Ryttsén, F. *et al.* Characterization of Single-Cell Electroporation by Using Patch-Clamp and Fluorescence Microscopy. *Biophys. J.* **79,** 1993–2001 (2000).

148. Rubinsky, B. Irreversible electroporation in medicine. *Technol. Cancer Res. Treat.* **6,** 255–260 (2007).

149. He, H., Chang, D. C. & Lee, Y.-K. Using a micro electroporation chip to determine the optimal physical parameters in the uptake of biomolecules in HeLa cells. *Bioelectrochemistry* **70,** 363–368 (2007).

150. Merrill, D. R., Bikson, M. & Jefferys, J. G. R. Electrical stimulation of excitable tissue: Design of efficacious and safe protocols. *Journal of Neuroscience Methods* **141,** 171–198 (2005).

151. Huang, C. Q., Carter, P. M. & Shepherd, R. K. Stimulus induced pH changes in cochlear implants: An in vitro and in vivo study. *Ann. Biomed. Eng.* **29,** 791–802 (2001).

152. Harnack, D. *et al.* The effects of electrode material, charge density and stimulation duration on the safety of high-frequency stimulation of the subthalamic nucleus in rats. *J. Neurosci. Methods* **138,** 207–216 (2004).

153. Schoen, I. & Fromherz, P. Extracellular stimulation of mammalian neurons through repetitive activation of Na+ channels by weak capacitive currents on a silicon chip. *J. Neurophysiol.* **100,** 346–57 (2008).

154. Hutzler, M. *et al.* High-resolution multitransistor array recording of electrical field potentials in cultured brain slices. *J. Neurophysiol.* **96,** 1638–45 (2006).

155. Wallrapp, F. & Fromherz, P. TiO2 and HfO2 in electrolyte-oxide-silicon configuration for applications in bioelectronics. *J. Appl. Phys.* **99,** (2006).

156. Ulbrich, M. H. & Fromherz, P. Opening of K+ channels by capacitive stimulation from silicon chip. *Appl. Phys. A Mater. Sci. Process.* **81,** 887–891 (2005).

157. Yin, J.-Y. *et al.* Establishing Prediction Model of Antiepileptic Drugs Response using Data Mining Approach. *CNS Neurosci. Ther.* **22,** 860–862 (2016).

158. Fellin, T. & Halassa, M. Neuronal network analysis : concepts and experimental approaches. (2012).

159. Kim, S., Quinn, C. J., Kiyavash, N. & Coleman, T. P. Dynamic and succinct statistical analysis of neuroscience data. *Proc. IEEE* **102,** 683–696 (2014).

160. Markets, R. and. *Medical Bionic Implant (Artificial Organs) Market - (Vision Bionics/Bionic Eye, Brain Bionics, Heart Bionics/Artificial Heart, Orthopedic Bionics and Ear Bionics) – Trends and Global Forecasts to 2017*. (2012).

161. Research, G. view. Artificial Organ And Bionics Market Analysis By Product (Artificial

Heart, Liver, Kidney, Pancreas, Bionic, Limbs, Heart Valves, Cardiac, Vision), By Technology (Mechanical, Electronic) And Segment Forecasts To 2020, June 2014. Grand View Research, Inc. *Gd. view Res.* (2014).

162. Information, K. *Market Research: Electro-stimulation devices*. (2012).

163. Reports, M. research. *Global Cochlear Implants Market 2014-2018*. (2013).